Doctoral Dissertation

Single-walled carbon nanotube field-effect transistor biosensor using small probe molecules

NGUYEN THANH TUNG

Supervisor: Prof. Yuzuru Takamura

Graduate School of Advanced Science and Technology
Japan Advanced Institute of Science and Technology
Materials Science
March 2019

Abstract

Field-effect transistor (FET)-based biosensors offer many advantages such as real-time, label-free, fast response, portability, and high density integration in addition to its high sensitivity. However, generally FET-based biosensors face a critical issue of the Debye shield (physical length of approximately 1 nm induced by counterions in physiological environment) which limits the selection of probe molecules. Besides, conventional probe molecule such as antibody – a product of *in vivo* biological protocol, which is large in size (10 – 12 nm) and suffered from batch to batch activity variation, critical storage condition and high cost, is not suitable for FET-based biosensors.

In this study, we demonstrated the utilization of small *in vitro* probe molecules such as peptide aptamer and glutamate-binding protein (GBP) integrated with single-walled carbon nanotube (SWCNT)-FET to overcome aforementioned problems. The peptide aptamer and GBP are *in vitro* chemically synthesized. Therefore, their activities are uniform regardless of batch with extended storage time; synthesis is quicker and inexpensive; especially they can be flexibly modified to approach wide variety of target while antibody is limited. To implement this research, the following works have been done.

First, SWCNT-FETs were fabricated on the Si/SO_2 substrate by growing SWCNTs on Co catalyst using catalytic alcohol chemical vapour deposition (CVD). We call this CVD-type SWCNT-FETs. On the other hand, to simplify the process of device fabrication and improve the reproducibility, a semiconducting SWCNT solution was used for the deposition of random network SWCNT. This technique is simple and fast, allowing a direct control of network density of SWCNT channel and hence the transistor characteristics. We call this network SWCNT-FET. Both CVD-type and network SWCNT-FETs exhibited typical p-type characteristics in ambient air and in solution as

well. The network SWCNT-FETs showed more reproducible operation than CVD-type SWCNT-FETs, but exhibited higher subthreshold swing value.

Second, we successfully integrated a novel peptide aptamer with the CVD-type SWCNT-FET to achieve highly sensitive and specific detection of biomarker. The novel peptide aptamer that specifically recognizes Cathepsin E (CatE) – a useful prognostic biomarker for cancer diagnosis, was utilized as probe molecule. The SWCNT channel was functionalized by no-covalent immobilization of the peptide aptamer using 1-pyrenebutanoic acid succinimidyl ester (PBASE) linker. As a result, the peptide aptamer-modified CVD-type SWCNT-FET could detect CatE at unprecedentedly low concentrations in both phosphate-buffered saline (0.1 ng/mL) and 10-times diluted human serum (10 ng/mL) and exhibited a high selectivity with no response to bovine serum albumin (BSA) and Cathepsin K (CatK)). The lowest detectable CatE of 10 ng/mL in serum is three time of magnitude lower than that of previous CatE biosensors. These results indicated that the use of small peptide aptamer is an effective strategy for realizing highly sensitive and selective FET-based biosensors. Our demonstrated sensor could be a promising platform for near-patient testing and point-of-care testing applications.

Third, we developed a new real-time monitoring Glutamate (Glu) sensor based on the integration of network SWCN-FET and glutamate-binding protein (GBP) for neuroscience application. Previous Glu sensors are suffered from the temporal and spatial resolution issues to monitor transient Glu. The bind and unbind event of Glu with its receptor is in millisecond range. Therefore, it is required to have a sensor system that is simple, miniaturizable and fast. The network SWCNT-FET appears as a promising candidate thanking to its properties of fast response, high reproducibility, real-time measurement and possibility to make a miniaturized device on flexible substrate. Additionally, the GBP exhibits rapid recognition to transient Glu. Therefore, in this study,

we attempt to combine the GBP with the network SWCNT-FET for real-time monitoring transient Glu. To do that, the GBP probe molecule was immobilized onto the network SWCNT channel of network SWCNT-FET via PBASE linker. The resulting GBP-modified network SWCNT-FET sensor exhibited a high selectivity with no response to Dopamine (DA) and could detect Glu at micro-molar range in real-time. These results indicated that our sensor could be a promising candidate for Glu monitoring in real-time.

In conclusion, we have successfully demonstrated, for the first time, the integration of small probe molecules (peptide aptamer and GBP) into SWCNT-based FETs. The proposed platforms are promising for clinical application as well as neuroscience study, and be applicable for various target biomarkers.

Keywords: SWCNT-FET, peptide aptamer, Cathepsin E, Glutamate-binding protein, Glutamate.

Contents

Acknowledgements

First and foremost, I would like to thank my thesis supervisor, Prof. Yuzuru Takamura, who gave me the freedom and flexibility to be creative in research. It was my great honor to be a member of his research group. His kind advices and encouragement regarding this research are invaluable to me.

I would like to thank my committee members: Prof. Kenzo Maehashi from Institute of Engineering, Tokyo University of Agriculture and Technology; Prof. Hiroshi Mizuta, Assoc. Prof. Yuichi Hiratsuka and Assoc. Prof. Hidekazu Tsutsui from School of Materials Science, JAIST. I thank all of them for their time and consideration in serving on my dissertation committee.

My special thanks go to Assistant Prof. Phan Trong Tue for his enthusiastic supports and advices. I would like to express my thanks to Prof. Truong Thi Ngoc Lien at Hanoi University of Science and Technology, Vietnam; Prof. Biyani at JAIST, Prof. Ohno at Tokushima University, Prof. Maehashi at Tokyo University of Agriculture and Technology, Prof. Matsumoto at ISIR of Osaka University; who have kindly contributed to my research with the stimulating discussions. I would also like to thank Prof. Koyano who helped me take Raman spectra.

I would like to thank for the support of the Ministry of Education, Culture, Sports, Science and Technology (MEXT) during my study in Japan.

Many thanks go to my Lab members for fun activities we have shared as well as nice discussion. I would also like to thank all of the Vietnamese students at JAIST for the wonderful time we had.

Finally, and most importantly, I express my deepest gratitude to my family for their undying love and encouragement during my doctoral course.

JAIST, November 20th, 2019

Nguyen Thanh Tung

Chapter 1: General introduction

1.1. Introduction to biosensors

Biosensors are analytical devices that measure the presence of specific biological molecules by generating signals, which are proportional to the concentration of analytes in the samples. Biosensors offer applications on monitoring disease in the early stage, detecting pollutants in the environment or food safety aiming to improve the quality of life. A typical biosensor consists of four components, namely probe molecule, linker, transducer and signal processing and displaying component (Figure 1.1).

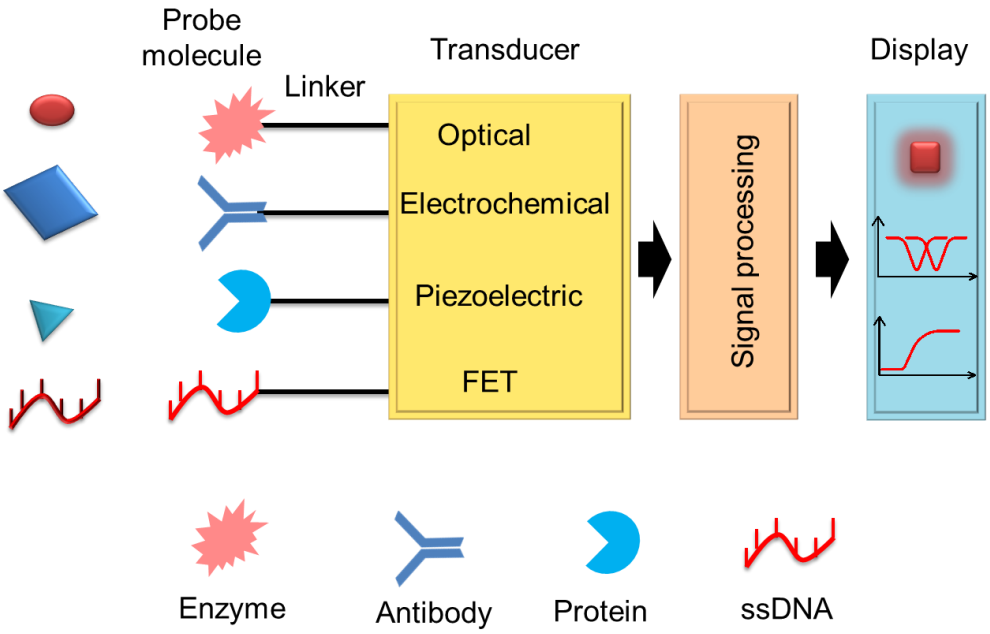

Figure 1.1: Schematic structure of a common biosensor.

- A probe molecule (or bioreceptor) is a biological molecule that specifically recognizes the analyte in sample. The examples of probe molecules are antibody [1, 2], DNA probe [3, 4], and aptamer [5, 6] that is able to make the specific interaction with the target analyte such as antigen, complementary DNA, and target of aptamer. The interaction of the probe molecule with the analyte is term biorecognition, which determines the both specificity and sensitivity properties of a biosensor.

- A linker is a part of a biosensor that is used to immobilize the probe molecule onto the device. In other words, linker is an intermediate that joins the organically biochemical element to organic substrate. Choosing the suitable linker is important. The linker needs ensuring not only the mechanical immobilization but also the transfer of biorecognition signal to the transducer.

- A transducer is a part of biosensor that converts the signal from the binding of target analyte and probe molecule into a measurable signal. This generated signal is directly or inversely proportional to the amount of analyte-probe molecule interactions. There are many types of transducer, namely electrochemical [7], optical [8], piezoelectric [9], thermal transducer [10], and micromechanical transducer (cantilever biosensor) [11, 12].

- A signal processing and displaying component is used to analyse the obtained signal then display on screen in a user-friendly way.

According to the principles of signal transduction (transducer) and birecognition element (probe molecule), biosensors can be classified as electrochemical biosensors (including potentiometric, amperometric and impedimetric biosnesors), calorimetric biosensors, optical biosensors, and acoustic biosensors (Table 1.1).

Table 1.1: The operation principle of biosensors.

Name	Principle of operation
Potentiometric biosensor	- A type of electrochemical biosensor. - The accumulation of a charge potential at working electrode is measured compared to the reference electrode when the current is equal or near zero.
Amperometric biosensor	- A type of electrochemical biosensor. - The current that results from the oxidation or reduction of an electroactive species in a biochemical reaction, is measured while a constant potential is applied between working and reference electrodes.
Impedimetric biosensor	- A type of electrochemical biosensor. - Based on monitoring the ability of an analyte to conduct an electrical current in a solution at constant voltage.
Calorimetric biosensor	- Based on measuring the change of temperature that is occurred in the reaction between biorecognition and analyte.
Optical biosensor	- Based on determining the change in light absorption between the reactants and products of a reaction or light emission.
Acoustic biosensor	- Based on piezoelectric phenomenon in which an oscillating crystal resonates at a natural resonance frequency.

Each type of biosensor has its own advantage and disadvantage as described in the Table 1.2.

Table 1.2: Advantage and disadvantage of biosensors.

Name	Advantage	Disadvantage
Potentiometric biosensor	- Simplicity of operation and the small size of the solid-state field effect transistor (FET) sensors.	- Less sensitivity (compared to amperometric biosensors) and nonspecific effects from other ion in the sample. - Signal to noise ratio is analytical problem which is difficult to tackle.
Amperometric biosensor	- More sensitive, rapid, and inexpensive compared to potentiometric and impedimetric biosensors. - More suitable for mass production rather than potentiometric biosensor.	- The main disadvantage is having an indirect sensing system.
Impedimetric biosensor	- Applying for some promising approaches such as hybridization of DNA fragments amplified by a polymerase chain reaction [13].	- False positive results due to electrolytes from the samples. - Less frequent than potentiometric and amperometric biosensors.
Calorimetric biosensor	- This method is capable in food industry and environmental monitoring [14].	- It is difficult to ensure that the temperature of the sample is constant.
Optical biosensor	- Providing label-free real time detection. - Can apply for single molecule detection [15].	- Expensive cost. - It takes several hours and a technical training.
Acoustic biosensor	- Providing label-free and low cost biosensor.	- Requiring high stability of circuit and extremely high phase stability [16].

1.2. Field effect transistor-based biosensors

FET has been used as an attractive platform for the fabrication of integrated biosensors, which have drawn much attentions of scientist around the world owing to their outstanding benefits, such as a greater signal-to-noise ratio, fast measurement abilities, and portable instrumentation [17]. The FET-based biosensors offer many applications on detecting target analytes in gases [18-21], in solution [22, 23], and biomolecules in sample [24-26]. A FET consists of semiconducting channel and three electrodes (including source, drain and gate electrode). The detection mechanism of the FET-based biosensors is when the target analyte is in vicinity of the semiconducting channel, leading to the conductance of its channel changes accordingly. Therefore, the output electrical signal is changed proportionally to the amount of analyte concentration. Figure 1.2 depicts an example of an example of a FET biosensor. In which probe molecules are immobilized onto the semiconducting channel. The target molecules that are specifically attached to probe molecules will cause the static charge inside the semiconducting channel, leading to the change in conductance. There are many types of semiconducting materials to make the channel of FET-based biosensors such as carbon nanotubes [27], silicon nanowire [28] and graphene [29]. In which single-walled carbon nanotubes (SWCNTs) manifest many overwhelming properties, especially its one-dimensional structure. Therefore, in this work, we focused on SWCNT-FET-based biosensor.

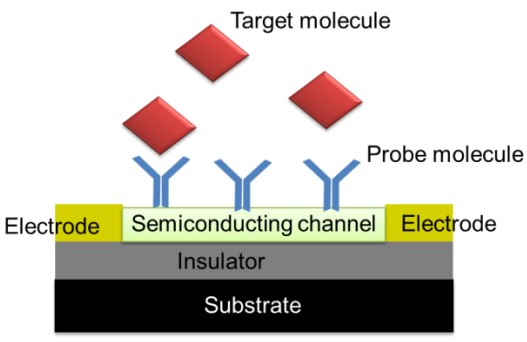

Figure 1.2: Schematic structure of a field effect transistor (FET) biosensor.

The major drawback of all type of FET-based biosensor is short Debye length. It is argued that a FET-based biosensor can only detect the target analyte in very short distance away from its channel surface. This is because of the electrical double layer which screens off the charged biomolecules out of its. The Debye screening length is approximately 1 nm in physiological condition (Figure 1.3). So far, there are several ways to tackle this issue such as increasing Debye screening length by lowering salt concentration [30, 31]; using polyethylene glycol (PEG) [32]; or applying alternating current to weaken the electrical double layer [33]. However, all of these approaches have limitations. For example, using low ionic strength buffer solution would result in weakening the target-probe binding affinity. The use of AC makes system complicated and difficult to control. Etc. Recently, researchers have demonstrated small probe molecules as an effective way to overcome the Debye issue [5, 6].

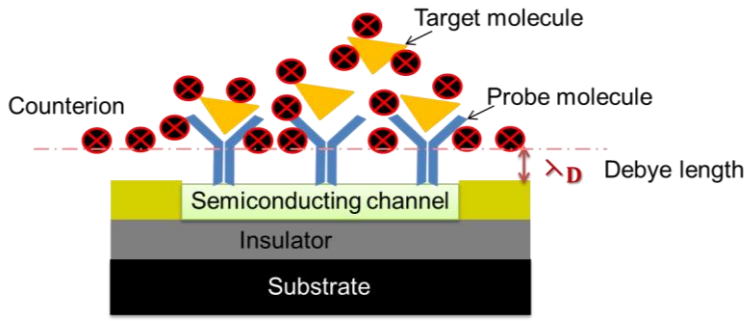

Figure 1.3: Biomolecules carry the zero net charge because of Debye screening effect.

1.3. Single-walled carbon nanotube field-effect transistor biosensors

SWCNT was firstly synthesized by Sumio lijima and Toshinari Ichihashi in 1993 [34]. The first FET based on SWCNT was reported by Tans et al. [35] and Kong et al. used it to develop the first chemical sensor [36]. The functionalization of SWCNT based on principle of molecular recognition induces SWCNT-FET as one of the most promising candidates for the development of highly sensitive and label-free biosensors. SWCNTs

which are inherently small size compatible with biomolecules are straightforward to be modified with probe molecules, facilitating the great improvement of the selectivity and sensitivity of the current methods. Table 1.3 shows the comparison of CNT-FET biosensors that employed different probe molecules. Debye screening is the main issue for FET-based biosensor in general and for SWCNT-based FET biosensor in particular. The use of small probe molecule to bring the binding events close to the sensing surface of CNT-FET could enhance the impact of field-effect from charged biomolecule target, hence improving the sensitivity. As a result, the CNT-FET biosensor using Fab fragment (3 – 5 nm) could improve the minimal detectable concentration down to 1 pg/mL comparing to CNT-FET using whole antibody (10 – 12 nm) with detectable concentration of 1 µg/mL. Additionally, the CNT-FET biosensors using DNA aptamer (1 -2 nm) and nanobody (2 -4 nm) probe molecules could detect IgE and GFP down to 250 pM and 1 pM, respectively. In this work, we focused on using small probe molecules such as peptide aptamer (< 2 nm) and GBP (~ 5 nm) for SWCNT-based FET.

Table 1.3: Comparison of CNT-FET biosensors employed different probe molecules.

Probe molecule	Analyte	Dyn. Range	Sample	Ref.
whole antibody (10 – 12 nm)	human IgG	~ 6.67 nM	10 mM buffer	[37]
Fab'2 fragment (5 – 8 nm)	human IgG	66.7 pM – 6.67 nM	10 mM buffer	[37]
Fab fragment (3 – 5 nm)	human IgG	6.67 – 666.67 fM	10 mM buffer	[37]
DNA aptamer (1 -2 nm)	IgE	250 pM – 160 nM	10 mM buffer	[6]
GFP specific nanobody (2 – 4 nm)	GFP	< 1 pM – 10 nM	100 mM buffer	[38]

Figure 1.4 shows the schematic structure of a SWCNT-FET that consists of Si/SiO_2 substrate, SWCNT channel and three electrodes (source, drain and gate electrodes). The carrier concentration inside SWCNT channel is manipulated by gate voltage. The negative or positive bias induces positive charges (holes) or negative charges (electrons), respectively [39]. SWCNT-FETs typically exhibit p-type characteristic under the ambient air because of the adsorption of oxygen molecules from air. The behaviour of SWCNT-FETs can change from p-type to n-type by passivation of SiN_x with exposed groove of SWCNT channel [40]. Besides, the n-type SWCNT-FET can be fabricated by doping source and drain region with potassium [41].

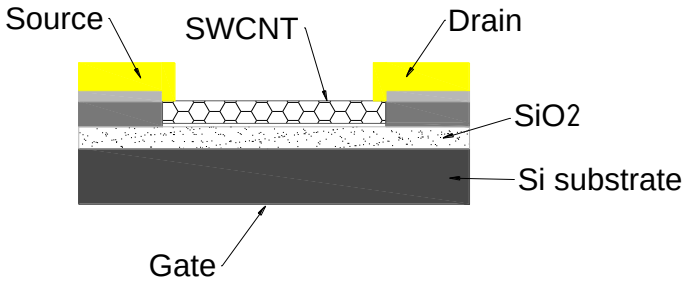

Figure 1.4: Schematic structure of a SWCNT-FET.

Figure 1.5 shows the schematic structure of a SWCNT-FET biosensor. The bioreceptors are immobilized onto SWCNT sidewall via linker. The target biomolecules come and specifically bind to bioreceptor inside the sensitive region of Debye length. Debye length is the distance around the SWCNTs that screen the surplus charge by the mobile carriers present in a material [42] (Figure 1.6). It depends on the salt concentration [C] with the formula $\lambda_D = 0.96\text{nm}\sqrt{0.1\text{M}/[\text{C}]}$. In SWCNT-FET biosensors, the current through source and drain is measured. The origin of the current change is the field effect or a variation in the potential which is affected by the analyte concentration in the sample solution. Therefore, SWCNT-FETs are classified as potentiometric biosensors.

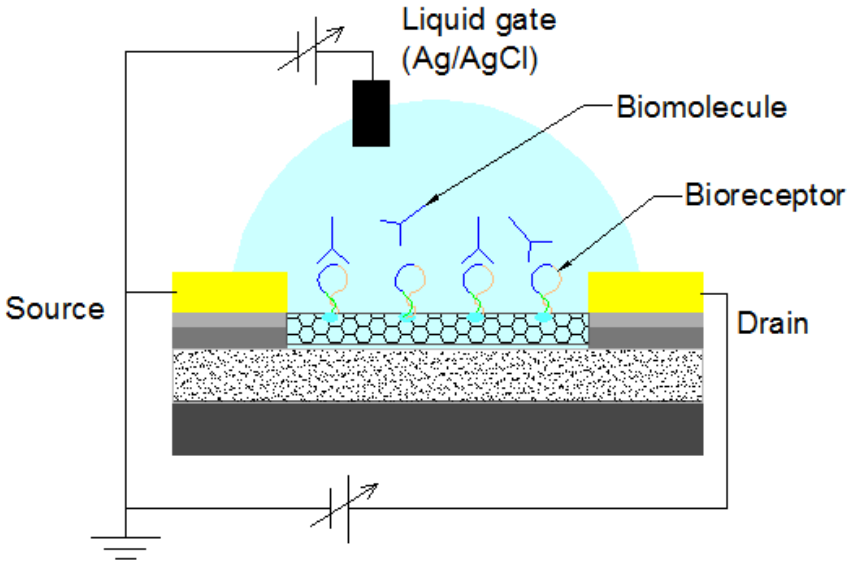

Figure 1.5: Schematic structure of s SWCNT-FET biosensor.

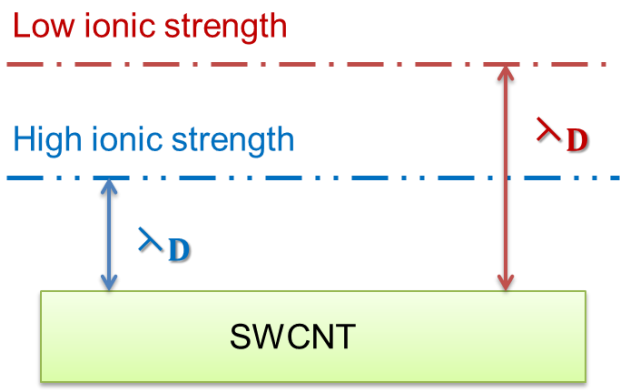

Figure 1.6: Schematic presentation of Debye length.

Consider a molecule in the vicinity of the CNTs, there are two main phenomena occurring. The first one is the charge transfer from the molecule to the CNTs channel. The second one is a scattering process in which the molecule acts as a scattering potential [43]. The charge transfer to the CNTs shifts the threshold voltage toward more positive or more negative direction in case of electron donation from the molecule to the CNTs or hole donation, respectively. If there is a scattering process, overall current decreases (Figure 1.7).

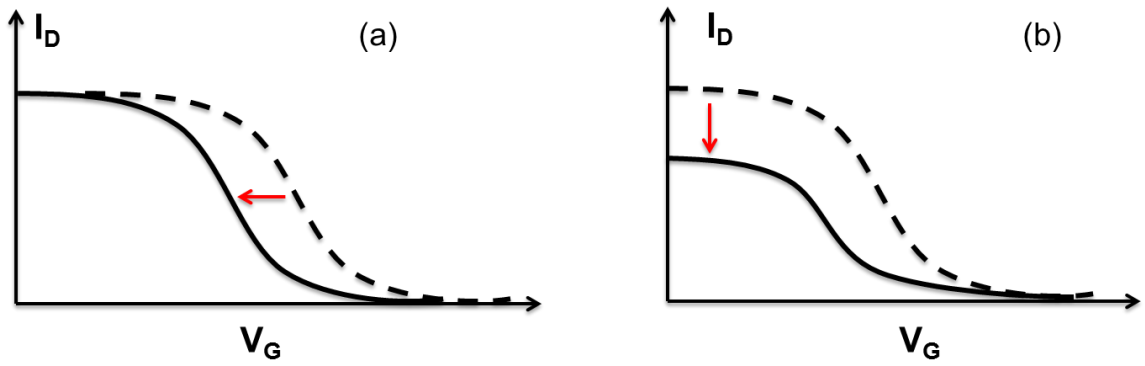

Figure 1.7: Current change in NTFET: (a) The effect of electron transfer from a protein to the CNTs; and (b) the reduction of carrier mobility by scattering potential created by a protein.

1.4. Carbon nanotubes synthesis

CNTs are made of carbon atom by rolling up a graphene sheet with tubular nanostructure. There are two types of CNTs, single-walled carbon nanotube (SWCNTs) and multi-walled carbon nanotube (MWCNTs) (Figure 1.8). SWCNTs are generated from single sheet of graphite called graphene. MWCNTs are produced from either multiple sheets of graphite that are arranged in concentric cylinders (Russian Doll model) or single sheet of graphite that is rolled up into a tube (Parchment model). The interlayer distance in MWCNTs is approximately 0.34 nm. The diameters of SWCNTs and MWCNTs are approximately 0.8 to 2 nm and 5 to over 100 nm, respectively. The CNTs length is from several ten nanometers to several hundred nanometers [44]. SWCNTs can be either semiconducting or metallic depending on their chirality. One-third of as-grown SWCNTs are metallic while the rest are semiconducting [45, 46]. In contrast, MWCNTs usually exhibit a metallic property.

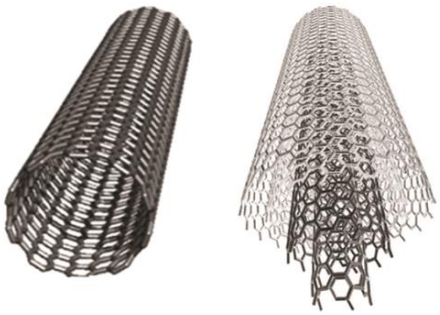

Figure 1.8: Schematic diagrams of SWCNT (left) and MWCNT (right) [47].

There are three main methods usually used to synthesize CNTs, namely arc discharge, laser ablation and chemical vapour deposition (CVD).

- Arc discharge is the method that was initially used by Iijima to discover CNTs in 1996 [48]. This technique generally consists of two high purity graphite electrodes called anode and cathode (Figure 1.9). The distance between anode and cathode is adjusted by moving the position of the anode. The inert gas is introduced at controlled pressure to make plasma between two electrodes. When the potential is applied between two electrodes, a discharge occurs, leading to formation of plasma. The products are obtained on the cathode. In case of no catalyst used, the products are the soot and deposit. The soot contains fullerenes while the carbon deposit contains MWCNTs together with graphite carbon nanoparticles. In case of a metal catalyst used along with graphite, most of nanotubes (SWCNTs and MWCNTs) are formed.

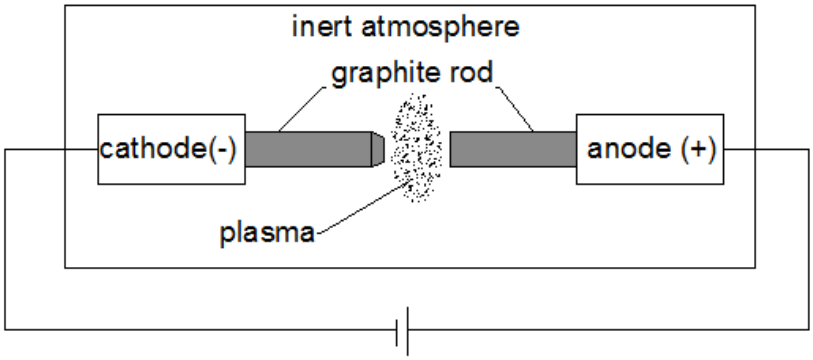

Figure 1.9: Schematic representation of arc discharge method.

- Laser ablation is the process in which an intense laser pulse is made to strike graphite target which contains small amount of metal catalyst such as nickel and cobalt, in a high temperature reactor with the presence of inert gas which vaporizes a graphite target (Figure 1.10). As a result, the inert gas is passed through the chamber carrying the synthesized nanotubes on the cooler surfaces of the reactor as the vaporized carbon condenses. This method chiefly produces SWCNT with higher purity than arc discharge process.

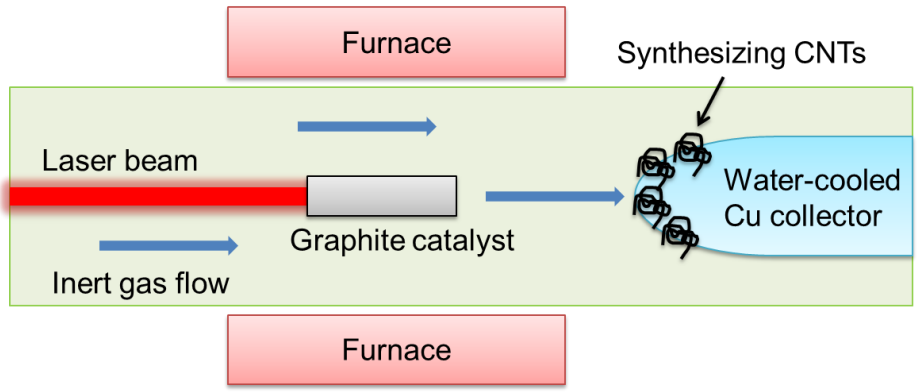

Figure 1.10: Schematic representation of laser ablation method.

Chemical vapour deposition (CVD) is the most popular method for high quality and large scale synthesis of carbon nanotubes. In this process, carbon feedstock gas (ethanol, ethylene, methanol or acetylene) is introduced into a high temperature (600 °C – 1200 °C) chamber that contains metal catalyst in either vacuum or atmospheric pressure (Figure 1.11). The catalytic metals are commonly Fe, Co and Ni because they make high solubility of carbon at high temperature and high carbon diffusion rate in these metals. Additionally, Fe, Co and Ni have stronger adhesion with the growing CNTs than other transition metals; hence enable to form high curvature CNTs such as SWCNTs [49].

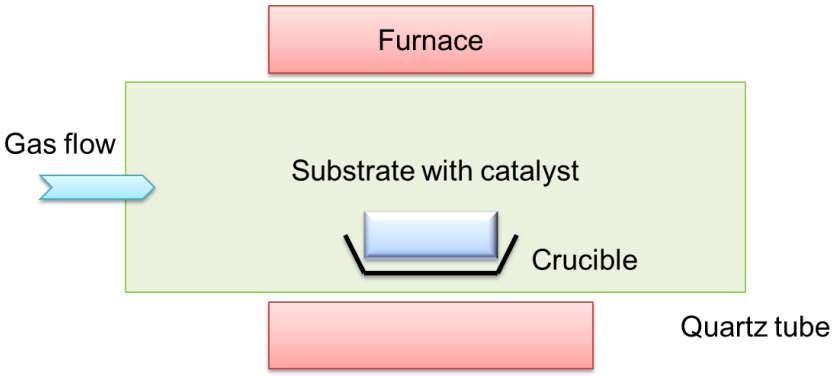

Figure 1.11: Schematic representation of chemical vapour deposition method.

Table 1.4 shows the comparison among three different methods for synthesizing CNTs. Compared to arc discharge and laser ablation methods, CVD method has many advantages. The energy required is lower. The carbon feedstocks are abundant and inexpensive. The setup of process is simple and it is easy to control and manipulate. In this process, CNTs are synthesized with high quality and large scale production [50]. The refining process is only necessary in case of further purification. Especially, CVD is unique method to produce well aligned CNTs which no other methods can make. With these aforementioned advantages, CVD method was chose to synthesize SWCNT in this work.

Table 1.4: Comparison of different synthesis methods of CNTs.

Method	**Arc discharge**	**Laser ablation**	**CVD**
Typical yield	30 – 90 %	Up to 70 %	20 – 100 %
SWCNT	Short tubes with diameter of 0.6 – 1.4 nm	Long bundles of tubes (5 – 20 µm) with individual diameter of 1 – 2 nm	Long tubes with diameter of 0.6 – 4 nm
Merits	- SWCNTs with few defects - MWCNTs without catalyst - Relatively cheap - Open air synthesis possible	- Primarily SWCNTs with good diameter control and few defects - Quite pure	- Easiest to scale up - Simple process - Long length - SWCNT diameter is controllable - Quite pure
Demerits	- Randomly short tube sizes and directions - Often needs purification	- Expensive because of costly lasers - High power requirement	- Usually MWCNTs - Often riddled with defects

In CVD method, CNTs are formed via “tip-growth model” and “base-growth model” as shown in Figure 1.12. First, the carbon feedstock gas is decomposed, then deposited on the methal catalyst, thence CNTs is grown. In the “tip-growth model” (Figure 1.11(a)), the adhesion between substrate and metal particle is weak. When the hydrocarbon decomposes onto the top surface of metal particle, carbon diffuses into interface of metal particle and substrate, forming the CNTs and lifting up the metal particle until the metal particle is fully covered with excess carbon. In the “base-growth model” (Figure 1.11(b)),

the adhesion between substrate and metal particles is strong. When the hydrocarbon decomposes onto the surface of metal particle, carbon diffuses into the interface of metal particle and substrate. But in this case, it fails to push the metal particle. Therefore, it is compelled to emerge, hence forming CNTs.

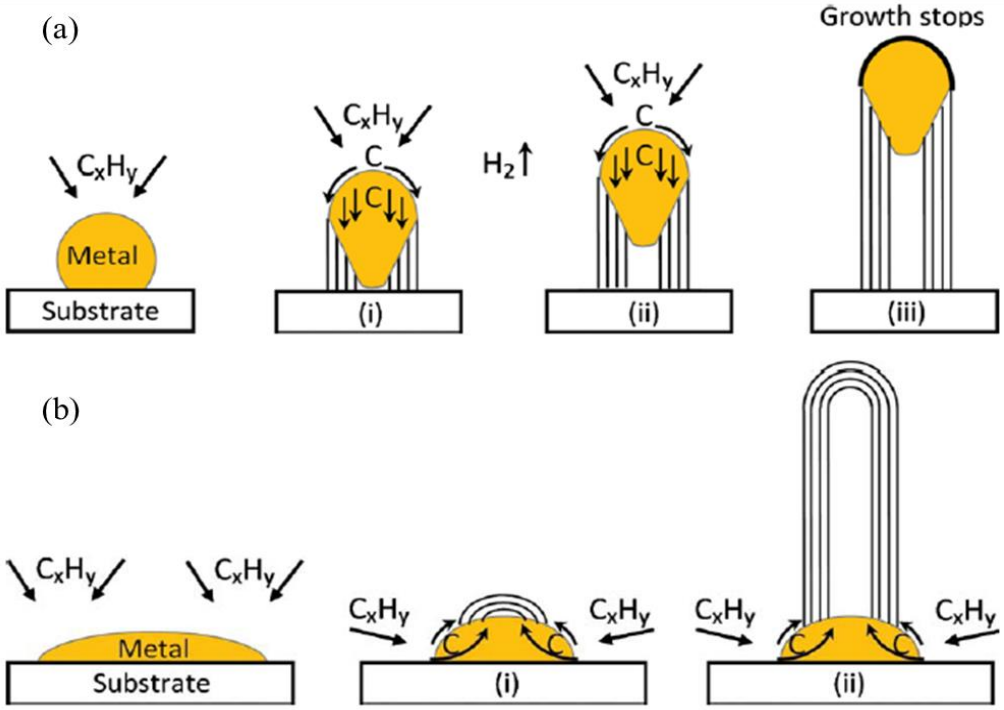

Figure 1.12: Growth mechanism of CNTs: (a) tip-growth model,

(b) base-growth model [49].

1.5. Bio-immobilization methods on carbon nanotubes

There are three types of adsorption methods: physical adsorption (physisorption), chemical adsorption (chemisorption) and entrapment method (Figure 1.13).

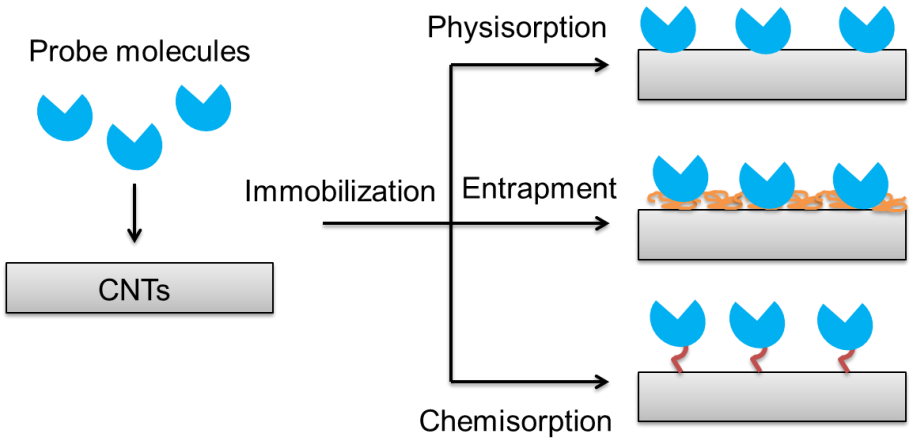

Figure 1.13: Three type of bioelement (probe molecule) immobilization.

Probe molecules can be immobilized onto sidewall of CNTs via covalent and nocovalent functionalization. In covalent method, probe molecules are immobilized directly onto defect of CNTs via covalent bond. In noncovalent method, probe molecules require a linker that mediates between them and CNTs.

Figure 1.14 shows the covalent functionalization of CNT's sidewall. Firstly, carboxyl groups are formed on the defect of CNT's sidewall by treating CNTs with strong acid like H_2SO_4 and HNO_3 [51]. These carboxyl groups are treated with N-hydroxysuccinimide (NHS) and 1-Ethyl-3-(3-dimethylaminopropyl)carbodiimide (EDC) to make the semi-stable NHS ester. Then the biorecptors that contain the amide group are immobilized via amide bond and release NHS groups.

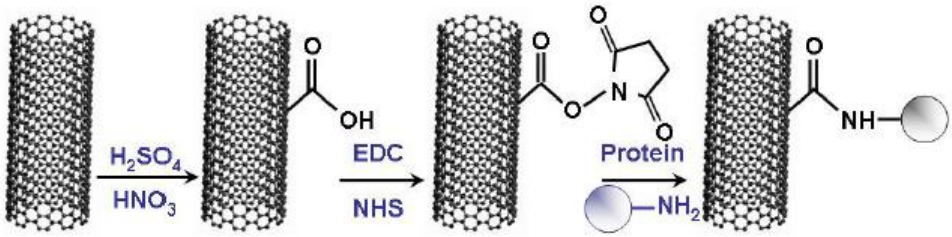

Figure 1.14: Covalent functionalization of CNT's sidewall [52]

Figure 1.15 shows noncovalent pi-stacking functionalization of SWCNT. The 1-pyrenebutanoic acid succinimidyl ester (PBASE) is used as the linker to immobilized bioreceptor onto surface of SWCNT [5, 6, 53]. PBASE consist of aromatic rings in one tail and NHS group in another tail. The aromatic rings make π- π interaction with surface of SWCNT while NHS group makes amide bond with bioreceptor.

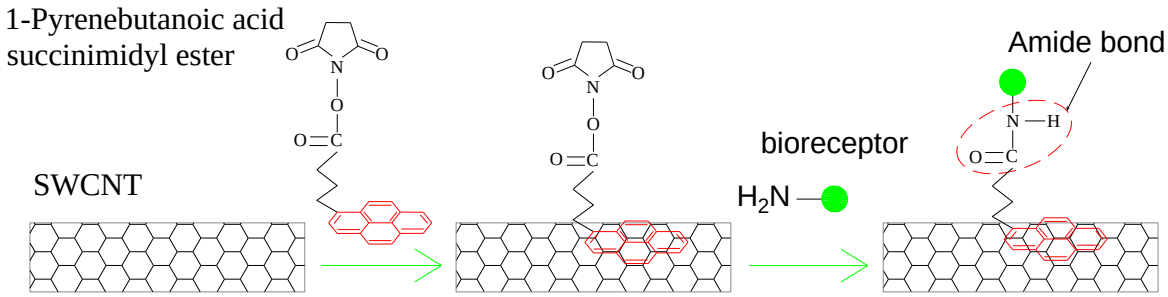

Figure 1.15: π- π stacking functionalization of SWCNT.

In addition, bimolecular receptors can be immobilized onto SWCNTs via polymeric layer functionalized with a molecular receptor, biotin that recognizes biomolecule, streptavidin [54] (Figure 1.16).

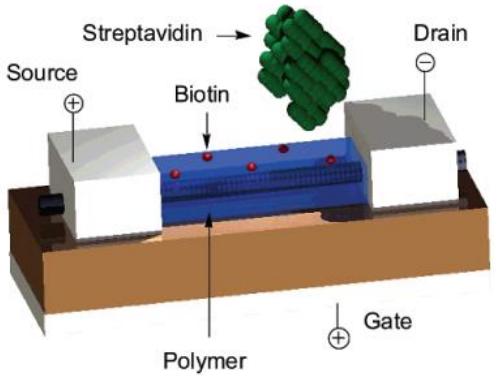

Figure 1.16: Modification of CNTs by polymeric layer containing biotin [54].

On the other hand, protein can directly bind to sensitive region of SWCNT-FET via electrostatic attraction. The substrate of SWCNT-FET is charged. Then protein with opposite charge comes and binds to the substrate [55] (Figure 1.17).

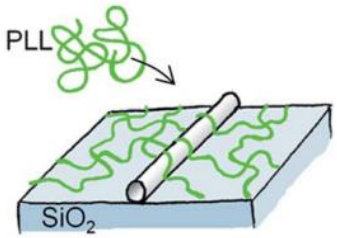

Figure 1.17: Schematic of poly-L-lysine (PLL) binding to SiO_2 and a CNT [55].

1.6. Introduction to peptide aptamer

The aptamers have been discovered and developed as a substitutable probe molecule of antibody. Aptamer was known as a short single stranded folded oligonucleotides and peptide that bind to molecular targets with high affinity and specificity. Table 1.5 shows the comparison between aptamer and antibody.

Table 1.5: Comparison between aptamer and antibody.

Aptamer	**Antibody**
Single stranded DNA or RNA oligonucleotide or peptides	Monoclonal or polyclonal
Product of *in vitro* chemical protocols, therefore can target any protein	Product of *in vivo* biological protocols, requires a biological system
Uniform activity regardless of batch	Varies from batch to batch
Stable at high temperature and can be extended storage time	Temperature sensitive and limited storage time
Investigator determines target site of protein, wide variety of chemical modifications to molecule for diverse functions	Immune system determines target site of protein, limited modifications of molecule
Low immunogenicity	High immunogenicity
Quicker and cheaper	Expensive

Recently, peptide aptamers have been developed since 1996 by Pierre Colas et al. [56]. Peptide aptamers are small artificial recognition proteins that consist a variable peptide sequence with affinity for a given target protein. This variable peptide sequence is inserted into the context of a small and very stable protein backbone, called "scaffold" [57-62]. Peptide aptamers can be produced and selected *in vivo* from combinatorial libraries on the basis of their affinity to the target protein and expressed in bacterial cells such as E. coli. Both termini of the variable peptide sequence are embedded ("double constrained") within an inert and constant scaffold protein. This double constraint distinguishes peptide aptamer from other classes of constrained combinatorial proteins (such as antibodies, antibody fragments and other non-antibody scaffold-based molecules) which consist of random peptide sequences embedded to a carrier protein [63] (Figure 1.18). These recognition molecules are more complex than peptide aptamers because target-binding surfaces consist of non-contiguous peptidic sequences disseminated on several secondary structural elements or across several variable loops. Moreover, these molecules require disulfide bonds to fold properly and are thus ill suited to target intracellular proteins [57].

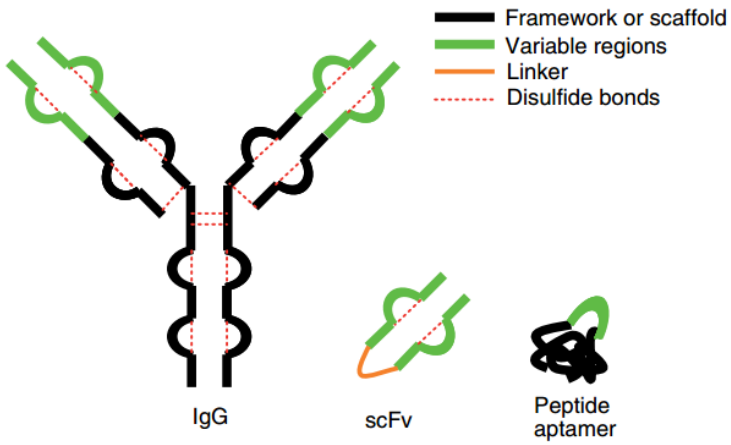

Figure 1.18: Comparison between different constrained combinatorial recognition proteins. IgG, immunoglobulin G; scFv, single-chain Fv antibody fragment [59].

Peptide aptamers show the molecular recognition properties similar to antibodies, but with overwhelming characteristics including their small size, simple design, high stability, high solubility, high yield bacterial expression and their disulphide-independent folding. The comparison of peptide aptamer versus antibody and DNA aptamer is briefly shown in Table 1.6.

Table 1.6: Comparison of antibody, DNA aptamer and peptide aptamer

(O and X indicate better and worse, respectively)

	Specificity	Stability	Cost	Diverse target	Size
Antibody	O	X	X	X	10 – 12 nm
DNA aptamer	X	O	O	X	1 – 2 nm
Peptide aptamer	O	O	O	O	< 2 nm

In comparison with DNA aptamers, peptide aptamers are relatively shorter in size with smaller binding footprint that allows more thorough and precise capture of target. Therefore, with the same surface area, peptide aptamers provide higher binding-site density and lower background signal that arises from the nonspecific binding of target analyte [64]. Additionally, DNA aptamer is created from the combination of 4 types of nucleotides (Adenine (A), Thymine (T), Guanine (G) and Cytosine (C)) while peptide aptamer was synthesized from the combination of 20 amino acids. Therefore, peptide aptamer is potential for approaching wide and diversity targets of biomarker.

1.7. Introduction to Glutamate-binding protein

Glutamate-binding protein (GBP) is glutamate/aspartate import solute-binding protein that specifically recognizes Glu (Glu) – a main excitatory neurotransmitter in the central nervous system. GBP is a kind of amino acid-binding protein which consists of two globular domains linked by hinges, and its ligand-binding site is located in the cleft

between the two domains. GBP was firstly discovered and purified from *E. coli* K12 [65, 66]. The biochemical and genetic properties of GBP has been well characterized [65-69]. The crystal structure of a periplasmic glutamate/aspartate binding protein molecule has been determined as an ellipsoid size of approximately 55 × 45 × 40 Å [70]. GBP binds to Glu through hydrogen bonds between side-chain and main-chain groups of GBP and the Glu as shown in Figure 1.19.

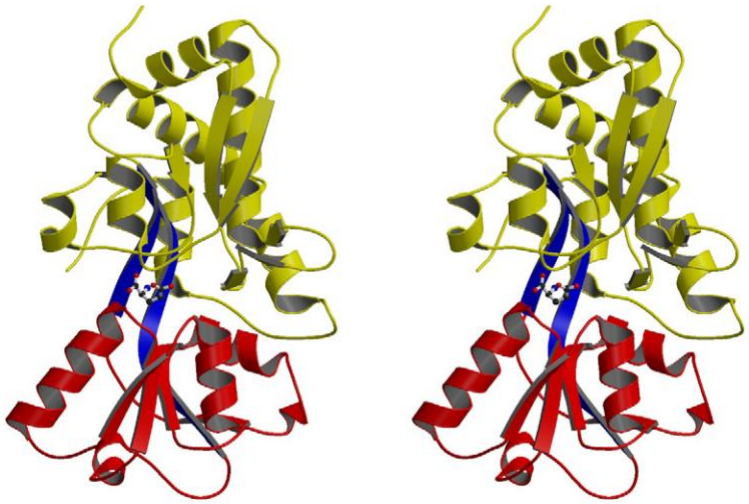

Figure 1.19: Structure of GBP. Domains I and II are colored yellow and red, respectively. The two β-strands that connect domains I and II are colored blue. The bound glutamate molecule is shown as ball-and-stick model [70].

Comparisons with several other periplasmic amino acid binding proteins indicate that GBP residues involved in the binding of α-amino and α-carboxylate groups of the ligand (Glu) and the pattern of hydrogen bond formation between these groups are very well conserved, but the binding pocket around the ligand side chain is not, leading to the specificity of GBP [70].

Recently, Loren Looger's lab developed the new GBP (iGluSnFr) by wedging green fluorescent protein (GFP) to periplasmic glutamate binding protein. When the resulting fusion protein binds to Glu, GBP's conformational change leads to an increase in

fluorescence intensity from the inserted GFP [71, 72]. The result of characterizing iGluSnFr *in vitro* shows that it is selectively activated by Glu and exhibits rapid recognition to transient Glu in around 5 ms. This process of Glu transmission, which is in millisecond range, is related to the ability of learning and memory. Therefore, GBP plays a promising probe molecule to develop biosensor that can monitor Glu released from neurons and other brain cells *in vivo* for studying Glu signalling and regulation.

1.8. Goal of study

In this study, we aimed to demonstrate the integration of small probe molecules (such as peptide aptamer and GBP) into SWCNT-based FET. Firstly, we proposed the first demonstration of the integration of a novel peptide aptamer with the CVD-type SWCNT-FET to achieve highly sensitive and specific detection of biomarker in order to early diagnose cancer disease in clinical application. Secondly, we proposed the first demonstration of the integration of GBP and the network SWCNT-FET for real-time monitoring of transient Glu, which contributes on neuroscience study.

1.9. Overview of dissertation

Chapter 2 discusses the fabrication and characterization of CVD-type SWCNT-FET and network SWCNT-FET. The details of microfabrication such as photolithography and CNTs growth by CVD method are described. The operation and stability of the both fabricated CVD-type SWCNT-FET and network SWCNT-FET were investigated and evaluated for biosensing application.

Chapter 3 details the first demonstration of the successful integration of a novel peptide aptamer with a liquid-gated CVD-tyep SWCNT FET to achieve highly sensitive and specific detection of CatE, a useful prognostic biomarker for cancer diagnosis. Novel peptide aptamers that are engineered by systemic in vitro evolution to specifically

recognize CatE are small probe molecule. The SWCNTs were firstly grown using the thermal CVD method and then were employed as a channel to fabricate a CVD-type SWCNT-FET device. Next, the SWCNTs were functionalized by noncovalent immobilization of the peptide aptamer using PBASE linker. The resulting peptide aptamer-modified CVD-tyep SWCNT-FET sensors exhibited a high selectivity (no response to BSA and CatK) and label-free detection of CatE at unprecedentedly low concentrations in both phosphate-buffered saline (0.1 ng/mL) and human serum (10 ng/mL). Our results highlight the use of peptide aptamer-modified CVD-type SWCNT-FET sensors as a promising platform for near-patient testing and point-of-care testing applications.

Chapter 4 presents the first successful demonstration of the novel FET biosensor for Glu monitoring by integrating GBP probe molecule into network SWCNT-FET transducer. A PBASE linker is used to immobilize GBP probe molecule onto the network SWCNT channel of network SWCNT-FET device. The GBP-modified network SWCNT-FET could monitor Glu at micromolar range in real-time with high selectivity (no response to Dopamine). This scheme could be promising candidate for Glu signalling to study neuroscience.

Chapter 2: Investigation of single-walled carbon nanotube field-effect transistors

2.1. Introduction

With aforementioned reasons, we need high performance CVD-type SWCNT-FET for the integration with peptide aptamer to develop high-performance sensor. And we need network SWCNT-FET with high reproducibility and fast response for the integration with GBP to develop Glu-monitoring sensor. Therefore, in this chapter, we fabricated and characterized the CVD-type SWCNT-FET and network SWCNT-FET. The CNTs were synthesized using CVD method. Cobalt (Co) and ethanol were used as the catalyst and carbon source for CNTs growth. The pressure, temperature and growth time are key factors for growing CNTs. We investigated the conditions for SWCNT growth by varying the temperature from 650 to 850 °C, and pressure from 220 to 1200 Pa while keeping constant growth time of 30 min. The optimal condition of 300 Pa, 850 °C and 30 min was chosen for SWCNT growth. The photolithography micro-fabrication was used for the fabrication of source and drain electrodes to complete CVD-type SWCNT-FET. A solution-process and photolithography techniques were used for the fabrication of random network SWCNT-FET. This technique is easy and fast, allowing a direct control of network density of channel and thus the transistor characteristics. At first, the SiO_2 surface of substrate was modified with (3-Aminopropyl)triethosysilane (APTES). A volume of commercial SWCNT was dropped on APTES-modified substrate and incubated to form the network SWCNT channel. The density of network SWCNT was investigated according to the incubation time of SWCNT solution from 20 min to 1h. The stabilities of operation of fabricated CVD-type SWCNT-FET and network SWCNT-FET were investigated.

2.2. Materials and apparatus

All chemicals and materials used in these experiments are listed in Table 2.1 below:

Table 2.1: List of chemicals and materials including their suppliers

Chemicals/materials and reagents	Suppliers
Sulphuric acid H_2SO_4	Sigma-Aldrich
Hydrogen peroxide H_2O_2	Wako Pure Chemical Industries, Ltd.
OAP photoresist	Tokyo Ohka Kogyo Co., Ltd., Japan
OFPR-800 photoresist	Tokyo Ohka Kogyo Co., Ltd., Japan
LOR-10B photoresist	MicroChem Corporation
Ethanol (super dehydrated, 95%)	Wako Pure Chemical Industries, Ltd.
(3-Aminopropyl)triethosysilane (APTES)	AVOCADO Research Chemicals Ltd., LANCS
SWCNT solution	Meijo Nano Carbon Co., Ltd.

A 10× PBS stock solution was prepared by adding 80 g NaCl, 2 g KCl, 14.4 g Na_2HPO_4 and 2.4 g KH_2PO_4 into 1 L milli-Q water. The pH of PBS was adjust by adding NaOH or HCl.

All the apparatuses are listed in Table 2.2 below:

Table 2.2: List of apparatuses and their suppiers

Apparatus	Suppliers
Sonicator	AS ONE, Japan
Spin coater	Mikasa, Japan
SiO_2 100 nm/ p^+-Si	KST World Corp., Japan
pH meter	Horiba, Japan
Mili Q system	Barnstead Milli Q-purification system
Autopipette	Eppendrof, Germany
Vortex	IKA, Japan
E-beam evaporator MUE-ECO-EB	ULVAC, Japan
Scanning electron microscope (SEM) model S-4500	Hitachi, Japan
Reference electrode Ag/AgCl	Bioanalytical Systems, West LaFayette, IN
Agilent 4156C Precision Semiconductor Parameter Analyzer	Measure Jig Co., Ltd., Japan

The SEM and Raman spectroscopy methods were used to characterize the as-grown SWCNTs. The AFM method was used to visualize the capture of CatE by the peptide aptamer, which was immobilized onto the SWCNTs. The Agilent 4156C Precision Semiconductor Parameter Analyzer was utilized for measuring the electrical performance

of the pristine SWCNT FET and the electrical signals of peptide aptamer-modified SWCNT FET induced from binding events.

2.3. Experimental

2.3.1. Single-walled carbon nanotube synthesis using chemical vapour deposition

In this work, CVD method was used to synthesize SWCNT. The schematic structure of CVD system is shown in Figure 2.1. In this system, ethanol was used as the carbon source to synthesize SWCNT. Temperature was controlled by a temperature controller. Argon gas, which was managed by a mass-flow controller, was used to keep the pressure inside the chamber stably before and after supplying ethanol. A rotary pump was used to make vacuum inside the chamber. Chamber's pressure value was displayed by a manometer.

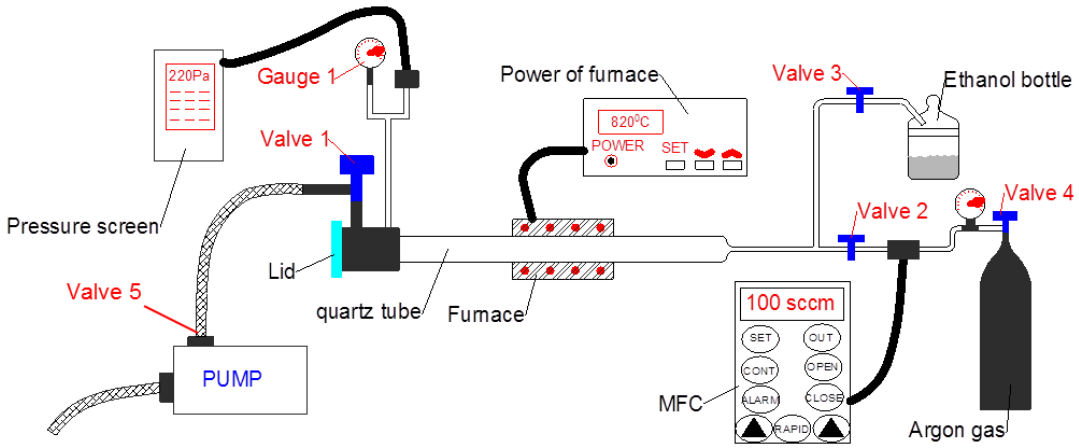

Figure 2.1: Schematic structure of the CVD system for SWCNT synthesis.

Figure 2.2 shows the procedure of SWCNT synthesis by using CVD method. Firstly, a commercial SiO_2 (100nm)/p^+-Si substrate was cleaned with piranha solution (a mixture of H_2SO_4 and H_2O_2 with ratio of 4:1 v/v). Then, two 5-nm-thick cobalt patterns were formed as the catalyst onto the substrate by using conventional photolithography and lift-off technology. The substrates were spin-coated with an OAP layer at 3000 rpm for 45

seconds followed by baking on a hot plate at 150 °C for 90 seconds. This OAP layer was used as a primer in order to improve adhesion between the substrate and photoresist. Next, OFPR-800 positive photoresist was spin-coated at 4000 rpm for 40 seconds, and then baked on a hot plate at 90 °C for 90 seconds. The samples were then exposed to UV light in a Double-View Mask Aligner PEM-800 for 3 seconds. The samples were developed in NMD3 for 60 seconds followed by rinsing with pure water. Next, cobalt thin film was deposited using an E-beam evaporator with deposition rate of 0.01 nm/s. The samples were then immersed in remover 106 for 15 minutes with sonication followed by rinsing with ethanol, 2-propanol and pure water to remove photoresist and residual organics. The substrate with Co catalyst patterns was introduced into the CVD system for SWCNT growth. Firstly, the quartz tube chamber was evacuated to around 10 Pa to pull out residual oxygen gas in the upper part of ethanol bottle at 800 °C. Then the furnace was cooled down in order to put the sample into chamber. The chamber was then evacuated while increasing temperature. After reaching a desired temperature, Ar gas (100 sccm) was introduced by mass flow controller for 10 minutes in order to get thermal equilibrium state of the whole system. Then ethanol was introduced into the chamber so that the pressure was kept fixed. After growing CNTs, the chamber was cooled down to room temperature naturally take out the sample.

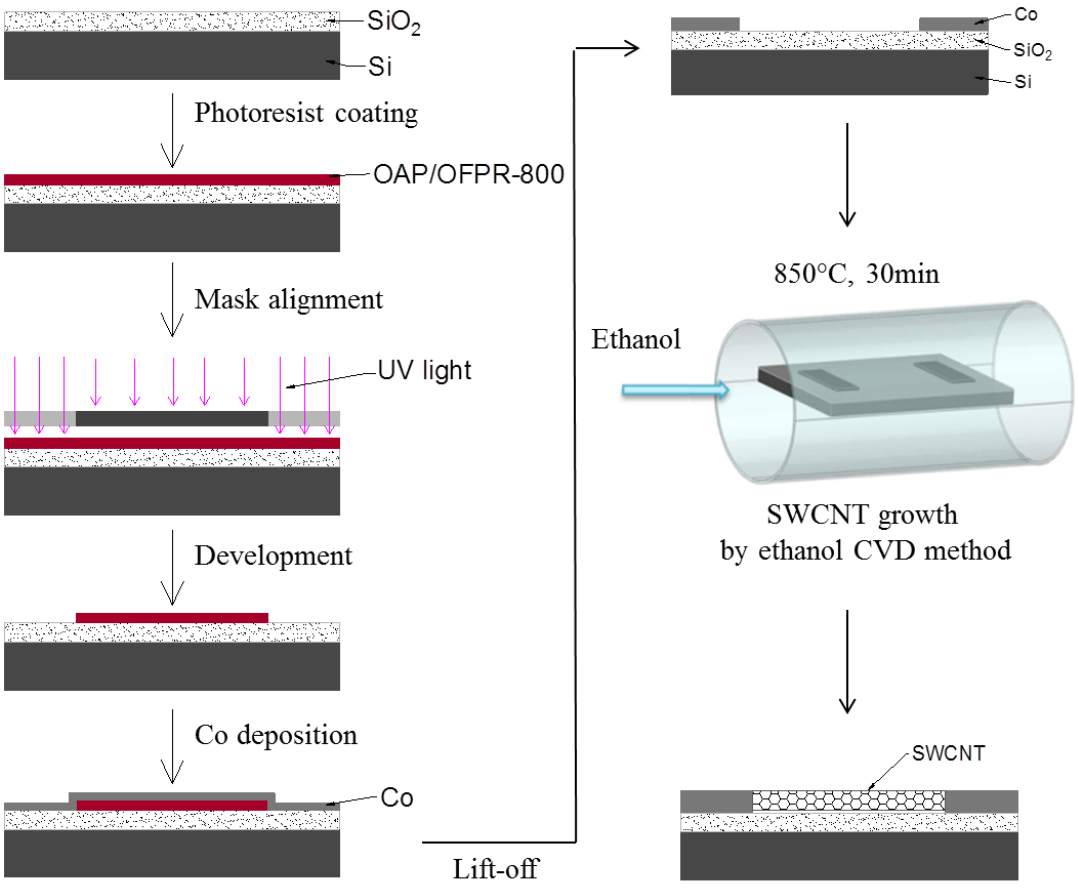

Figure 2.2: The procedure of SWCNT synthesis.

In this work, two important parameters of the CVD process including growth temperature and pressure were investigated for optimizing SWCNT growth. In case of temperature dependence, CNTs growth was implemented at pressure of 1200 Pa for 30 minutes with variant temperatures. In case of pressure dependence, SWCNT growth was carried out at 850 °C for 30 minutes with variant pressures. The as-grown SWCNTs were confirmed by Raman spectroscopy. The morphology of as-grown SWCNTs was observed via SEM and AFM.

2.3.2. Fabrication of single-walled carbon nanotube field-effect transistor

After growing SWCNT, an array of Ti/Au (2 nm/45 nm) source and drain electrode pads were formed by using photolithography and lift-off technology (Figure 2.3). The distance between source and drain electrode was approximately 3 µm. The sample was

spin-coated with LOR 10B at 3000 rpm for 45 seconds, then baked on a hot plate at 150 °C for 3 minutes. This LOR 10B under layer was used to aid for the next metal lift-off process. OFPR-800 resist was then spin-coated at 4000 rpm for 40 seconds then baked on a hot plate at 90 °C for 90 seconds. Next, the samples were exposed to UV light in a contact aligner for 5 seconds. The samples were developed in NMD3 for 18 seconds followed by rinsing with pure water. Next, Ti (2 nm) and Au (45 nm) thin films were deposited by using e-beam evaporation with deposition rate of 0.01 nm/s and 0.03 nm/s, respectively. The samples were then immersed in remover 106 for 30 minutes at 70 °C in a hot plate followed by rinsing with ethanol, 2-propanol and pure water to remove photoresist and excess metal.

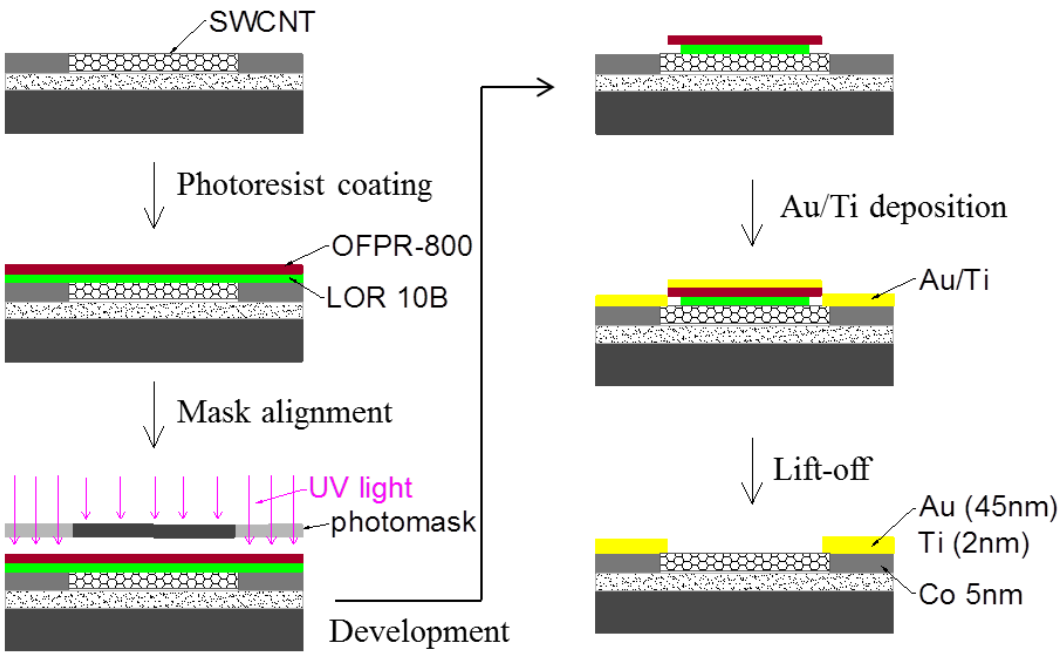

Figure 2.3: Deposition of Ti/Au electrodes to make CVD-type SWCNT-FET.

2.3.3. Fabrication of network single-walled carbon nanotube field-effect transistor

We fabricated an array of network SWCNT-FETs onto a heavily doped p^+-Si substrate capped with a 100 nm-thick thermally grown SiO_2 layer. The p^+-Si substrate was used as a back-gate electrode. First, a commercial SiO_2(100nm)/p^+-Si substrate was

cleaned with piranha solution (a mixture of H_2SO_4 and H_2O_2 with ratio of 4:1 v/v) at 100 °C for 10 min to modify SiO_2 surface with hydroxyl group, followed by rinsing with milliQ water and drying with nitrogenous gas. An array of Ti/Au (2 nm/45 nm) source and drain electrode pads were formed by using photolithography and lift-off technique (Figure 2.4). The distance between source and drain electrodes was vary from 3 to 10 µm. The sample was spin-coated with LOR 10B at 3000 rpm for 45 seconds, then baked on a hot plate at 150 °C for 3 minutes. This LOR 10B under layer was used to aid for the next metal lift-off process. OFPR-800 resist was then spin-coated at 4000 rpm for 40 seconds then baked on a hot plate at 90 °C for 90 seconds. Next, the samples were exposed to UV light in a contact aligner for 5 seconds. The samples were developed in NMD3 for 18 seconds followed by rinsing with pure water. Next, Ti (2 nm) and Au (45 nm) thin films were deposited by using e-beam evaporation with deposition rate of 0.01 nm/s and 0.03 nm/s, respectively. The samples were then immersed in remover 106 for 30 minutes at 70 °C in a hot plate followed by rinsing with ethanol, 2-propanol and pure water to remove photoresist and excess metal.

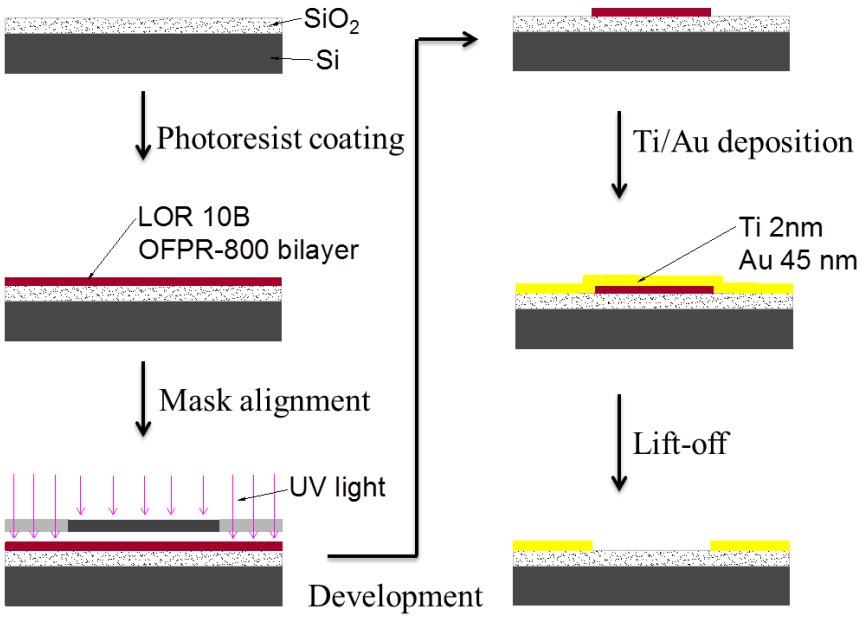

Figure 2.4: Deposition of Ti/Au to make an array of source and drain electrode pads.

After making source and drain electrode pads, the network SWCNT was deposited onto the device as depicted in Figure 2.5. The SiO_2 surface was modified with amine terminated groups of APTES self-assembled monolayer (SAM) by dropping a fresh solution of 5% APTES, 5% water and 90% pure ethanol for 2h at room temperature, followed by rinsing thoroughly with milli-Q water. Then the commercial SWCNT solution was dropped onto the APTES-modified substrate and incubated at room temperature for variant time (from 10 min to 1h) to form a network SWCNT, the specimen was rinsed with milli-Q water and dried with nitrogen gas. The device was baked at 200 °C for 30 min to remove the surfactant and to form good contacts between SWCNTs and electrodes.

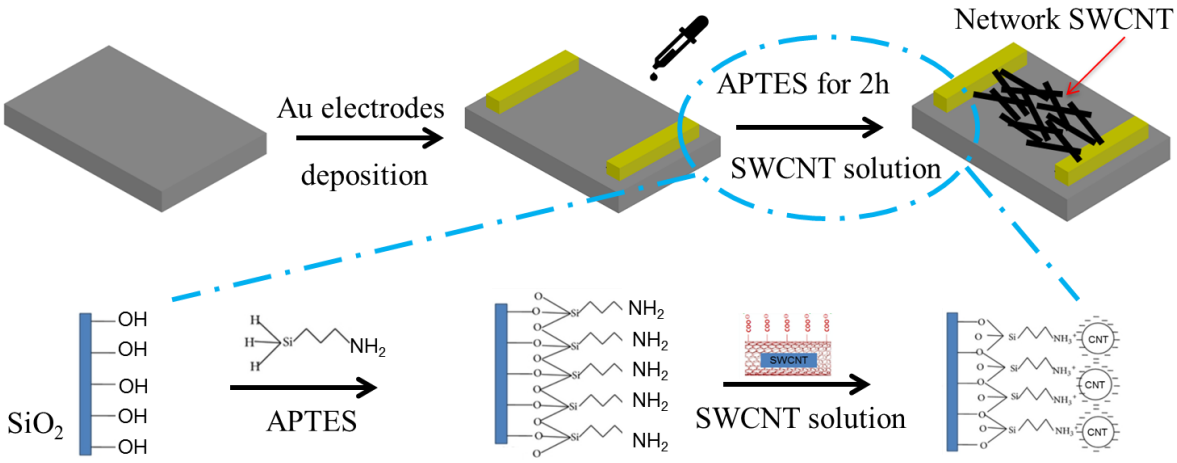

Figure 2.5: Fabrication of network SWCNT-FET.

2.3.4. Characterization of CVD-type SWCNT-FET and network SWCNT-FET

In the FET, CVD-type SWCNTs and network SWCNTs function as a semiconducting channel. The both fabricated CVD-tyep SWCNT-FETs and network SWCNT-FETs were characterized with back-gated measurement setup by using Agilent 4156C Precision Semiconductor Parameter Analyzer as shown in Figure 2.6. The source electrode was grounded. In transfer characteristic ($I_D - V_G$) measurement, drain current was measured at a constant drain voltage and variant back-gated voltages. In output

characteristic (I_D – V_D) measurement, drain current was measured with a constant back-gated voltage and variant drain voltages.

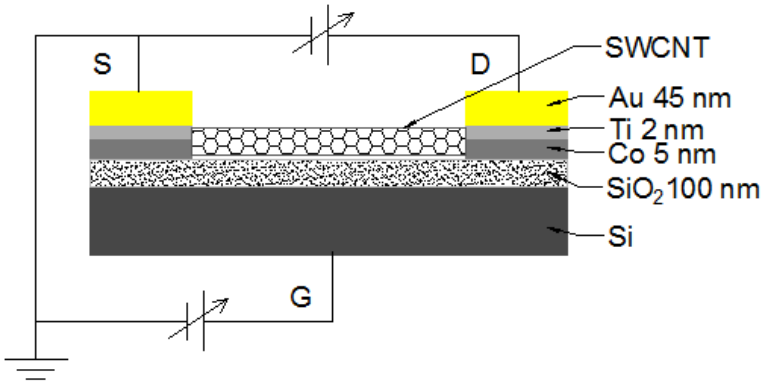

Figure 2.6: Back-gated schematic circuit for measuring the electrical characteristics of both fabricated CVD-type SWCNT-FET and network SWCNT-FET.

The liquid-gated schematic circuit for measuring the electrical characteristics of fabricated CVD-type SWCNT-FETs and network SWCNT-FETs were carried out in order to compare the stable operation between back-gated and liquid-gated scheme (Figure 2.7). The source electrode was grounded. The drain current was measured at a constant drain voltage of 200 mV and variant liquid-gated voltages from 0 to -0.6 V.

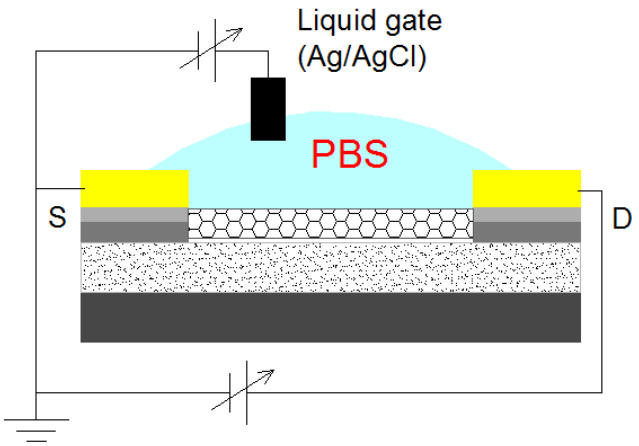

Figure 2.7: Liquid-gated schematic circuit for measuring the electrical characteristics of both fabricated CVD-type SWCNT-FET and network SWCNT-FET.

2.4. Results and discussion

2.4.1. Temperature and pressure dependence of SWCNT growth

The CNTs were grown between two cobalt patterns at a given pressure of 1200 Pa for 30 minutes. Figure 2.8 shows the SEM images of CNTs growth as a function of growth temperatures (650, 700, 750, 800, and 850 °C). The results indicated that SWCNTs started growing at 800 °C with increases in density and length.

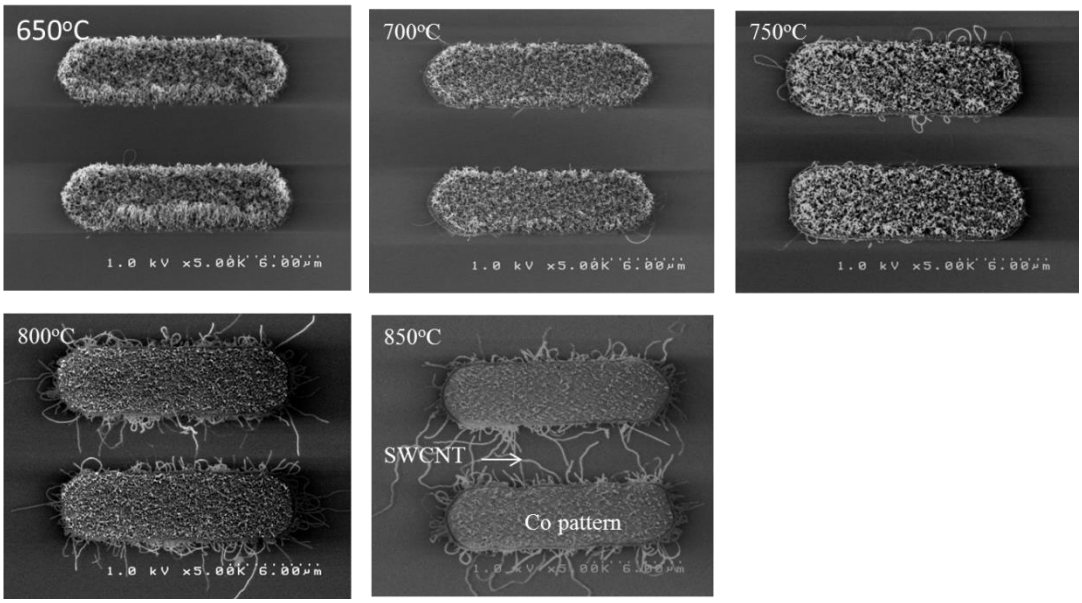

Figure 2.8: SEM image of temperature dependence of SWCNT growth.

In order to confirm the as-grown SWCNTs, the Raman spectrum of SWCNTs was taken. Figure 2.9 shows the Raman spectrum of SWCNT grown at 1200 Pa of ethanol, 850°C for 30 minutes. These results clearly indicated that SWCNTs were successfully synthesized by CVD method. The characteristic radial breathing mode (RBM) of SWCNT was observed at 170 cm^{-1} corresponding to as-grown SWCNT's diameter of around 1.4 nm [73].

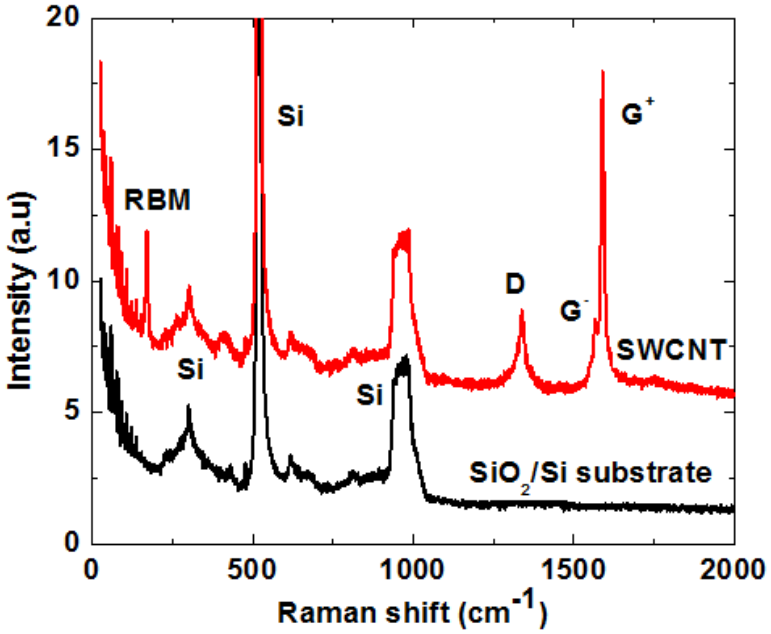

Figure 2.9: Raman spectra of SWCNT that was synthesized at 1200 Pa of ethanol, 850°C for 30 minutes. Characteristic radial breathing mode (RBM) observed indicated SWCNT.

At lower temperatures (650°C, 700°C, 750°C), introduced ethanol might not be pyrolyzed properly, leading to the formation of multi-walled carbon nanotubes (MWCNTs). This result was confirmed by Raman spectrum as shown in Figure 2.10 with the G band at 1591 cm^{-1} assigned to the in-plane vibration of C-C bond and D band at 1342 cm^{-1} activated by the presence of disorder in carbon systems [74].

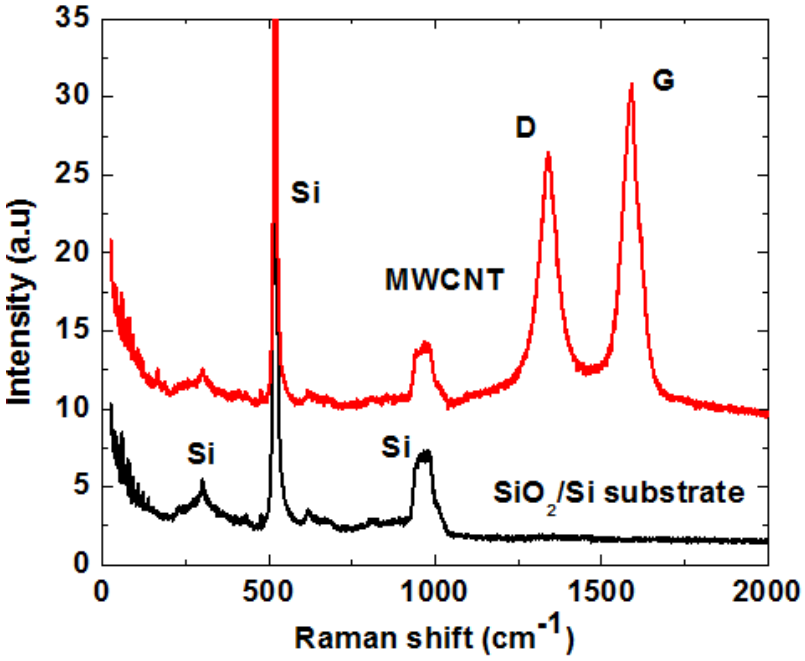

Figure 2.10: Raman spectra of single-walled nanohorn (SWNH) or damaged grapheme in case of CNTs synthesized at 1200 Pa of ethanol, 650°C for 30 minutes.

SWCNTs grown at 850°C appeared long enough to bridge between two cobalt patterns. Further, the SWCNT grown at 850°C also exhibited highest density compared to the other conditions. This fact could enable successful fabrication of CVD-type SWCNT-FET in which the grown SWCNT played a role as the transistor's semiconducting channel. Based on this investigation, 850°C was selected as the temperature for CNT growth.

Figure 2.11 shows the SEM images of SWCNTs as a function of pressure (220, 410, 610, 800, and 1200 Pa) at 850°C for 30 min. SWCNTs were sparse at 220 Pa and denser at higher pressures (610 Pa, 800 Pa, and 1200 Pa). The flow rate of ethanol introduction is proportional with chamber pressure. At 220 Pa, a less amount of ethanol source was supplied, leading to sparse SWCNTs growth. At higher pressure, a larger amount of ethanol source was introduced, resulting in denser SWCNTs growth. These results indicated that SWCNTs could be able to synthesize in wide range of pressure (from 220 Pa to 1200 Pa) using CVD method.

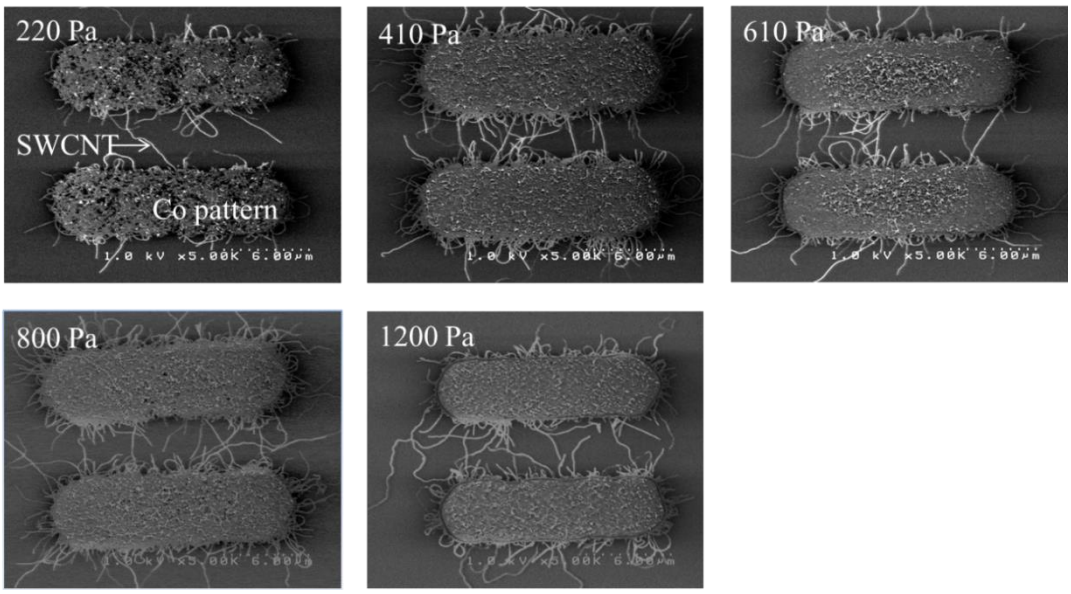

Figure 2.11: SEM image of the pressure dependence of SWCNT growth.

2.4.2. Characterization of fabricated CVD-type SWCNT-FETs

Figure 2.12 shows the SEM image, taken at 1.0 keV acceleration voltage, of fabricated CVD-type SWCNT-FET focused on an area between source and drain electrodes. It is clearly seen that SWCNT was successfully bridged between these source and drain electrodes.

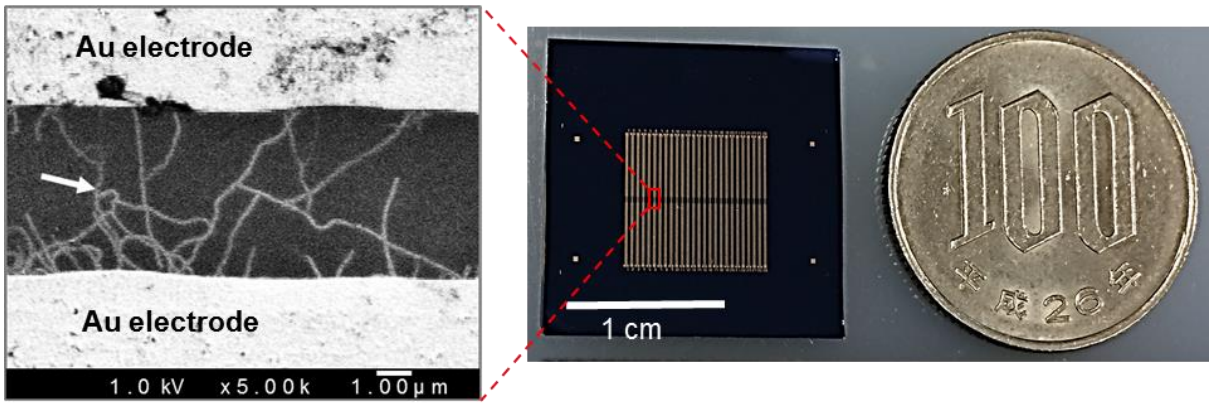

Figure 2.12: SEM image of fabricated CVD-type SWCNT-FET (white arrow indicates the SWCNT) and real photo of a fabricated chip, which contains an array of 52 SWCNT-FETs.

Figure 2.13 shows the transfer characteristics of 10 different CVD-type SWCNT-FETs devices. The back-gate in air was scanned from -5 to 5 V while drain voltage was kept constant of 0.5 V. The transfer curves vary from device to device. This variation may be due to the uncontrollable SWCNT growth during the CVD processes.

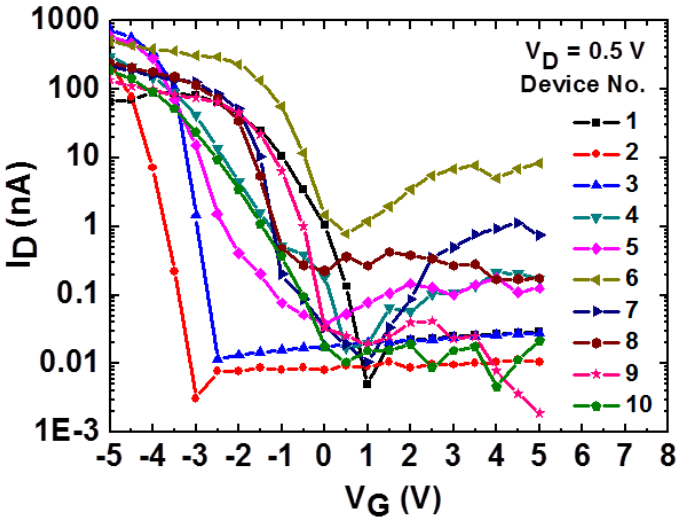

Figure 2.13: Transfer characteristics of 10 fabricated CVD-type SWCNT-FET devices

Figure 2.14 shows the transfer characteristics of the fabricated CVD-type SWCNT-FET were measured using back-gated and top liquid-gated schemes. The back-gate bias in air was swept from -3.0 to 1.5 V. The liquid-gated bias was scanned from 0 to -0.6 V. Such a small liquid-gated voltage was used to prevent undesirable electrochemical reactions between the source/drain metal electrodes and the liquid [75]. In both measurements, the drain currents decreased with increasing gate voltage, indicating that hole conduction was dominant in the fabricated SWCNT FET. A similar tendency of the drain current versus gate voltage was also observed in the output characteristics (Figure 2.15). The top liquid-gated device exhibited a smaller subthreshold swing factor (S) (85.7 mV/decade) compared with that of the back-gated device (337 mV/decade). This small S-factor of the liquid-gated CVD-type SWCNT-FET was due to a large capacitance induced by the formation of an ultrathin electrical double layer in the vicinity of the SWCNT channel [76].

Generally, in the case of FET-based biosensors, a smaller S-factor indicates greater sensitivity.

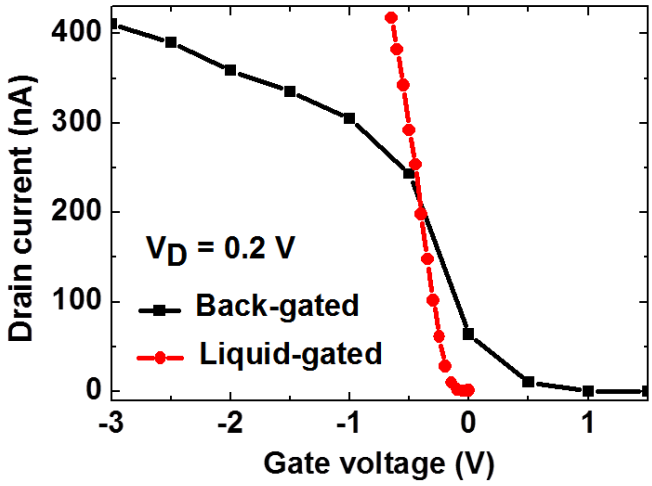

Figure 2.14: Transfer characteristics of fabricated CVD-type SWCNT-FET using back-gated (black) and liquid-gated (red) measurement.

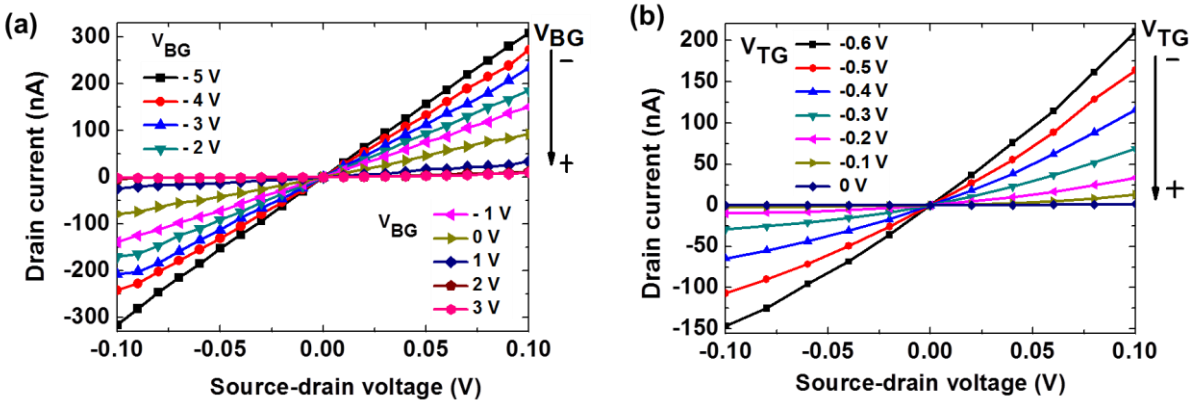

Figure 2.15: Output characteristics of fabricated CVD-type SWCNT-FET using (a) back-gated and (b) top-liquid-gated schemes. In both measurements, at source-drain voltage of 0.1 V, the drain currents decreased with increasing gate voltage.

Figure 2.16 shows the operation stability of CVD-type SWCNT-FET in air versus in liquid. The variation of transfer curves (ΔV) at drain current of 80 nA are 345 mV and 29 mV, corresponding to back-gated and top liquid-gated scheme, respectively. The result indicated that the fabricated CVD-type SWCNT-FET manifested stable operation in

liquid-gated scheme rather than in ambient air scheme. This stability stems from the SWCNT channel being covered by the liquid, thereby preventing the effects of the surrounding environment. In addition, the use of an Ag/AgCl reference electrode can minimize voltage fluctuations [77]. These stability properties are critically important for realizing reliable biosensing devices.

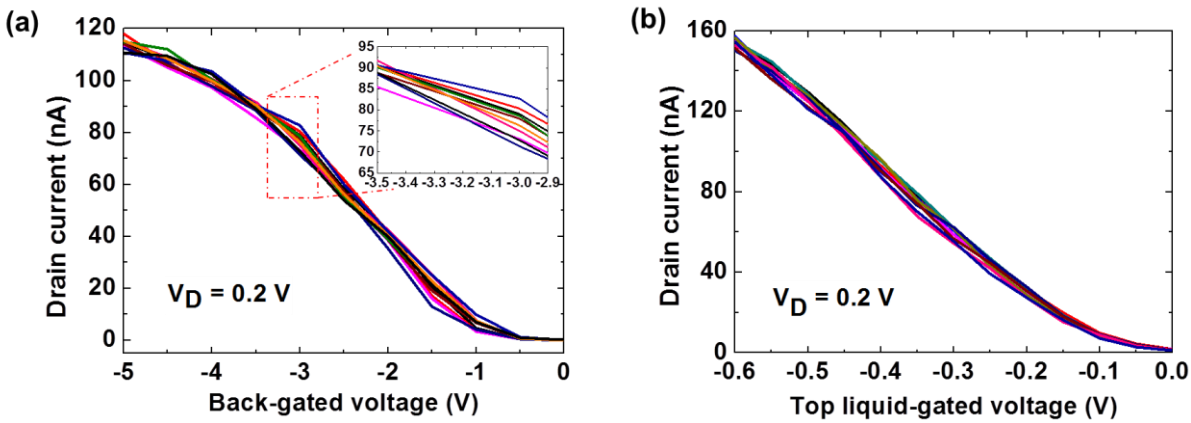

Figure 2.16: Operation stability of CVD-type SWCNT-FET in air versus in liquid: The transfer characteristics of fabricated CVD-type SWCNT-FET with 10 measurements, using (a) back-gated scheme and (b) top liquid-gated scheme.

2.4.3. Investigation of network SWCNT

The network SWCNT was evenly formed on the SiO_2/Si substrate via APTES (Figure 2.17 (b)) in contrast to the substrate without APTES treatment (Figure 2.17 (a)). The surface of substrate, which was modified with amine-terminated groups by APTES, is able to make the electrostatic attraction to the carboxyl groups of SWCNT. Therefore, the network SWCNT was deposited evenly on the APTES-modified Si/SiO_2 substrate. On the other hand, the surface of substrate without APTES treatment, which was decorated by hydroxyl groups by treating with piranha solution, is not able to be deposited by SWCNTs.

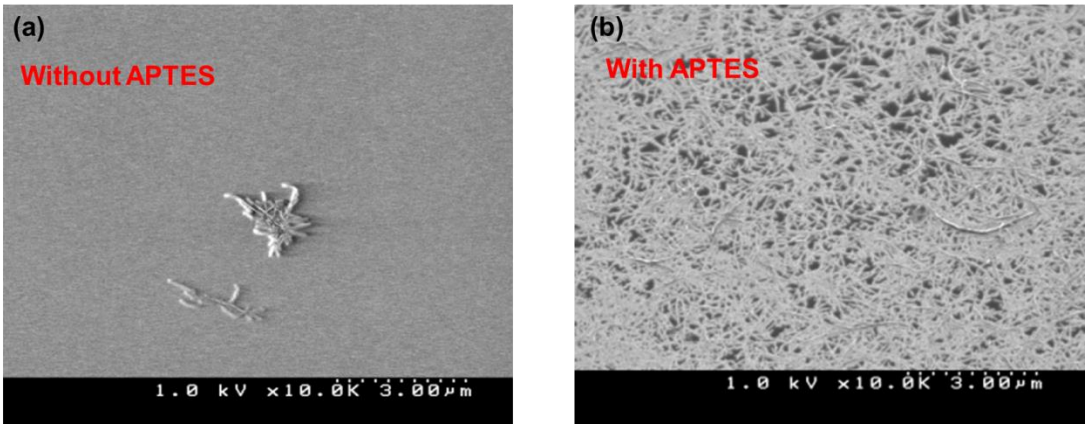

Figure 2.17: SEM images of network SWCNT on Si/SO_2 substrate (a) without and (b) with APTES treatment. SWCNT solution was incubated for 40 min.

Figure 2.18 shows incubation time dependence of network SWCNT density. The density of SWCNT is denser with longer incubation time. It is due to the accumulation of SWCNTs in the solution.

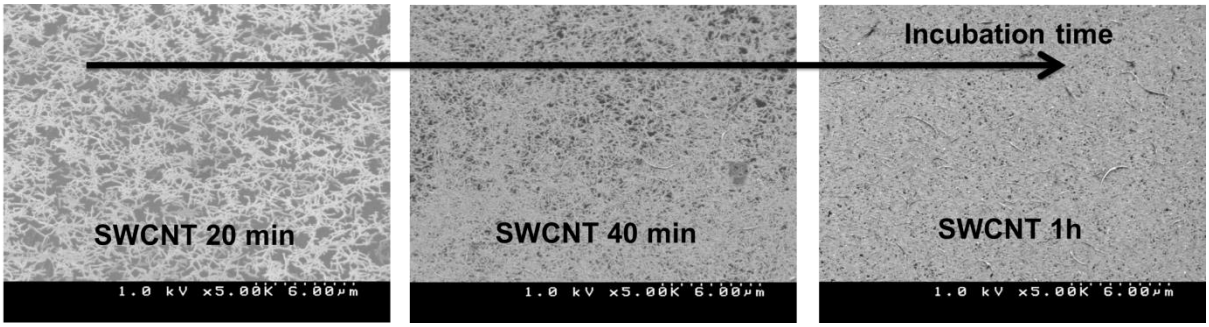

Figure 2.18: SEM images of network SWCNT on APTEST-modified Si/SiO_2 substrate with variant incubation time of SWCNT solution from 20 min to 1h.

2.4.4. Characterization of fabricated network SWCNT-FETs

Figure 2.19 shows the SEM image of a network SWCNT-FET device with the semiconducting network SWCNT channel connecting two Au source and drain electrodes.

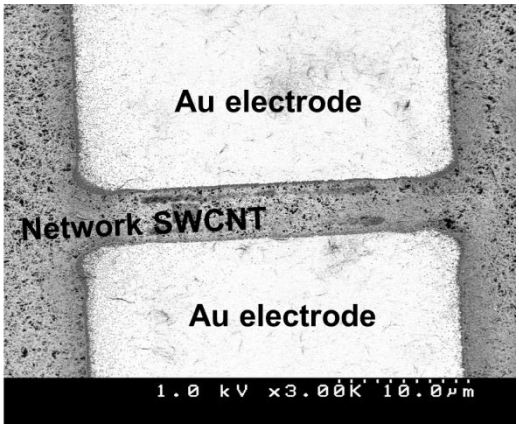

Figure 2.19: SEM image of a network SWCNT-FET with incubation time of SWCNT solution of 40 min.

The transfer characteristics of fabricated network SWCNT-FET with variant incubation time of SWCNT solution of 20, 40 and 60 min as shown in Figure 2.20. The back-gate in air was scanned from -10 to 10 V while drain voltage was kept constant of 0.2 V. The drain current decreases with increasing back-gated voltage. These results indicate that the fabricated network SWCNT-FET devices exhibit typical p-type characteristic. The both "on" and "off" currents of transfer curves increase with increasing incubation time of SWCNT solution from 20 to 60 min. This is due to the increase of carrier density inside network SWCNT channel which is originated from the denser network SWCNT formation at longer incubation time of SWCNT solution as aforementioned in Figure 2.18. The transfer curves of devices are unstable in case of sparse network SWCNT channel (Figure 2.20 (a)) and more stable in case of denser network SWCNT channel (Figure 2.20 (b, c)). This may because of the inhomogeneous or impure SWCNT solution. It is difficult to completely remove the contamination or filter the semiconducting SWCNT from mixture of metallic and semiconducting SWCNT solution. With the devices fabricated in case of the incubation time of SWCNT solution of above 1h, the "on/off" ratio becomes smaller (data is not shown). It is due to the high amount of metallic SWCNT existing in the network SWCNT channel. Additionally, in case of long incubation time of SWCNT

solution, the SWCNTs were accumulated and created thick film of network SWCNT. Therefore, higher back-gated voltage is required to deplete the hole carrier inside the network SWCNT channel. Based on these investigations, 40 min and 1 h are selected as the good condition for fabrication of network SWCNT-FET devices. Moreover, compared with the operation of the SWCNT-FET devices which were fabricated based on CVD method (as mentioned before in Figure 2.13), the operation of network SWCNT-FETs shows better stability from device to device. The stability of operation can be expected to be improved by using more homogeneous or pure SWCNT solution.

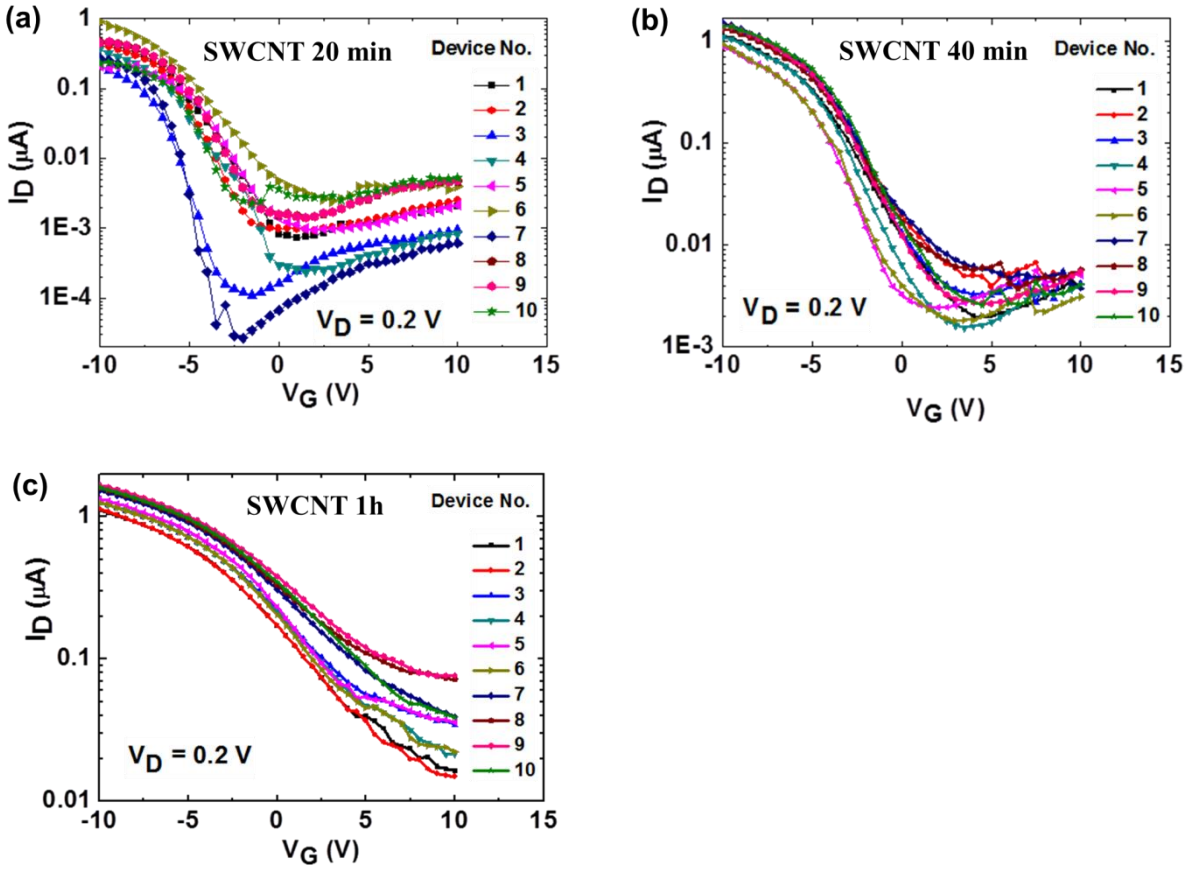

Figure 2.20: Transfer characteristics of network SWCNT-FETs with different incubation time of SWCNT solution: (a) 20 min, (b) 40 min and (c) 1h.

Figure 2.21 shows the transfer characteristics of the fabricated network SWCNT-FET were measured using back-gated and top liquid-gated schemes. The drain current was

kept constant at 0.2 V for both cases. The back-gate bias in air was swept from -5.0 to 1 V. The liquid-gated bias was scanned from 0 to -0.6 V. Such a small liquid-gated voltage was used to prevent undesirable electrochemical reactions between the source/drain metal electrodes and the liquid. In both measurements, the drain currents decreased with increasing gate voltage, indicating that hole conduction was dominant in the fabricated network SWCNT FET. The top liquid-gated device exhibited a smaller subthreshold swing factor (S) (110 mV/decade) compared with that of the back-gated device (1.821 V/decade). This small S-factor of the liquid-gated network SWCNT-FET was due to a large capacitance induced by the formation of an ultrathin electrical double layer in the vicinity of the SWCNT channel.

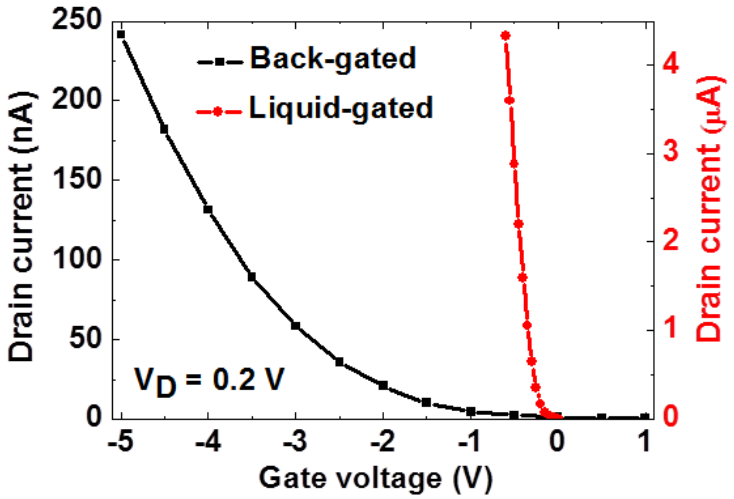

Figure 2.21: Transfer characteristics of fabricated network SWCNT-FET using back-gated (black) and liquid-gated (red) measurement.

Figure 2.22 shows the operation stability of fabricated network SWCNT-FET in air versus in liquid. The variation of transfer curves (ΔV) at drain current of 100 nA are 147 mV and 12.7 mV, corresponding to back-gated and top liquid-gated scheme, respectively. The result indicated that the fabricated SWCNT FET manifested stable operation in liquid-gated scheme rather than in ambient air scheme. This stability stems from the SWCNT

channel being covered by the liquid, thereby preventing the effects of the surrounding environment. In addition, the use of an Ag/AgCl reference electrode can minimize voltage fluctuations. These stability properties are critically important for realizing reliable biosensing devices.

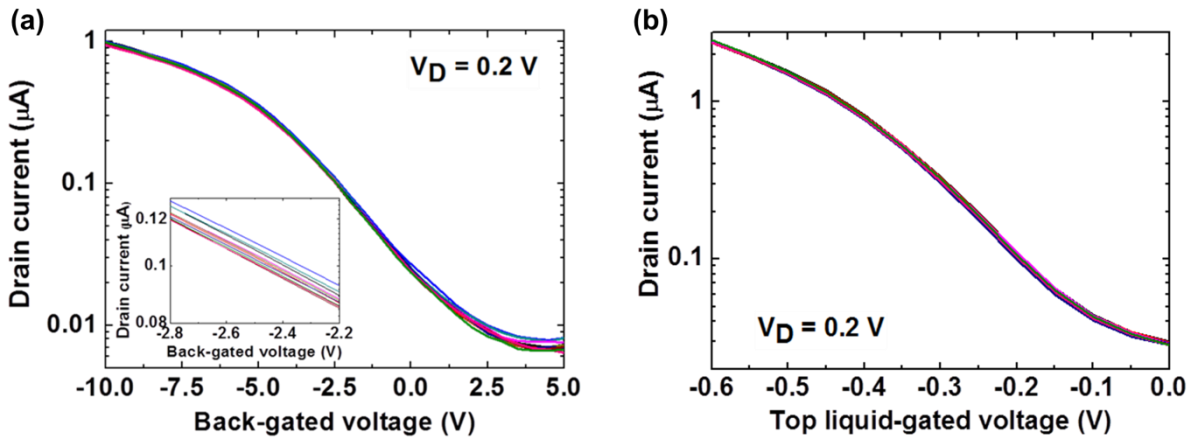

Figure 2.22: Operation stability of network SWCNT-FET in air versus in liquid: The transfer characteristics of fabricated network SWCNT-FET with 10 measurements, using (a) back-gated scheme and (b) top liquid-gated scheme.

2.5. Conclusion

In this chapter, we first synthesized and optimized SWCNT growth by using the CVD method. Using the optimized SWCNT, we proceeded to the fabrication of CVD-type SWCNT-FET device. To simplify the process on fabricating device, a solution-process and photolithography technique were used for the fabrication of random network SWCNT-FET. The operation and stability of the both fabricated CVD-type SWCNT-FET and network SWCNT-FET were investigated and evaluated for biosensing application. The main achievements are summarized below:

- The CVD conditions such as growth temperature and pressure were systematically investigated for SWCNT growth. We found that the density, length and purity of grown

CNTs were strongly dependent on the growth temperature, but not gas pressure. The optimal growth temperature was found to be 850 °C, whereas the growth pressure could be in a range of 220 – 1200 Pa. Such a high temperature is needed for sufficient pyrolysis of the supplied ethanol as carbon source. At the optimal growth condition, the diameter of SWCNT was approximately 1.4 nm which is consistent with standard SWCNT diameter. The length of as-grown SWCNTs was more than 5 μm which is long enough to bridge source and drain electrodes of CVD-type SWCNT-FETs.

- The CVD-type SWCNT-FETs were successfully fabricated and their operations were confirmed in both back- and top-gate schemes. The top liquid-gated device exhibited a smaller subthreshold swing factor (S) (85.7 mV/decade) compared with that of the back-gated device (337 mV/decade). Additionally, the fabricated CVD-type SWCNT-FET manifested more stable operation in liquid-gated scheme rather than in ambient air scheme. The performances of fabricated CVD-type SWCNT-FETs are applicable for biosensing.

- The network SWCNT was evenly formed on the SiO_2/Si substrate via APTES by simply dropping and washing commercial SWCNT solution. We found that the density as well as thickness of network SWCNT was remarkably dependent on the incubation time of SWCNT solution. The longer incubation time results in the denser network SWCNT.

- The network SWCNT-FETs were successfully fabricated and their operation were investigated. The network SWCNT-FETs showed reproducible transfer characteristics in case of incubation time of SWCNT solution of 40 and 60 min. The operation of network SWCNT-FETs manifested more stability than that of CVD-type SWCNT-FET devices.

- The operation of network SWCNT-FETs were characterized in both back- and top-gate schemes. The top liquid-gated device exhibited a smaller subthreshold swing factor (S) (110 mV/decade) compared with that of the back-gated device (1.821 V/decade). Additionally, the fabricated network SWCNT-FET exhibited more stable operation in

liquid-gated scheme rather than in ambient air scheme. The performances of fabricated network SWCNT-FETs are applicable for biosensing.

Chapter 3: Peptide aptamer-modified CVD-type SWCNT-FET biosensor

3.1. Introduction

The emergence of biosensor devices that convert a biological response into an electrical signal can address the rapidly increasing need in the point-of-care testing (POCT) market and achieve wide-scale application. However, the utilization of biosensor devices has yet to become a mainstream, particularly for near-patient testing, mainly because of the difficulty in harnessing the combination of two key prerequisites: "sensitivity" and "selectivity". To address the sensitivity issue, one-dimensional conductive nanomaterials such as CNT-based FETs have emerged as an effective transducer for label-free nanoelectronic platforms because of their exquisite electrical sensitivity toward minute variations in their surrounding environment [27, 78-80]. However, the use of CNT-FETs in practical applications in clinical diagnostics remains a challenging issue because the obvious essential requirement of POCT is to recognize targets specifically in the presence of thousands-fold excesses of interfering species within a complex biological sample. For example, human serum contains hundreds of thousands of different protein molecules, of which 97% are composed of the 20 most abundant proteins [81]. Therefore, in this work, our intention is to focus on the selectivity issue while maintaining the greater sensitivity of semiconductor electronics devices. Because the large specific surface area (SSA) in CNTs, which enables immobilization of a large number of functional units at the carbon nanotube surface, increases with a decreasing number of walls, we preferred to use SWCNTs to improve the signal-to-noise ratio.

The bioelectronics interface interaction of CNTs with biological molecules has quite recently become the topic of focus after the discovery of a monoclonal antibody [82] and peptide [83] capable of selectively binding to the surface of CNTs. Interestingly, a dodecapeptide capable of self-assembly into peptide nanowires on graphene has recently

been reported [84]. Therefore, peptide-based probes enable new approaches to develop CNT-based biosensors. To take a further step, our philosophy is to develop a new generation of biosensing technology by introducing evolutionary molecularly engineered peptide aptameric reagents [85] as a smart probe molecule onto SWCNT-FETs to combine the high sensitivity of SWCNTs with the outstanding binding properties of the peptide aptamer to achieve excellent selectivity. Previously, the DNA aptamer-based CNT-FETs were fabricated and evaluated the detection of IgE with higher sensitive performance [6, 75]. However, peptide-based aptamers, which are comparatively smaller in molecular weight, exhibit a smaller binding footprint, allowing for a more thorough and precise interrogation of the target than that afforded by nucleic acid-based aptamers [57]. Most importantly, a peptide aptamer can be engineered on-demand through an in vitro selection procedure and can thus be targeted to the detection of biological molecules that are fundamentally unable to be detected via conventional approaches. Besides, antibody-based recognition elements with heights greater than 10 nm remain outside the electrical double layer (Debye length) and are thus unfit for use in a SWCNT-FETs biosensor [53, 86]. Interestingly, the smaller size of a peptide aptamer (less than a few nanometers) enables the detection of proteins in solutions of high ionic strength (i.e., approaching the ionic strengths found in physiological environments) and beyond the electrical double layer using SWCNT-FETs.

Recently, the application of repeats of amino acids integrated with CNT-FET sensor has been developed for the detection of heavy-metal ions such as Ni^{2+}, Cu^{2+} [87], and environmentally toxic chemicals such as decabrominated diphenyl ether (DBDE) [88] and 2,4,6-Trinitrotoluene (TNT) [89]. In this work, we fabricated CVD-type SWCNT-FETs and investigated the integration and application of an engineered peptide aptamer for the highly selective and sensitive detection of unreached biomarkers for POCT application

(Figure 3.1). To do so, we modified the channels of CVD-type SWCNT-FETs by novel peptide aptamers that were engineered with a selective affinity for CatE via systemic in vitro evolution [90]. We identified an alpha-strand peptide scaffold and conjugated it to a novel peptide aptamer with high binding affinity (0.954 nM) for CatE. This conjugated peptide was then grafted onto an SWCNT via noncovalent bonding. As a result, this FET device provides a strong yet selective capture of target CatE molecules; consequently, extremely sensitive detection of CatE can be achieved using this FET sensor system. Our device exhibited good selectivity (no response for BSA and CatK) and a low detection limit. The sensitivity of this device could improve the limit of detection of CatE in human serum by at least three orders of magnitude compared with a conventional ELISA-based system using a similar peptide aptamer [91].

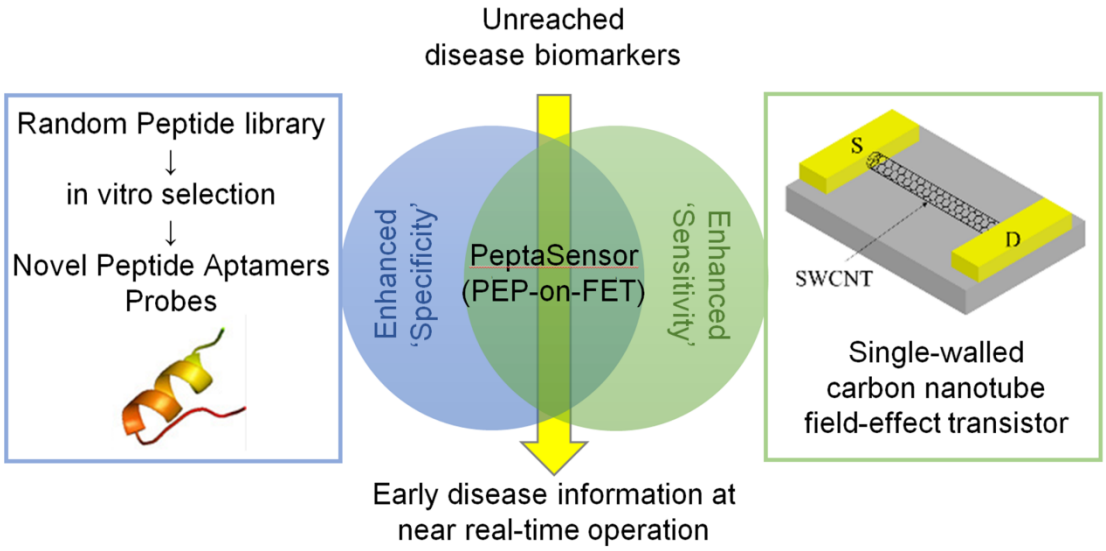

Figure 3.1: The integration of novel peptide aptamer with CVD-type SWCNT-FET to achieve highly selective and sensitive biosensing of unreached biomarkers.

This work details the successful fabrication and demonstration of a liquid-gated CVD-type SWCNT-FET sensor modified with CatE-binding peptide aptamers as an attractive platform for POCT application for the detection of unreached disease biomarkers such as serum CatE, which has recently been highlighted as a novel prognostic biomarker

for cancer because the reduction of serum level of CatE has been associated with poor prognosis in breast cancer patients [92]. To the best of our knowledge, this work represents the first report of an FET-type sensor utilizing peptide aptamer-modified SWCNTs; this novel sensor can lead to the development of a portable and affordable sensing system for high-performance near-patient testing.

3.2. Materials and apparatus

All chemicals and materials used in these experiments are listed in Table 3.1 below:

Table 3.1: List of chemicals and materials including their suppliers

Chemicals/materials and reagents	Suppliers
Dimethylformamide (DMF) (98%)	Wako Pure Chemical Industries, Ltd., Japan
1-pyrenebutanoic acid succinimidyl ester (PBASE)	Thermo Fisher Scientific Inc., Japan
Peptide aptamer	Scrum, Inc., Japan
Cathepsin E (CatE)	BioVision, Inc. (CA, USA)
Cathepsin K Active human (CatK)	Sigma-Aldrich Co. LLC., Japan
Bovine Serum Albumin (BSA)	Wako Pure Chemical Industries, Ltd., Japan

The PBASE linker was dissolved in DMF. CatE samples were prepared in 1× PBS pH 10 and 10-fold-diluted human serum, which was diluted with 1× PBS pH 7.4 and then stored at -20°C until use. CatK and BSA were prepared in PBS and then stored at -20°C.

The 0.0005× PBS pH 4 was prepared by diluting 10× PBS with milli-Q water and then adding HCl to adjust the pH value to 4. The peptide aptamer with a sequence of SCGGI IIISC IAVIS LIPGR IGCIR AKAAAK that specifically recognizes CatE was custom-made by Scrum, Inc., Japan.

All the apparatuses are listed in Table 3.2 below:

Table 3.2: List of apparatuses and their suppiers

Apparatus	**Suppliers**
Biacore X100	GE Healthcare Life Sciences
Reference electrode Ag/AgCl	Bioanalytical Systems, West LaFayette, IN

A Biacore X100 instrument was used to characterize the binding features of the peptide aptamer to CatE. The AFM method was used to visualize the capture of CatE by the peptide aptamer, which was immobilized onto the SWCNTs. The Agilent 4156C Precision Semiconductor Parameter Analyzer was utilized for measuring the electrical performance of the pristine SWCNT FET and the electrical signals of peptide aptamer-modified SWCNT FET induced from binding events.

3.3. Experimental

3.3.1. Peptide aptamer characterization

A novel peptide aptamer that specifically recognizes CatE was engineered via systemic in vitro evolution. We characterized the binding affinity of the peptide aptamer and CatE using a Biacore X100 instrument. The Surface Plasmon Resonance (SPR) analysis for the affinity binding of the peptide aptamer to CatE used a single-cycle mode

with an aptamer level of 1000 RU and sequential injections of five ascending concentrations of analyte CatE (858.37, 171.67, 34.33, 6.87, 1.37 ng/mL). A steady-state affinity binding plot was calculated from the end of the association phases against the analyte concentration.

3.3.2. Surface modification of the CVD-type SWCNT-FET and CatE detection scheme

The CatE-specified peptide aptamer probe molecule was immobilized onto the SWCNT channel of the CVD-type SWCNT-FET via the PBASE linker. First, the PBASE linker was immobilized onto the SWCNT channel by dropping PBASE solution onto the device and then incubating for 1 h at room temperature. Afterwards, peptide aptamer dissolved in DMF was dropped onto the device, which was then incubated for 1 h at room temperature, rinsed thoroughly with DMF and then dried with nitrogen gas. The concentration of PBASE and peptide aptamer for immobilization was investigated systematically. The PBASE can bind by noncovalent π-stacking with the sidewall of SWCNTs via its aromatic ring. The peptide aptamer probe molecule covalently binds to the linkers via its succinimidyl ester functional group. The unreacted PBASE linker was blocked with 100 mM ethanolamine for 30 min. The devices were subsequently subjected to various CatE concentrations (from 0.1 to 1 ng/mL) in 1× PBS pH 10, incubated for 10 min at 25°C to capture the CatE target, rinsed thoroughly with 0.0005× PBS pH 4 and then dried with nitrogen gas. Finally, a Parafilm cavity was attached to the device to contain the PBS buffer solution during electrical measurements.

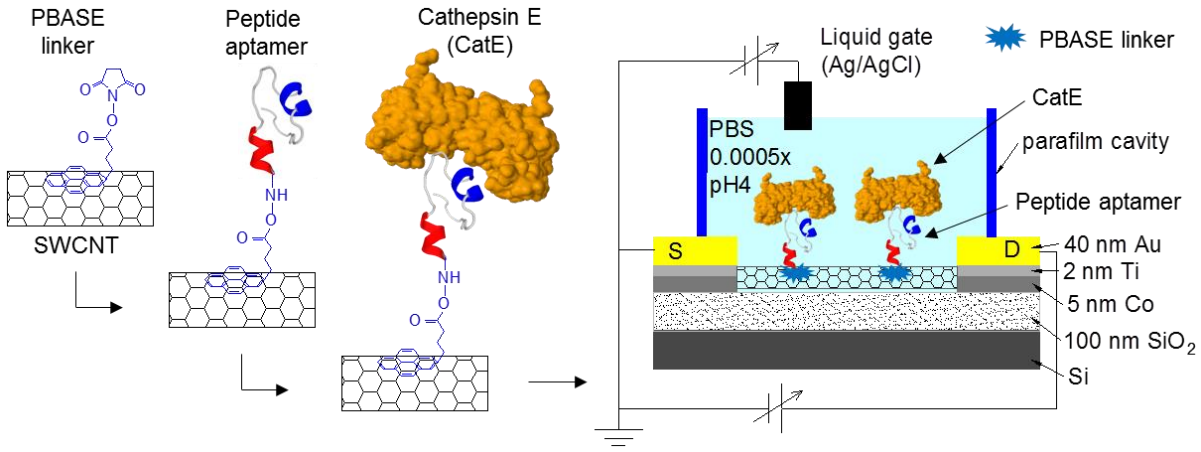

Figure 3.2: The immobilization of peptide aptamer onto the surface of SWCNT and the operating setup of liquid-gated SWCNT FET device for CatE detection.

Figure 3.2 shows the schematic scheme for immobilization of peptide aptamer onto the sidewall of SWCNT and schematic diagram of experimental setup. We measured the transfer characteristics of the fabricated sensor using a top liquid-gated scheme in 0.0005× PBS pH 4. The source electrode was grounded. A 0.2 V bias voltage was applied between the source and drain electrodes to monitor the electrical conductance of the SWCNT channel while a top liquid-gated potential with respect to the grounded source electrode was scanned from 0 to -0.6 V. A reference electrode (Ag/AgCl, Bioanalytical Systems, West LaFayette, IN) was used to apply potential to the top liquid gate to avoid sensing an artifact from the environment [77].

To test the selectivity of our sensor, the peptide aptamer-modified SWCNT FETs were subjected to 1 ng/mL BSA for 10 min, and 0.1 and 1 ng/mL CatK for 10 min, separately, rinsed thoroughly with 0.0005× PBS pH 4 and then dried with nitrogen gas prior to collection of their transfer curves.

The non-specific binding of CatE molecules onto SWCNT was examined via an experiment in which the PBASE linker was immobilized onto a SWCNT FET without the peptide aptamer probe molecule, followed by blocking with 100 mM ethanolamine for 30

min. The PBASE linker-modified SWCNT FETs were then subjected to 1 ng/mL CatE for 10 min, rinsed thoroughly with 0.0005× PBS pH 4 and then dried with nitrogen gas prior to collection of their transfer curves.

3.3.3. AFM preparation of CatE captured on the peptide aptamer-modified CVD-type SWCNT-FET

The 10 ng/mL CatE in 1× PBS pH 10 was dropped onto the peptide aptamer-modified SWCNT FET and then incubated at 25°C for 10 min, rinsed completely with 0.0005× PBS pH 4 and dried with nitrogenous gas. The morphology of bare SWCNT, peptide aptamer-modified SWCNT and CatE-captured peptide aptamer-modified SWCNT FETs were visualized using AFM images.

3.3.4. Quantitative detection of CatE in 10-fold-diluted human serum

The peptide aptamer-modified SWCNT FETs were exposed to various CatE concentrations (from 10 ng/mL to 100 ng/mL), which were prepared in 10-fold diluted human serum and then incubated for 20 min at 25°C, rinsed thoroughly with milli-Q water and 0.0005× PBS pH 4 and then dried with nitrogen gas. The transfer characteristics of the sensors were measured in 0.0005× PBS pH 4 for each CatE concentration using the top liquid-gated scheme.

3.4. Results and discussion

3.4.1. Characterization of the peptide aptamer probe molecule

A *de novo* simulated model of the peptide aptamer with selective affinity for CatE is shown in Figure 3.3(a). CatE is composed of an in vitro-selected peptide aptamer (24 amino acids comprising two peptide blocks of 12- and 8-amino acids paired by a 4-amino

acid linker) and a short alpha-strand peptide scaffold (7-amino acids). A Biacore X100 instrument was used to characterize the binding features of the peptide aptamer to CatE. A free N-terminal end of the peptide aptamer is necessary for its correct folding as a basis for the formation of the binding complex with the target. Therefore, the C-terminal end of the peptide aptamer with biotin-streptavidin chemistry was immobilized onto a CM5 sensor chip, and then CatE was injected as the analyte across this surface for interaction with the peptide aptamer. The dissociation constant (K_d) for the CatE was calculated as 9.548×10^{-10} M. Figure 3.3(b) shows the result of the Biacore measurement of the peptide aptamer. In the surface plasmon resonance (SPR) analysis, it is expected to get similar results for similar experiments.

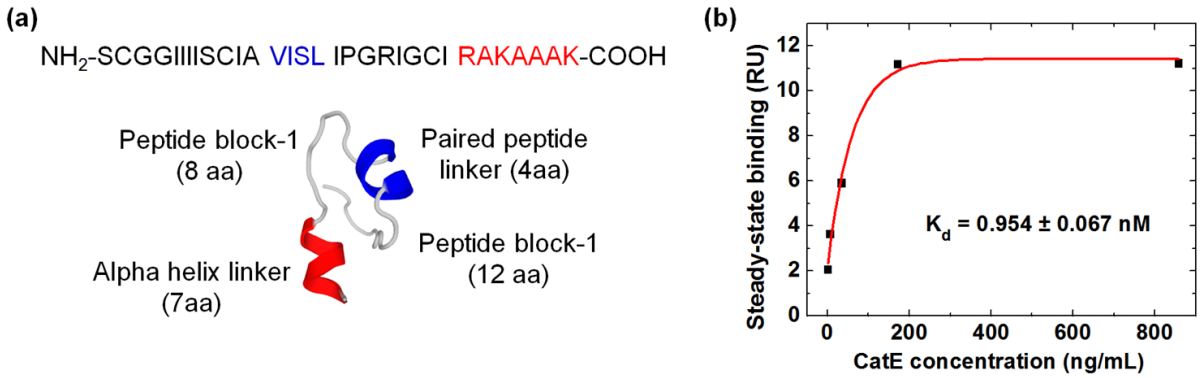

Figure 3.3: Peptide aptamer characterization. (a) The sequence and a cartoon model of selected peptide aptamer; and (b) SPR analysis for the affinity binding of peptide aptamer to Cathepsin E. Steady-state affinity binding plot was calculated from the end of the association phases against analyte concentration.

3.4.2. Quantitative detection of CatE in PBS buffer using the peptide aptamer-modified CVD-type SWCNT-FET biosensor

After fabricating the CVD-type SWCNT-FET, we immobilized the CatE-binding peptide aptamer onto the SWCNT channel via PBASE linker to develop a peptide aptamer-modified CVD-type SWCNT-FET sensor for CatE detection. The immobilization

of the PBASE linker and peptide aptamer were systematically investigated (Figure 3.4). The relative decrease in the "on" current ($\Delta I/\Delta I_{max}$), where ΔI_{max} represents the decrease in the "on" current at a saturation level due to the interaction between PBASE and SWCNT FETs, increased with increasing PBASE concentration from 3 to 50 mM and appeared to be saturated at 50 mM (Figure 3.4(a)). The π-π interaction between the PBASE and SWCNT might affect the hole carrier inside the SWCNT channel, leading to the observed decrease in $\Delta I/\Delta I_{max}$ [93]. This observation indicates the success of the PBASE linker immobilization. Therefore, 50 mM PBASE was selected for the subsequent experiments. Figure 3.4(b) shows that the relative decrease in the "on" current ($\Delta I/\Delta I_{max}$), where ΔI_{max} represents the decrease in the "on" current at a saturation level due to the interaction between peptide aptamers and CVD-type SWCNT-FETs, increased with increasing peptide aptamer concentration in the range from 1 to 120 μM and then became saturated near 120 μM. The immobilization time of 60 min was selected as the optimal condition because aggregation of the peptide aptamer occurred at longer incubation times. The $\Delta I/\Delta I_{max}$ indicated the successful immobilization of the peptide aptamer probe molecules onto the SWCNT channel. The peptide aptamer, which has an isoelectric point of 9.77, exhibits positive charge in PBS pH 4. This positive charge of the peptide aptamer might affect the hole carrier inside the SWCNT channel, leading to the $\Delta I/\Delta I_{max}$. A large coverage of peptide aptamer over the SWCNT channel is critically important because it maximizes the target capturing efficiency. Therefore, 120 μM was chosen as the optimal concentration of the peptide aptamer. The fabricated sensors could be stored in the dried form at cool temperature of less than or equal to 4 °C.

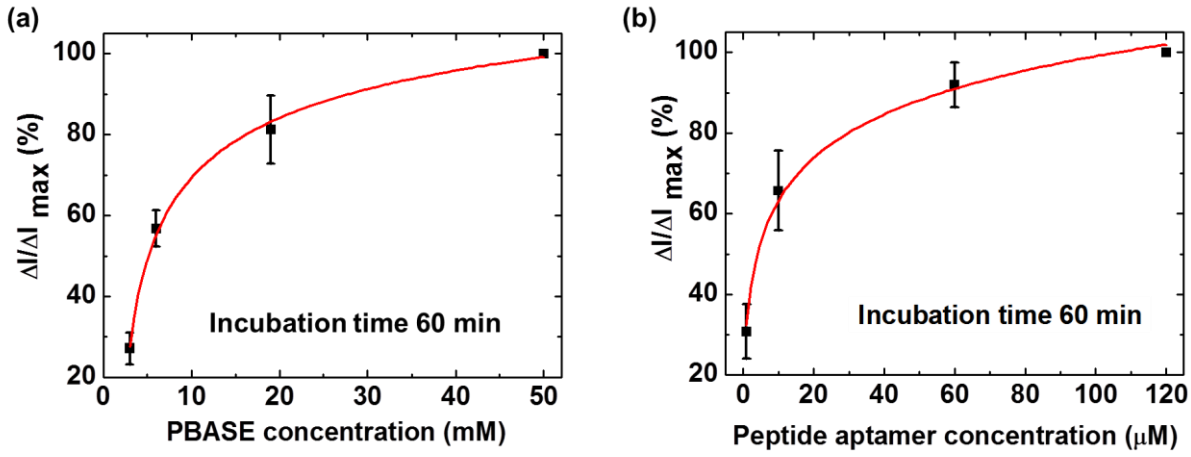

Figure 3.4: The investigation of (a) PBASE linker concentration (n = 5); and (b) peptide aptamer concentration (n = 5).

The peptide aptamer was immobilized onto the SWCNT channel via the PBASE linker prior to the capture of CatE. Next, the sensor was exposed to 0.0005× PBS pH 4 for electrical measurements. Figure 3.5(a) shows the transfer characteristics of the peptide aptamer-functionalized CVD-type SWCNT-FET biosensor for various CatE concentrations ranging from 0.1 to 1 ng/mL. The transfer curve of the CVD-type SWCNT-FET initially shifted toward the negative bias direction after the immobilization of the peptide aptamer. With increasing CatE concentrations from 0.1 to 0.6 ng/mL, the curve further shifted toward the same direction. This phenomenon is attributed to the positively charged CatE molecules at PBS pH 4 (the isoelectric point of CatE is 4.69) inducing the gradual reduction of hole carriers in the SWCNT channel via a field effect [94]. At concentrations greater than this concentration, the shift of the transfer curve is no longer observed because all peptide aptamer probe molecules are occupied by CatE molecules. The relative decrease in the "on" current ($\Delta I/\Delta I_{max}$), where ΔI_{max} represents the decrease in "on" current at a saturation level due to the interaction between CatE and peptide aptamer-modified CVD-type SWCNT-FETs, at a top liquid-gated voltage of -0.6 V was plotted as a function of CatE concentration, as shown in Figure 3.5(b). The results reveal that $\Delta I/\Delta I_{max}$

increased as a function of CatE concentration from 0.1 to 0.6 ng/mL and then saturated with a further increase of the CatE concentration. The minimal detectable concentration of 0.1 ng/mL is comparable with that of CatE ELISA Kit (0.156 ng/mL). The inset of figure 3.5(b) shows the dependence of CatE concentration $C_{CatE}/(\Delta I/\Delta I_{max})$ as a function of CatE concentrations. The good linear fitting of the experimental results indicates that the capture of CatE on the peptide aptamer-functionalized SWCNT is in accordance with the Langmuir adsorption isotherm given by:

$$\frac{(\Delta I/\Delta I_{max})}{(\Delta I/\Delta I_{max})_{max}} = \frac{C_{CatE}}{K_d + C_{CatE}}$$

Or

$$\frac{C_{CatE}}{(\Delta I/\Delta I_{max})} = \frac{1}{(\Delta I/\Delta I_{max})_{max}} C_{CatE} + \frac{K_d}{(\Delta I/\Delta I_{max})_{max}}$$

Where K_d is the dissociation constant of the reaction between CatE molecules and the CatE-specified peptide aptamer probe molecules and $(\Delta I/\Delta I_{max})_{max}$ is the saturated amount of the relative decrease in the "on" current. From the fitting, K_d was estimated to be 0.12 ng/mL or 2.769 pM, which is approximately 2 order smaller than that estimated from the SPR-based titration (40.9 ng/mL or 0.954 nM). This difference is attributed to the difference in the range of CatE concentrations. In case of using SPR, the range of CatE was from 1.37 to 858.37 ng/mL. In case of using FET, the range of CatE was from 0.1 to 1 ng/mL. Additionally, the hydrophobic interaction between the SWCNT and the CatE may affect to the decrease in the dissociation rate constant, resulting in the smaller dissociation constant K_d.

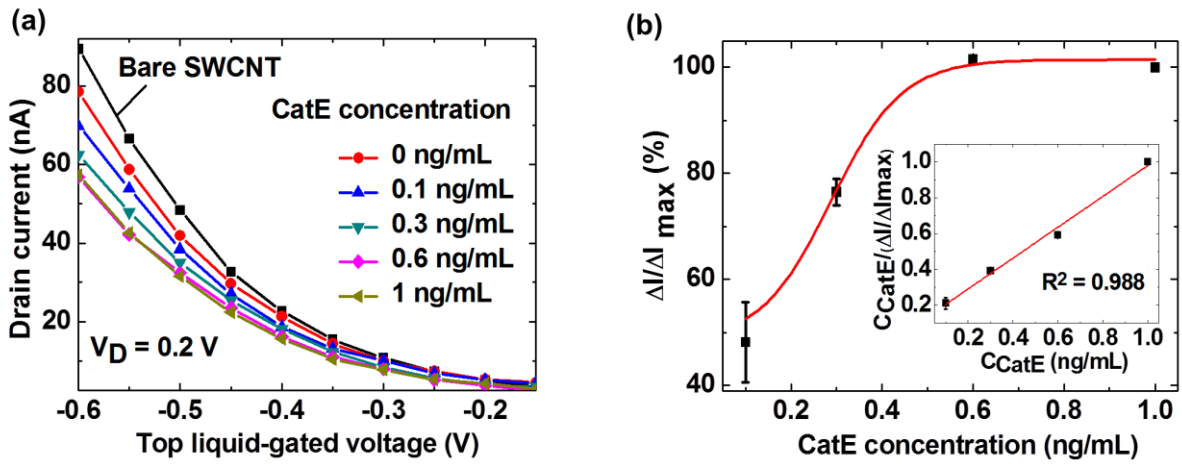

Figure 3.5: Quantitative detection of CatE in phosphate-buffered saline. (a) Transfer characteristics of peptide aptamer-modified CVD-type SWCNT-FET for various CatE concentrations; (b) The relative decrease in "on" current ($\Delta I/\Delta I_{max}$) as a function of CatE concentration (n = 3). Inset figure shows the CatE concentration/($\Delta I/\Delta I_{max}$) as a function of CatE concentration.

Figure 3.6(a) shows the result for the PBASE-modified CVD-type SWCNT-FET without the peptide aptamer probe molecule for CatE detection. There was almost no change observed in the drain current. Figure 3.6(b) shows the comparison of the SWCNT FETs with and without peptide aptamer probe molecules responding to 1 ng/mL CatE. The normalization of "on" current ($\Delta I/I_o$), where I_o represents the "on" current in presence or absence of target, was used for this comparison. The apparent change in ($\Delta I/I_o$) was observed in case of SWCNT FETs with peptide aptamer while negligible change was observed in case of SWCNT FETs without peptide aptamer. This result indicates that the non-specific binding of CatE was successfully suppressed.

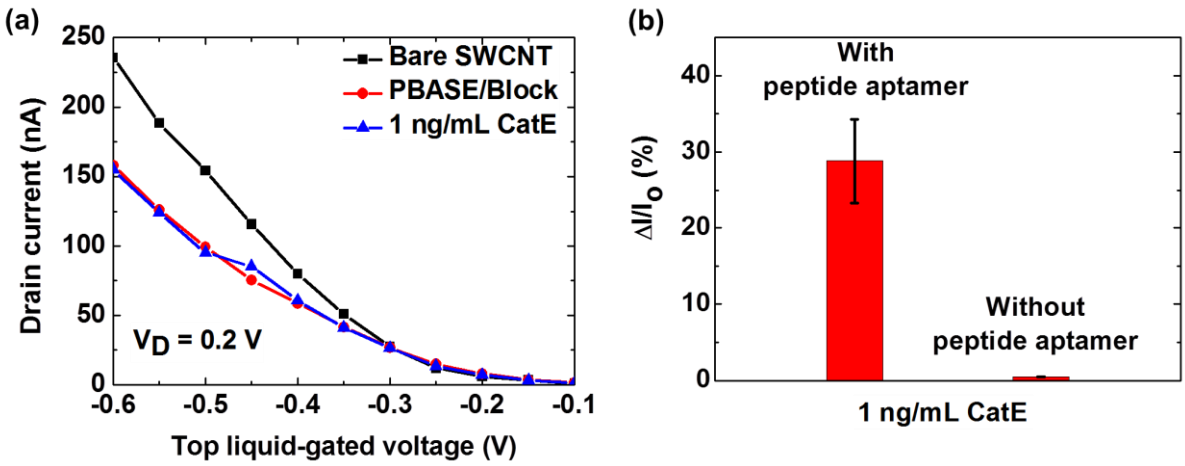

Figure 3.6: (a) Transfer characteristics of PBASE-modified CVD-type SWCNT-FET without peptide aptamer for 1 ng/mL CatE. (b) Comparison of response signal from 1 ng/mL CatE using CVD-type SWCNT-FET with and without peptide aptamer probe molecule.

Figure 3.7(a) and 3.7(b) show the results for the response of the peptide aptamer-modified SWCNT FET biosensor for BSA and CatK detections, respectively. The changes in the drain currents were hardly observed in both cases, indicating that the device was able to distinguish among the CatE target and interfering BSA, CatK molecules.

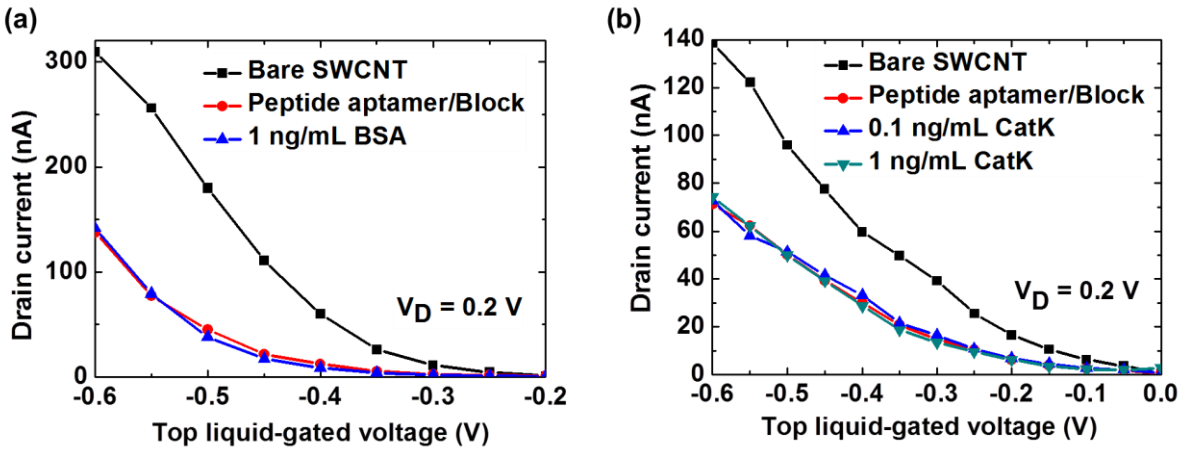

Figure 3.7: Transfer characteristics of peptide aptamer-modified SWCNT FETs for (a) 1 ng/mL BSA and (b) 0.1 and 1 ng/mL CatK.

By using the normalization of "on" current ($\Delta I/I_o$), where I_o represents the "on" current in presence or absence of target, the responses of the peptide aptamer-modified SWCNT FETs to concentration of CatE, BSA and CatK were plotted as shown in figure 3.8. The obvious changes in $\Delta I/I_o$ were observed after the introduction of CatE concentration while the small changes in $\Delta I/I_o$ in the opposite direction were observed after the introduction of BSA as well as CatK. These results suggest that high selectivity originated from the specific binding of the CatE target and peptide aptamer probe molecules, as anticipated from the Biacore measurements.

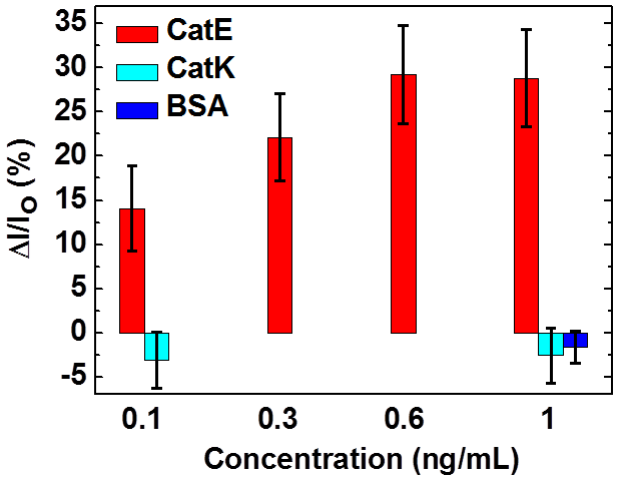

Figure 3.8: The relative change in "on" current ($\Delta I/I_o$) versus concentration was plotted for CatE, BSA and CatK (where I_o is the value of "on" current for 0 ng/mL) (n = 3).

Figure 3.9 shows the AFM images of a bare SWCNT, a peptide aptamer-immobilized SWCNT, and a CatE-captured SWCNT. No change in the height of the SWCNT before (Figure 3.9 (a)) and after peptide aptamer immobilization (Figure 3.9 (b)) was observed. The peptide aptamer molecules with the short length of 31 amino acids might lie down on the sensor surface, as measured in a dried form, resulting in no obvious difference in the observed height. By contrast, the height increased from 1.5 nm to 2.5 nm after CatE addition (Figure 3.9 (c)), which further confirmed that CatE molecules were captured by the peptide aptamer probe molecules.

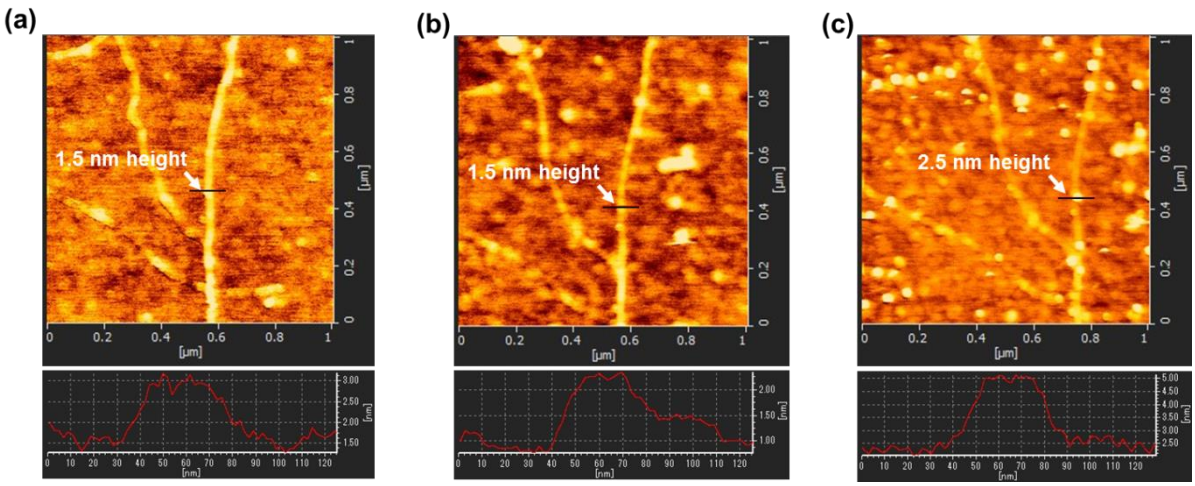

Figure 3.9: The AFM microphotographs of device before and after capture of CatE. (a) bare SWCNT, (b) peptide aptamer-immobilized SWCNT and (c) CatE captured on peptide aptamer, which was immobilized on SWCNT.

3.4.3. Quantitative detection of CatE in human serum

From a point-of-care perspective, the direct and facile measurement of a cancer biomarker in blood serum is necessary. However, in the absence of a blocking treatment, a certain amount of response can be expected because of the non-specific adsorption or noise generated by bulk proteins present in human serum. To reduce such non-specific adsorption, we introduced the well-known blocking reagent, ethanolamine [95]. We further explored the potential application of our biosensor to detect CatE in a human serum sample by measuring the transfer characteristics of the peptide aptamer-modified SWCNT FET as a function of the CatE concentrations (from 10 to 100 ng/mL) in 10-fold diluted human serum (Figure 3.10). Similar to the observations for the device in the PBS buffer, the transfer curve of the SWCNT FET initially shifted toward the negative bias direction after immobilization of the peptide aptamer and the addition of CatE target with concentrations from 10 ng/mL to 60 ng/mL (Figure 3.10 (a)). However, no response was observed above the CatE concentration of 60 ng/mL. This result indicates that the limit of detection in the presence of 10-fold diluted serum (i.e., 10 ng/mL) was impaired by two

orders of magnitude compared with the limit in the presence of PBS (i.e., 0.1 ng/mL). A calibration curve was obtained as a function of serum CatE concentration using the normalization of the relative decrease in "on" current ($\Delta I/\Delta I_{max}$), where ΔI_{max} represents the decrease in "on" current at a saturation level due to the interaction between serum CatE and peptide aptamer-modified SWCNT FETs (Figure 3.10 (b)).

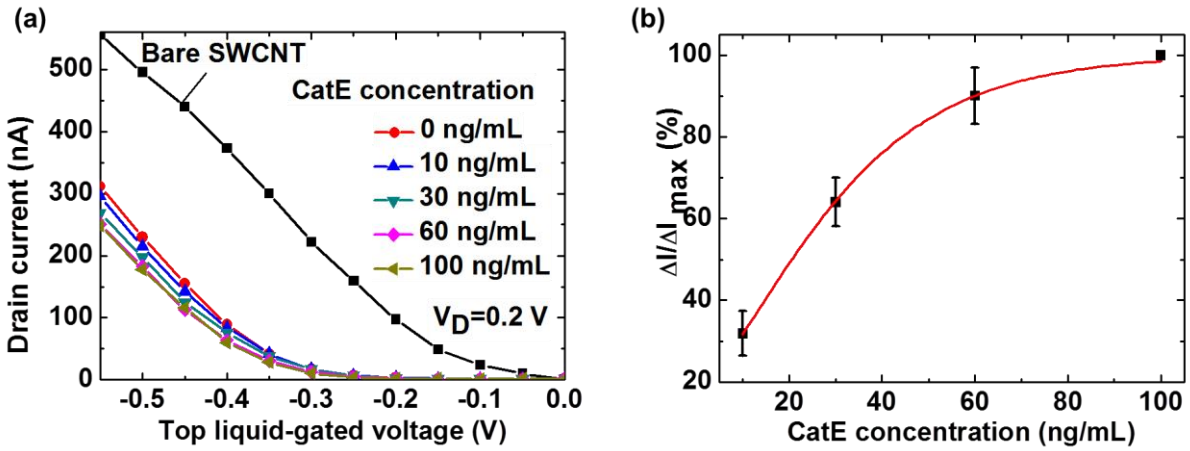

Figure 3.10: (a) Transfer characteristics of peptide aptamer-modified SWCNT FET for various CatE concentrations in 10-fold diluted human serum; and (b) The relative decrease in "on" current ($\Delta I/\Delta I_{max}$) as a function of CatE concentration (n = 3).

The other (contaminating) proteins in human serum may affect responses in two ways. First, the non-specific adsorption of charged proteins onto the PBASE-modified SWCNT surface may lead to a shift in the transfer curve. In addition, the non-specific proteins, which are larger, may be adsorbed or hindered from moving onto the surface of the probe molecules and thus hide the recognition/binding site of the peptide aptamer, leading to a decrease in the response caused by the target protein. To address these challenges, a microfluidic approach can be used to reduce the possible non-specific interactions. Our sensor provided an improvement of sensitivity of serum CatE by at least three orders of magnitude compared to a conventional ELISA system using a similar peptide aptamer [91]. Table 3.3 shows the comparison among the methods for CatE

detection. Given this observation and with implementation of further improvements in the sampling process, our peptide-modified SWCNT FET biosensor could offer an attractive approach to detect CatE in a real clinical sample with higher selectivity and the desired sensitivity.

Table 3.3: Comparison of CatE-detecting biosensors.

Method	**Probe molecule**	**Lowest detectable CatE concentration**	**Ref.**
Fluorescence Resonance Energy Transfer (FRET)	Peptide probe	2.27 nM in 50 mM sodium acetate buffer (pH 4)	[96]
SWCNT-FET	Peptide aptamer	2.3 pM (or 0.1 ng/mL) in buffer	Our study
ELISA	Peptide aptamer	10 µg/mL Serum containing buffer (pH 4.5)	[91]
SWCNT-FET	Peptide aptamer	10 ng/mL in 10-times diluted serum in buffer	Our study

3.5. Conclusion

In this chapter, we presented the first demonstration of the successful integration of a novel peptide aptamer with a liquid-gated CVD-type SWCNT-FET to achieve highly sensitive and specific detection of CatE. The main achievements are summarized below:

- The immobilization of peptide aptamer onto sidewall of SWCNT channel of CVD-type SWCNT-FET was systematically investigated. The concentration of 50 mM and incubation time of 1h were optimal conditions for immobilization of PBASE linker. The 120 µM and 1h were chosen as the optimal concentration of the peptide aptamer and

incubation time, respectively, for the immobilization of peptide aptamer onto SWCNT channel.

- The fabricated peptide aptamer-modified CVD-tyep SWCNT-FET sensors were successfully fabricated for the label-free detection of CatE at at unprecedentedly low concentrations. The minimal detectable CatE concentration of 0.1 ng/mL in PBS was achieved with highly suppressing nonspecific binding (no response to CatE when using CVD-type SWCNT-FET without peptide aptamer probe molecule).

- The fabricated peptide aptamer-modified CVD-type SWCNT-FET sensors exhibited a high selectivity (no response to BSA and CatK).

- The fabricated sensors showed the minimal detectable CatE concentration of 10 ng/mL in 10-diluted human serum. Our sensor provided an improvement of sensitivity of serum CatE by at least three orders of magnitude compared to a conventional ELISA system using a similar peptide aptamer. Our results suggest that the integration of a highly specific peptide aptamer and a SWCNT FET transducer can be a platform for near-patient detection of biomarkers and thus could be widely used for human health monitoring and early disease diagnosis.

Chapter 4: Glutamate-binding protein modified network SWCNT-FET biosensor

4.1. Introduction

Glutamate (Glu) is one of the key excitatory neurotransmitters in human center nervous system [97]. It is released from presynapse of the axon terminal and picked up by receptors on the postsynapse of dendrite. Glu is abundant in the human body, but particularly in the nervous system and especially prominent in the human brain [98]. Since it is a primary fast excitatory neurotransmitter, Glu plays a role in learning and memory in brain [99, 100]. An accurate sensor could help us to better understand these processes. Additionally, the abnormal release of Glu accounts for the pathogenesis of brain or spinal cord injury [101] and the neuronal disorder such as Alzheimer's, Huntington's and Parkinson's diseases [102, 103]. The normal concentrations of Glu in extracellular fluid and inside the cells are a few micromolar and approximately 1 to 10 mM level, respectively. The highest concentration of Glu is about 100 mM inside synaptic vesicles. The normal concentration of Glu in the cerebrospinal fluid is about 1 µM, but it can increase to 20 µM under the abnormal conditions [104] (Figure 4.1).

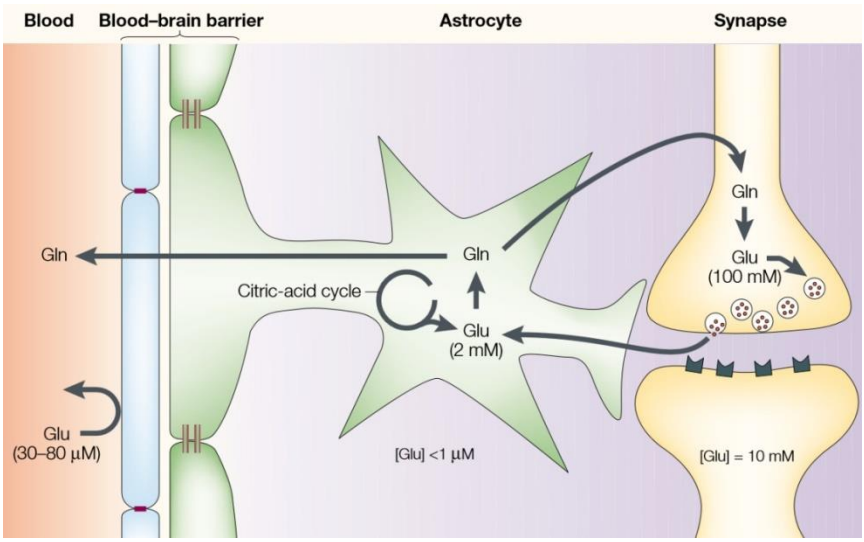

Figure 4.1: Compartmentalization of brain glutamate. Glutamine is taken up by neurons and converted to glutamate before being packaged into synaptic vesicle [105].

Currently, there are two common types of Glu-detection sensors: electrochemical sensors and optical sensors. Previous enzymatic-based Glu sensors using glutamate oxidase [106, 107] or glutamate dehydrogenase [108-110] have been reported, however most of them display the poor selectivity because many other electroactive species in the biological fluids can also be oxidized causing signal interference [111]. In order to overcome this issue, GBP that specifically recognizes the Glu was used as the probe molecule in this work to eliminate the biofouling occurrence or minimize the interference. Additionally, the fluorescent sensors used for Glu detection [71, 112] are also suffered from the issue of assay fluorescence interference [113]. To overcome this issue, network SWCNT-FET sensor, which provides label-free detection, was developed in this work. In addition, network SWCNT-FET appears as one of the most promising candidates for real-time sensitive and selective detection of biomolecule. Therefore, combination of network SWCNT-FET and GBP probe is expected to provide an effective platform for Glu sensing.

Recently, the application of glutamate oxidase with CNT-FET [114] or floating-gate FET [115] sensors has been developed for the detection of Glu. However, this enzyme-immobilized assay could also provide the biofouling due to the oxidization of the other electroactive speciese in the physiological environment.

Additionally, the bind and unbind of Glu is just several milliseconds. The current methods, which are bulky, complicated operation, or suffered from the temporal or spatial resolutions, are not suitable for *in vivo* Glu monitoring. Therefore, it is required the instrument that is miniaturized size, simple operation and fast response. The network SWCNT-FET exhibits promising candidate to fulfil these requirement thanking to its properties of fast response, stable operation, reproducibility, real-time measurement and be flexible to make miniaturized device on flexible substrate. Recent publication shows that the GBP exhibits rapid recognition to Glu (< 5 ms) [71]. Therefore, in this work, we report

the first successful demonstration of the integration of the GBP with liquid gated network SWCNT-FET for real-time monitoring of transient Glu. The GBP probe molecule was immobilized onto the surface of network SWCNT channel via PBASE linker. The fabricated GBP-modified network SWCNT-FET could monitor Glu at micromolar range in real-time with high selectivity (no response to Dopamine). The initial results showed that the GBP-modified network SWCNT-FET could be a promising candidate for real-time Glu monitoring.

4.2. Materials and apparatus

All chemicals and materials used in these experiments are listed in Table 4.1 below:

Table 4.1: List of chemicals and materials including their suppliers

Chemicals/materials and reagents	Suppliers
Glutamate-binding protein (GBP) pRSET.Glt1253-cpGFP.L1LV/L2NP	Addgene
Glutamate (Glu)	Wako
Dopamine (DA)	Sigma-aldrich

The sequence of GBP is MRGSH HHHHH GMASM TGGQQ MGRDL YDDDD KDRWG SAAGS TLDKI AKNGV IVVGH RESSV PFSYY DNQQK VVGYS QDYSN AIVEA VKKKL NKPDL QVKLI PITSQ NRIPL LQNGT FDFEC GSTTN NVERQ KQAAF SDTIF VVGTR LLTKK GGDIK DFANL KDKAV VVTSG TTSEV LLNKL NEEQK MNMRI ISAKD HGDSF RTLES GRAVA FMMDD VLLAG ERAKA KKPDN WEIVG KPQSQ EAYGC MLRKD DPQFK KLMDD TIAQV QTSGE AEKWF DKWFK

NPILV SHNVY IMADK QRNGI KANFK IRHNI EDGGV QLAYH YQQNT PIGDG PVLLP DNHYL STQSK LSKDP NEKRD HMVLL EFVTA AGITL GMDEL YKGGT GGSMV SKGEE LFTGV VPILV ELDGD VNGHK FSVSG EGEGD ATYGK LTLKF ICTTG KLPVP WPTLV TTLTY GVQCF SRYPD HMKQH DFFKS AMPEG YIQER TIFFK DDGNY KTRAE VKFEG DTLVN RIELK GIDFK EDGNI LGHKL EYNFN NPLNM NFELS DEMKA LFKEP NDKAL K.

All the apparatuses are listed in Table 4.2 below:

Table 4.2: List of apparatuses and their suppiers

Apparatus	**Suppliers**
Spectrofluorometer	JASCO corporation
Cuvette	JASCO corporation

The spectrofluorometer was used to characterize the binding affinity between GBP and Glu.

4.3. Experimental

4.3.1. Glutamate-binding protein characterization

The GBP obtained was characterized by fluorescence spectroscopy using emission mode. The wavelength was scanned from 480 to 600 nm. The 50 µL of 2 mM, 20 mM and 200 mM Glu sample was prepared in PBS prior to measurement. The 2 mL PBS was added to cuvette. At first, 2 µL of GBP sample was added to 2 mL PBS cuvette for measurement of zero Glu concentration. The 2 µM Glu measurement was carried out by adding 2 µL of 2 mM Glu to cuvette. The 20 µM, 40 µM, 80 µM and 120 µM Glu

measurements were carried out by adding 2 µL, 2 µL, 4 µL and 4 µL of 20 mM Glu to cuvette, respectively. The 320 µM, 520 µM, 720 µM and 920 µM Glu measurements were implemented by adding each 2 µL of 200 mM Glu to cuvette, respectively. All the fluorescence measurements were carried out at room temperature.

4.3.2. Surface modification of network SWCNT-FET and Glutamate detection scheme

The GBP was immobilized onto the network SWCNT channel of FET via the PBASE linker. First, the PBASE linker was immobilized onto the SWCNT channel by dropping 50 mM PBASE solution onto the device and then incubating for 1 h at room temperature, followed by washing thoroughly with DMF, milli-Q water, then drying with nitrogenous gas. Afterwards, a volume of 2 mg/mL GBP in PBS was dropped onto the device for overnight at 4 °C, followed by rinsing thoroughly with pure water and drying with nitrogen gas. The PBASE can bind with the sidewall of SWCNTs by noncovalent π-stacking via its aromatic ring. The GBP probe molecule covalently binds to the PBASE linker via amide bond to its succinimidyl ester functional group. The unreacted PBASE linker was blocked with 100 mM ethanolamine for 30 min. Figure 4.2 depicted the schematic scheme for the immobilization of GBP onto the sidewall of network SWCNT channel.

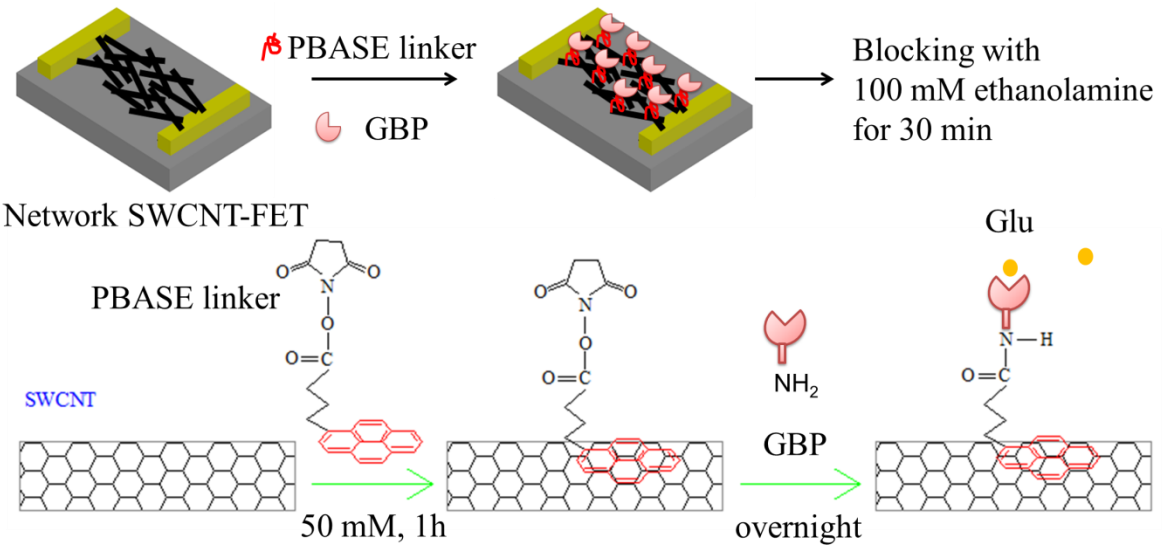

Figure 4.2: Schematic scheme for the immobilization of GBP onto surface of network SWCNT channel of network SWCNT-FET device.

Finally, a Parafilm cavity was attached to the device to contain the PBS buffer solution for real-time measurement of Glu target molecule from 1 to 100 µM (Figure 4.3). We measured the source-drain current versus time of the fabricated GBP-modified network SWCNT-FET sensor using a top liquid-gated scheme in 0.01× PBS pH 7.5. The source electrode was grounded. A 0.2 V bias voltage was applied between the source and drain electrodes to monitor the electrical conductance of the network SWCNT channel while the top-gated potential with respect to the grounded source electrode was kept constant. A reference electrode (Ag/AgCl, Bioanalytical Systems, West LaFayette, IN) was used to apply potential to the top liquid gate to avoid sensing an artefact from the environment.

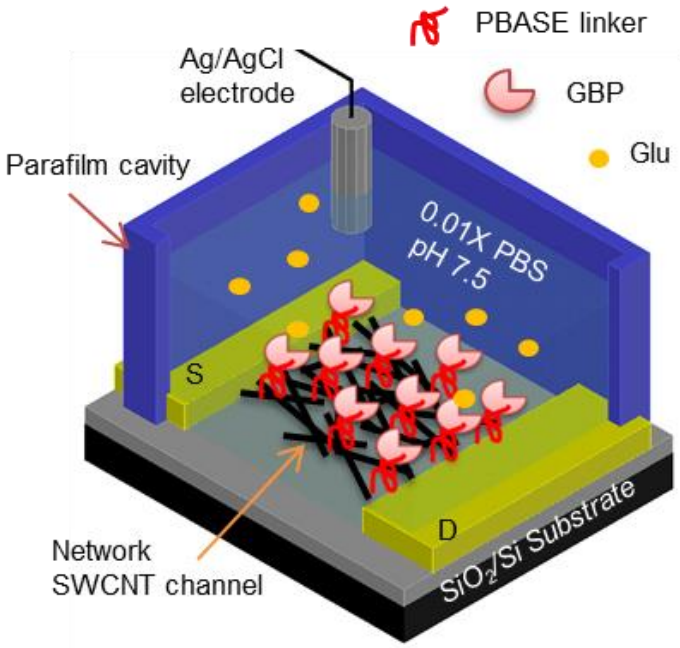

Figure 4.3: Structural illustration of GBP-modified network SWCNT-FET for Glu detection.

The non-specific binding of Glu molecules onto network SWCNT channel was examined via an experiment in which the PBASE linker was immobilized onto the network SWCNT channel of the device without the GBP probe molecule, followed by blocking with 100 mM ethanolamine for 30 min. The PBASE linker-modified network SWCNT-FETs were then subjected to various Glu concentrations from 1 to 100 µM. The drain current was recorded versus time in real-time measurement.

To test the selectivity of our sensor, the fabricated GBP-modified network SWCNT-FETs were subjected to various Dopamine concentrations from 0.1 to 100 µM. The drain current was recorded versus time in real-time measurement.

4.4. Results and discussion

4.4.1. Characterization of GBP probe molecule

The GBP used is fluorescence protein which can give fluorescence spectrum by fluorescence spectroscopy. Figure 4.4 shows the fluorescence spectra of GBP to various Glu concentrations from 0 to 920 µM. The intensity of spectra increased with increasing the Glu concentration from 2 to 320 µM then got saturation because all GBPs were occupied by Glu. The increase of fluorescence intensity was due to the binding between Glu and GBP which induced the fluorophore of GBP to give the higher fluorescence intensity.

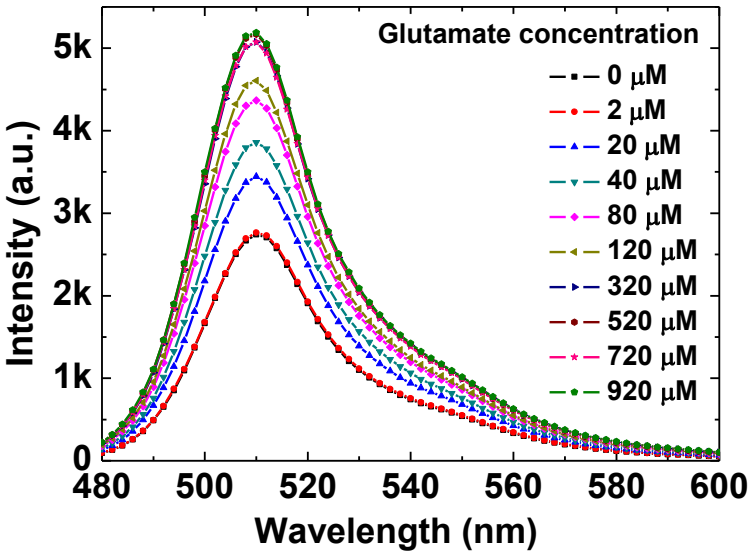

Figure 4.4: Fluorescence spectra of GBP to various Glu concentrations from 0 to 920 µM.

In the Figure 4.4, the emission at 510 nm is the highest point of a fluorescence spectrum. By plotting the fluorescence intensity at emission wavelength according to the Glu concentration, the intensity is as a function of Glu concentration as shown in Figure 4.5. The changes in fluorescence emission from titration experiments were fitted in accordance with hyperbolic isotherm. The dissociation constant of GBP towards Glu is

estimated to be 44 µM. These results indicated that the binding affinity between GBP and Glu was confirmed.

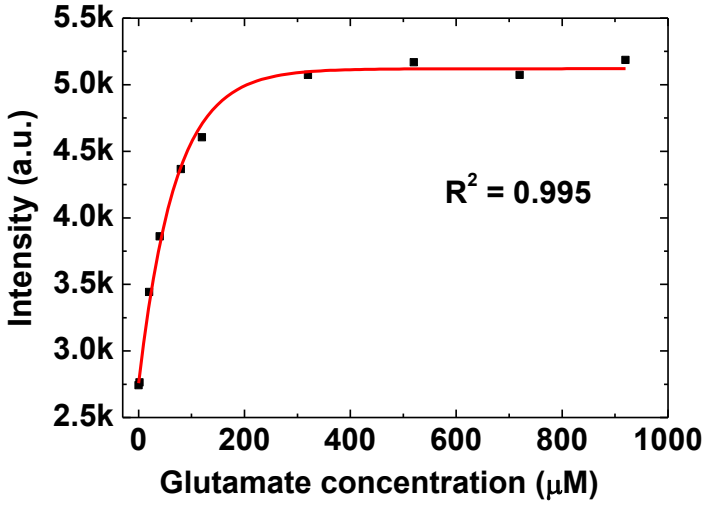

Figure 4.5: Titration of GBP with various Glu concentration from 2 to 920 µM.

4.4.2. Glutamate detection using GBP-modified network SWCNT-FET sensor

After fabricating the network SWCNT-FET, we immobilized the GBP probe molecule onto the network SWCNT channel via PBASE linker to develop a GBP-modified network SWCNT-FET sensor for Glu detection. Figure 4.6 shows the transfer characteristics of network SWCNT-FET before and after immobilization of PBASE linker (red curve) and GBP probe molecule (blue curve) using liquid-gated measurement. After immobilization of PBASE, the transfer curve of device shifted towards negative direction. This is due to the π-π interaction between the PBASE and SWCNTs, which might affect the hole carrier inside the network SWCNT channel [93]. This observation indicates the success of the PBASE linker immobilization. The transfer curve of device shifted towards positive direction after immobilization of GBP probe molecule (from red curve to blue curve). This shift is due to the interaction between GBP probe molecule and network SWCNT-FET. The GBP, which has an isoelectric point of 6.44, exhibits the negative charge in PBS pH 7.5. This negative net charge of GBP might affect the hole carrier inside

the network SWCNT channel, leading to the shift of transfer curve towards positive direction. This result indicates that the GBP probe molecule was successfully immobilized onto the network SWCNT channel via PBASE linker. The fabricated sensors could be stored in the dried form at cool temperature of less than or equal to 4 °C.

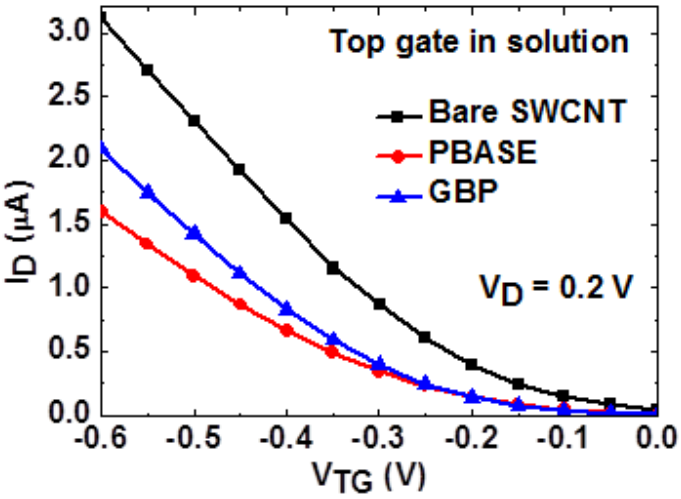

Figure 4.6: Transfer characteristics of fabricated network SWCNT-FET with bare network SWCNT (black), after immobilization of PBASE linker (red) and GBP (blue).

The GBP probe molecule was immobilized onto the netowrk SWCNT channel via the PBASE linker prior to the capture of Glu. Next, the sensor was exposed to 0.01× PBS pH 7.5 for electrical measurements. Figure 4.7 shows the real-time measurement of Glu using network SWCNT-FET with and without GBP probe molecule. The GBP-modified network SWCNT-FET sensor responds to the variant Glu concentration from 1 to 100 µM with response time from 16 to 40 s (black plot). The drain current (I_D) started increasing at 10 µM Glu, and then gradually increased with increasing Glu concentration upto 50 µM. This phenomenon is attributed to the negative charged Glu molecules at PBS pH 7.5 (the isoelectric point of Glu is 3.22), which induces the gradual increase of hole carriers inside the network SWCNT channel vial field effect [94]. At concentrations greater than this concentration, the raise of drain current is no longer observed because all GBP probe

molecules are occupied by Glu molecules. The decrease in drain current at 100 µM could be attributed to the effect of decreased pH of the sampling solution due to the addition of excessive Glu molecules, which exhibits acidic nature. The red plot shows the result for the PBASE-modified network SWCNT-FET without GBP probe molecule exposing to Glu from 1 to 100 µM. There was no significant change observed in drain current fro Glu concentration from 1 to 50 µM. This result indicates that the non-specific binding of Glu was successfully suppressed. The drain current also drops sharply at 100 µM because of decreased pH. The increase in drain current was observed in case of using network SWCNT-FET with GBP probe molecule while no significant change was observed in case of using network SWCNT-FET without probe molecule. This result indicates that the increase in drain current is originated from the specific binding between GBP probe molecule and Glu molecule.

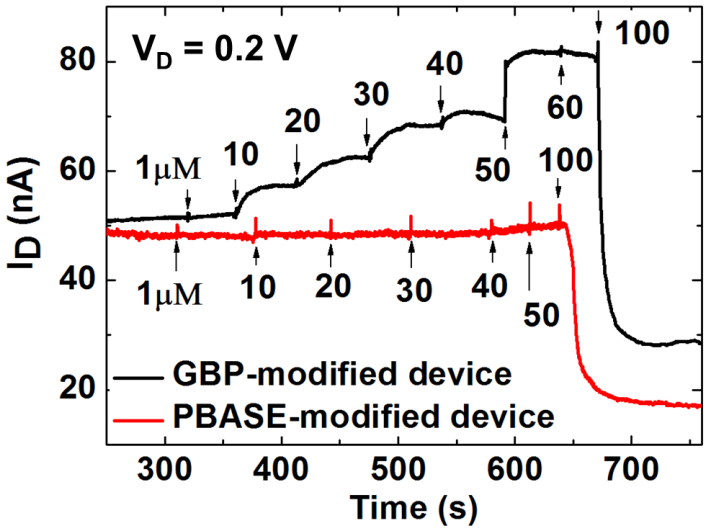

Figure 4.7: Real-time measurement of Glu (1 to 100 µM) using network SWCNT-FET with (black) and without (red) GBP probe molecule.

Figure 4.8 shows the result for the response of the GBP-modified network SWCNT-FET biosensor for DA detection. There was no obvious change in the drain

current, indicating that the device was able to distinguish among the Glu target and another interfering neurotransmitter, DA.

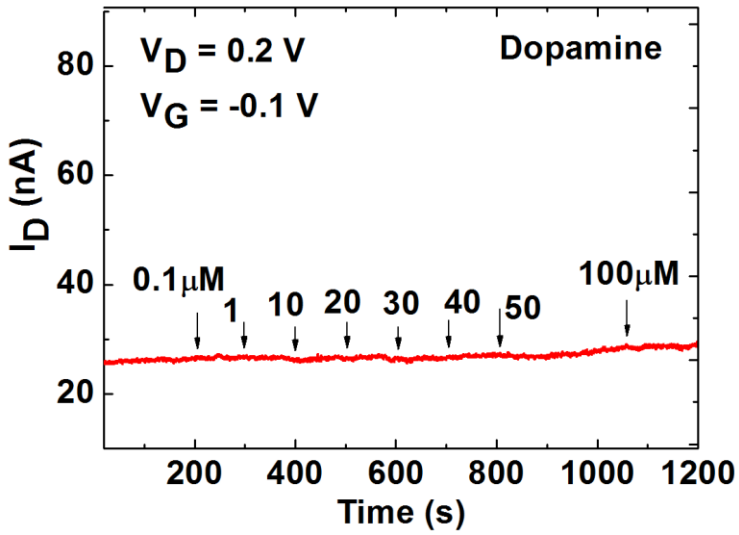

Figure 4.8: The GBP-modified network SWCNT-FET exposing to various Dopamine concentrations (0.1 to 100 μM).

4.5. Conclusion

In this chapter, we presented the first demonstration of the novel FET biosensor for Glu detection by integrating GBP probe molecule into network SWCNT-FET transducer. The main achievements are summarized below:

- The GPB probe molecule was immobilized successfully onto the surface of network SWCNT-FET via the PBASE linker to complete the GBP-modified network SWCNT-FET sensor.

- The GBP-modified network SWCNT-FET could monitor Glu at micromolar range in real-time with high selectivity (no response to Dopamine).

- Our sensor could be a promising candidate for Glu signaling to study neuroscience. This scheme of the integration of amino acid-binding protein and network

SWCNT-FET could be a platform for the label-free detection of small molecule such as amino acids in real-time.

Chapter 5: Conclusion

5.1. Conclusion

In this work, we presented the first demonstration of the integration of small probe molecules (peptide aptamer and GBP) and SWCNT-based FET devices (CVD-type SWCNT-FET and network SWCNT-FET). The main achievements are summarized below:

- The CVD-type SWCNT-FET and network SWCNT-FET were successfully fabricated and their operation exhibited typical p-type characteristics, which are applicable for biosensing.

- The first demonstration of the integration of peptide aptamer and CVD-type SWCNT-FET offered the sensitive and selective CatE detection. This scheme can be applied for various target biomarkers in clinical application.

- The first demonstration of the integration of GBP and network SWCNT-FET could monitor Glu at micromolar range in real-time with high selectivity. The fabricated sensor could be a promising candidate for Glu signalling to study neuroscience.

References

1. Truong, L.T.N., et al., *Labelless impedance immunosensor based on polypyrrole–pyrolecarboxylic acid copolymer for hCG detection.* Talanta, 2011. **85**(5): p. 2576-2580.
2. Truong TN Lien, N.X.V., Miyuki Chikae, Yoshiaki Ukita, Yuzuru Takamura, *Development of Label-Free Impedimetric Hcg-Immunosensor Using Screen-Printed Electrode.* J Biosens Bioelectron, 2011. **2:107**: p. (doi:10.4172/2155-6210.1000107).
3. Gui, E.L., et al., *DNA Sensing by Field-Effect Transistors Based on Networks of Carbon Nanotubes.* Journal of the American Chemical Society, 2007. **129**(46): p. 14427-14432.
4. Star, A., et al., *Label-free detection of DNA hybridization using carbon nanotube network field-effect transistors.* Proceedings of the National Academy of Sciences of the United States of America, 2006. **103**(4): p. 921-926.
5. Okuda, S., et al., *Horizontally Aligned Carbon Nanotubes on a Quartz Substrate for Chemical and Biological Sensing.* The Journal of Physical Chemistry C, 2012. **116**(36): p. 19490-19495.
6. Maehashi, K., et al., *Label-Free Protein Biosensor Based on Aptamer-Modified Carbon Nanotube Field-Effect Transistors.* Analytical Chemistry, 2007. **79**(2): p. 782-787.
7. Grieshaber, D., et al., *Electrochemical Biosensors - Sensor Principles and Architectures.* Sensors (Basel, Switzerland), 2008. **8**(3): p. 1400-1458.
8. Kleinjung, F., et al., *Fibre-optic genosensor for specific determination of femtomolar DNA oligomers.* Analytica Chimica Acta, 1997. **350**(1): p. 51-58.
9. Tombelli, S., et al., *A DNA piezoelectric biosensor assay coupled with a polymerase chain reaction for bacterial toxicity determination in environmental samples.* Analytica Chimica Acta, 2000. **418**(1): p. 1-9.
10. Ramanathan, K., M. Khayyami, and B. Danielsson, *Enzyme Biosensors Based on Thermal Transducer/Thermistor*, in *Enzyme and Microbial Biosensors: Techniques and Protocols*, A. Mulchandani and K.R. Rogers, Editors. 1998, Humana Press: Totowa, NJ. p. 175-186.
11. Hansen, K.M. and T. Thundat, *Microcantilever biosensors.* Methods, 2005. **37**(1): p. 57-64.
12. Lang, H.P., M. Hegner, and C. Gerber, *Cantilever array sensors.* Materials Today, 2005. **8**(4): p. 30-36.
13. Davis, F., et al., *Single Gene Differentiation by DNA-Modified Carbon Electrodes Using an AC Impedimetric Approach.* Analytical Chemistry, 2007. **79**(3): p. 1153-1157.
14. Maskow, T., et al., *Rapid analysis of bacterial contamination of tap water using isothermal calorimetry.* Thermochimica Acta, 2012. **543**: p. 273-280.
15. Moerner, W.E. and D.P. Fromm, *Methods of single-molecule fluorescence spectroscopy and microscopy.* Review of Scientific Instruments, 2003. **74**(8): p. 3597-3619.
16. Eichelbaum, F., et al., *Interface circuits for quartz-crystal-microbalance sensors.* Review of Scientific Instruments, 1999. **70**(5): p. 2537-2545.
17. Jeho Park, H.H.N., Abdela Woubit, Moonil Kim, *Applications of Field-Effect Transistor (FET)-Type Biosensors.* Appl. Sci. Converg. Technol., 2014. **23**(2): p. 61-71.

18. Ganhua, L., E.O. Leonidas, and C. Junhong, *Reduced graphene oxide for room-temperature gas sensors.* Nanotechnology, 2009. **20**(44): p. 445502.
19. Mao, S., et al., *Tuning gas-sensing properties of reduced graphene oxide using tin oxide nanocrystals.* Journal of Materials Chemistry, 2012. **22**(22): p. 11009-11013.
20. Abbas, A.N., et al., *Black Phosphorus Gas Sensors.* ACS Nano, 2015. **9**(5): p. 5618-5624.
21. Cui, S., et al., *Ultrahigh sensitivity and layer-dependent sensing performance of phosphorene-based gas sensors.* Nature Communications, 2015. **6**: p. 8632.
22. Zhou, G., et al., *Real-Time, Selective Detection of Pb2+ in Water Using a Reduced Graphene Oxide/Gold Nanoparticle Field-Effect Transistor Device.* ACS Applied Materials & Interfaces, 2014. **6**(21): p. 19235-19241.
23. Chen, K., et al., *Hg(II) Ion Detection Using Thermally Reduced Graphene Oxide Decorated with Functionalized Gold Nanoparticles.* Analytical Chemistry, 2012. **84**(9): p. 4057-4062.
24. Mao, S., et al., *Direct Growth of Vertically-oriented Graphene for Field-Effect Transistor Biosensor.* Scientific Reports, 2013. **3**: p. 1696.
25. Chang, J., et al., *Single-walled carbon nanotube field-effect transistors with graphene oxide passivation for fast, sensitive, and selective proteindetection.* Biosensors and Bioelectronics, 2013. **42**: p. 186-192.
26. Mao, S., et al., *Specific Protein Detection Using Thermally Reduced Graphene Oxide Sheet Decorated with Gold Nanoparticle-Antibody Conjugates.* Advanced Materials, 2010. **22**(32): p. 3521-3526.
27. Liu, S. and X. Guo, *Carbon nanomaterials field-effect-transistor-based biosensors.* Npg Asia Materials, 2012. **4**: p. e23.
28. Chen, K.-I., B.-R. Li, and Y.-T. Chen, *Silicon nanowire field-effect transistor-based biosensors for biomedical diagnosis and cellular recording investigation.* Nano Today, 2011. **6**(2): p. 131-154.
29. Mohanty, N. and V. Berry, *Graphene-Based Single-Bacterium Resolution Biodevice and DNA Transistor: Interfacing Graphene Derivatives with Nanoscale and Microscale Biocomponents.* Nano Letters, 2008. **8**(12): p. 4469-4476.
30. Zheng, G., et al., *Multiplexed electrical detection of cancer markers with nanowire sensor arrays.* Nature Biotechnology, 2005. **23**: p. 1294.
31. Stern, E., et al., *Importance of the Debye Screening Length on Nanowire Field Effect Transistor Sensors.* Nano Letters, 2007. **7**(11): p. 3405-3409.
32. Gao, N., et al., *General Strategy for Biodetection in High Ionic Strength Solutions Using Transistor-Based Nanoelectronic Sensors.* Nano Letters, 2015. **15**(3): p. 2143-2148.
33. Kulkarni, G.S. and Z. Zhong, *Detection beyond the Debye Screening Length in a High-Frequency Nanoelectronic Biosensor.* Nano Letters, 2012. **12**(2): p. 719-723.
34. Iijima, S. and T. Ichihashi, *Single-shell carbon nanotubes of 1-nm diameter.* Nature, 1993. **363**: p. 603.
35. Tans, S.J., A.R.M. Verschueren, and C. Dekker, *Room-temperature transistor based on a single carbon nanotube.* Nature, 1998. **393**: p. 49.
36. Kong, J., et al., *Nanotube Molecular Wires as Chemical Sensors.* Science, 2000. **287**(5453): p. 622-625.
37. Kim, J.P., et al., *Ultrasensitive carbon nanotube-based biosensors using antibody-binding fragments.* Analytical Biochemistry, 2008. **381**(2): p. 193-198.
38. Filipiak, M.S., et al., *Highly sensitive, selective and label-free protein detection in physiological solutions using carbon nanotube transistors with nanobody receptors.* Sensors and Actuators B: Chemical, 2018. **255**: p. 1507-1516.

39. McEuen, P.L., *Single-wall carbon nanotubes.* Physics World, 2000: p. 31-36.
40. Yasuki, Y., et al., *Electrical Detection of Negatively Charged Proteins Using n-Type Carbon Nanotube Field-Effect Transistor Biosensors.* Japanese Journal of Applied Physics, 2010. **49**(2S): p. 02BD10.
41. Javey, A., et al., *High Performance n-Type Carbon Nanotube Field-Effect Transistors with Chemically Doped Contacts.* Nano Letters, 2005. **5**(2): p. 345-348.
42. DEBYE, P., *Dieletric Properties of Pure Liquids.* Chem. Rev., 1936. **19**(3): p. 171–182.
43. Gruner, G., *Carbon nanotube transistors for biosensing applications.* Analytical and Bioanalytical Chemistry, 2006. **384**(2): p. 322-335.
44. De Volder, M.F.L., et al., *Carbon Nanotubes: Present and Future Commercial Applications.* Science, 2013. **339**(6119): p. 535-539.
45. Dresselhaus, M.S., et al., *Raman spectroscopy of carbon nanotubes.* Physics Reports, 2005. **409**(2): p. 47-99.
46. Odom, T.W., et al., *Atomic structure and electronic properties of single-walled carbon nanotubes.* Nature, 1998. **391**: p. 62.
47. Veena Choudhary, A.G., *Polymer/Carbon Nanotube Nanocomposites.* (doi: 10.5772/18423), 2011.
48. Iijima, S., *Helical microtubules of graphitic carbon.* Nature, 1991. **354**: p. 56.
49. Mukul, K. and A. Yoshinori, *Chemical Vapor Deposition of Carbon Nanotubes: A Review on Growth Mechanism and Mass Production.* J. Nanosci. Nanotechnol., 2010. **10**: p. 3739–3758.
50. Cassell, A.M., et al., *Large Scale CVD Synthesis of Single-Walled Carbon Nanotubes.* The Journal of Physical Chemistry B, 1999. **103**(31): p. 6484-6492.
51. Singh, P., et al., *Organic functionalisation and characterisation of single-walled carbon nanotubes.* Chemical Society Reviews, 2009. **38**(8): p. 2214-2230.
52. Poulpiquet, A.D., et al., *Carbon Nanotube-Enzyme Biohybrids in a Green Hydrogen Economy.* DOI: 10.5772/51782.
53. So, H.-M., et al., *Single-Walled Carbon Nanotube Biosensors Using Aptamers as Molecular Recognition Elements.* Journal of the American Chemical Society, 2005. **127**(34): p. 11906-11907.
54. Star, A., et al., *Electronic Detection of Specific Protein Binding Using Nanotube FET Devices.* Nano Letters, 2003. **3**(4): p. 459-463.
55. Leyden, M.R., et al., *Increasing the detection speed of an all-electronic real-time biosensor.* Lab on a Chip, 2012. **12**(5): p. 954-959.
56. Colas, P., et al., *Genetic selection of peptide aptamers that recognize and inhibit cyclin-dependent kinase 2.* Nature, 1996. **380**(6574): p. 548-550.
57. Baines, I.C. and P. Colas, *Peptide aptamers as guides for small-molecule drug discovery.* Drug Discovery Today, 2006. **11**(7-8): p. 334-341.
58. Hoppe-Seyler, F. and K. Butz, *Peptide aptamers: powerful new tools for molecular medicine.* Journal of Molecular Medicine, 2000. **78**(8): p. 426-430.
59. Colas, P., *The eleven-year switch of peptide aptamers.* Journal of Biology, 2008. **7**(1): p. 2.
60. Hoppe-Seyler, F., et al., *Peptide aptamers: new tools to study protein interactions.* The Journal of Steroid Biochemistry and Molecular Biology, 2001. **78**(2): p. 105-111.
61. Crawford, M., *Peptide aptamers: Tools for biology and drug discovery.* Briefings in Functional Genomics and Proteomics, 2003. **2**(1): p. 72-79.
62. Hoppe-Seyler, F., et al., *Peptide Aptamers: Specific Inhibitors of Protein Function.* Current Molecular Medicine, 2004. **4**(5): p. 529-538.

63. Mascini, M., I. Palchetti, and S. Tombelli, *Nucleic Acid and Peptide Aptamers: Fundamentals and Bioanalytical Aspects.* Angewandte Chemie International Edition, 2012. **51**(6): p. 1316-1332.
64. Biyani, M., et al., *PEP-on-DEP: A competitive peptide-based disposable electrochemical aptasensor for renin diagnostics.* Biosensors and Bioelectronics, 2016. **84**: p. 120-125.
65. Willis, R.C. and C.E. Furlong, *Interactions of a glutamate-aspartate binding protein with the glutamate transport system of Escherichia coli.* Journal of Biological Chemistry, 1975. **250**(7): p. 2581-2586.
66. Willis, R.C. and C.E. Furlong, *Purification and properties of a periplasmic glutamate-aspartate binding protein from Escherichia coli K12 strain W3092.* Journal of Biological Chemistry, 1975. **250**(7): p. 2574-2580.
67. Oshima, T., et al., *A 718-kb DNA Sequence of the Escherichia coli K-12 Genome Corresponding to the 12.7–28.0 min Region on the Linkage Map (Supplement).* DNA Research, 1996. **3**(3): p. 211-223.
68. Blattner, F.R., et al., *The Complete Genome Sequence of Escherichia coli K-12.* Science, 1997. **277**(5331): p. 1453-1462.
69. Fan, C.-P., et al., *A Periplasmic Glutamate/Aspartate Binding Protein from Shigella flexneri: Gene Cloning, Over-Expression, Purification and Preliminary Crystallographic Studies of the Recombinant Protein.* Protein & Peptide Letters, 2006. **13**(5): p. 513-516.
70. Hu, Y., et al., *Crystal Structure of a Glutamate/Aspartate Binding Protein Complexed with a Glutamate Molecule: Structural Basis of Ligand Specificity at Atomic Resolution.* Journal of Molecular Biology, 2008. **382**(1): p. 99-111.
71. Marvin, J.S., et al., *An optimized fluorescent probe for visualizing glutamate neurotransmission.* Nature methods, 2013. **10**(2): p. 162-170.
72. Marvin, J.S., et al., *Stability, affinity, and chromatic variants of the glutamate sensor iGluSnFR.* Nature methods, 2018. **15**(11): p. 936-939.
73. Basirjafari, S., S.E. Khadem, and R. Malekfar, *Radial breathing mode frequencies of carbon nanotubes for determination of their diameters.* Current Applied Physics, 2013. **13**(3): p. 599-609.
74. Bokobza, L. and J. Zhang, *Raman spectroscopic characterization of multiwall carbon nanotubes and of composites.* Express Polymer Letters, 2012. **6**(7): p. 601 - 608.
75. Maehashi, K. and K. Matsumoto. *Aptamer-based label-free immunosensors using carbon nanotube field-effect transistors*. in *SENSORS, 2009 IEEE*. 2009.
76. Du, H., et al., *Electric double-layer transistors: a review of recent progress.* Journal of Materials Science, 2015. **50**(17): p. 5641-5673.
77. Minot, E.D., et al., *Carbon nanotube biosensors: The critical role of the reference electrode.* Applied Physics Letters, 2007. **91**(9): p. 093507.
78. Kenzo, M., et al., *Ultrasensitive Detection of DNA Hybridization Using Carbon Nanotube Field-Effect Transistors.* Japanese Journal of Applied Physics, 2004. **43**(12A): p. L1558.
79. Sharma, A., et al., *Single-walled carbon nanotube based transparent immunosensor for detection of a prostate cancer biomarker osteopontin.* Analytica Chimica Acta, 2015. **869**: p. 68-73.
80. Ordinario, D.D., et al., *Sequence Specific Detection of Restriction Enzymes at DNA-Modified Carbon Nanotube Field Effect Transistors.* Analytical Chemistry, 2014. **86**(17): p. 8628-8633.

81. Nanjappa, V., et al., *Plasma Proteome Database as a resource for proteomics research: 2014 update.* Nucleic Acids Research, 2014. **42**(D1): p. D959-D965.
82. Erlanger, B.F., et al., *Binding of an Anti-Fullerene IgG Monoclonal Antibody to Single Wall Carbon Nanotubes.* Nano Letters, 2001. **1**(9): p. 465-467.
83. Wang, S., et al., *Peptides with selective affinity for carbon nanotubes.* Nature Materials, 2003. **2**: p. 196.
84. Hayamizu, Y., et al., *Bioelectronic interfaces by spontaneously organized peptides on 2D atomic single layer materials.* Scientific Reports, 2016. **6**: p. 33778.
85. Kitamura, K., et al., *Development of Systemic in vitro Evolution and Its Application to Generation of Peptide-Aptamer-Based Inhibitors of Cathepsin E.* Journal of Molecular Biology, 2009. **387**(5): p. 1186-1198.
86. Chu, C.-H., et al., *Beyond the Debye length in high ionic strength solution: direct protein detection with field-effect transistors (FETs) in human serum.* Scientific Reports, 2017. **7**(1): p. 5256.
87. Forzani, E.S., et al., *Tuning the Chemical Selectivity of SWNT-FETs for Detection of Heavy-Metal Ions.* Small, 2006. **2**(11): p. 1283-1291.
88. Jin, H.-E., et al., *Selective and Sensitive Sensing of Flame Retardant Chemicals Through Phage Display Discovered Recognition Peptide.* Nano Letters, 2015. **15**(11): p. 7697-7703.
89. Kim, T.H., et al., *Selective and Sensitive TNT Sensors Using Biomimetic Polydiacetylene-Coated CNT-FETs.* ACS Nano, 2011. **5**(4): p. 2824-2830.
90. Kitamura, K., et al., *Provenin vitroevolution of protease cathepsin E-inhibitors and -activators at pH 4.5 using a paired peptide method.* Journal of Peptide Science, 2012. **18**(12): p. 711-719.
91. Kitamura, K., et al., *Peptide Aptamer-Based ELISA-Like System for Detection of Cathepsin E in Tissues and Plasma.* Journal of Molecular Biomarkers & Diagnosis, 2011. **02**(01).
92. Kawakubo, T., et al., *Repression of cathepsin E expression increases the risk of mammary carcinogenesis and links to poor prognosis in breast cancer.* Carcinogenesis, 2014. **35**(3): p. 714-726.
93. Star, A., et al., *Interaction of Aromatic Compounds with Carbon Nanotubes: Correlation to the Hammett Parameter of the Substituent and Measured Carbon Nanotube FET Response.* Nano Letters, 2003. **3**(10): p. 1421-1423.
94. Artyukhin, A.B., et al., *Controlled Electrostatic Gating of Carbon Nanotube FET Devices.* Nano Letters, 2006. **6**(9): p. 2080-2085.
95. Frederix, F., et al., *Reduced nonspecific adsorption on covalently immobilized protein surfaces using poly(ethylene oxide) containing blocking agents.* Journal of Biochemical and Biophysical Methods, 2004. **58**(1): p. 67-74.
96. Abd-Elgaliel, W.R. and C.-H. Tung, *Selective detection of Cathepsin E proteolytic activity.* Biochimica et Biophysica Acta (BBA) - General Subjects, 2010. **1800**(9): p. 1002-1008.
97. Zhou, Y. and N.C. Danbolt, *Glutamate as a neurotransmitter in the healthy brain.* Journal of Neural Transmission, 2014. **121**(8): p. 799-817.
98. Meldrum, B.S., *Glutamate as a Neurotransmitter in the Brain: Review of Physiology and Pathology.* The Journal of Nutrition, 2000. **130**(4): p. 1007S-1015S.
99. McEntee, W.J. and T.H. Crook, *Glutamate: its role in learning, memory, and the aging brain.* Psychopharmacology, 1993. **111**(4): p. 391-401.
100. Brun, M.A., et al., *A Semisynthetic Fluorescent Sensor Protein for Glutamate.* Journal of the American Chemical Society, 2012. **134**(18): p. 7676-7678.

101. Choi, D.W., *Excitotoxic cell death.* Journal of Neurobiology, 1992. **23**(9): p. 1261-1276.
102. Parsons, C.G., W. Danysz, and G. Quack, *Glutamate in CNS disorders as a target for drug development: an update.* Drug News & Perspectives, 1998. **11**(9): p. 523.
103. Gsell, W., et al. *Neurochemical abnormalities in Alzheimer's disease and Parkinson's disease — a comparative review*. 1997. Vienna: Springer Vienna.
104. Danbolt, N.C., *Glutamate uptake.* Progress in Neurobiology, 2001. **65**(1): p. 1-105.
105. Nedergaard, M., T. Takano, and A.J. Hansen, *Beyond the role of glutamate as a neurotransmitter.* Nature Reviews Neuroscience, 2002. **3**(9): p. 748-755.
106. Mikeladze, E., et al., *Characterization of a Glutamate Biosensor Based on a Novel Glutamate Oxidase Integrated into a Redox Hydrogel.* Electroanalysis, 2002. **14**(15-16): p. 1052-1059.
107. Schuvailo, O.M., et al., *Highly selective microbiosensors for in vivo measurement of glucose, lactate and glutamate.* Analytica Chimica Acta, 2006. **573-574**: p. 110-116.
108. Chakraborty, S. and C. Retna Raj, *Amperometric biosensing of glutamate using carbon nanotube based electrode.* Electrochemistry Communications, 2007. **9**(6): p. 1323-1330.
109. Tang, L., et al., *Amperometric glutamate biosensor based on self-assembling glutamate dehydrogenase and dendrimer-encapsulated platinum nanoparticles onto carbon nanotubes.* Talanta, 2007. **73**(3): p. 438-443.
110. Tang, L., et al., *An enhanced biosensor for glutamate based on self-assembled carbon nanotubes and dendrimer-encapsulated platinum nanobiocomposites-doped polypyrrole film.* Analytica Chimica Acta, 2007. **597**(1): p. 145-150.
111. Rocchitta, G., et al., *Enzyme Biosensors for Biomedical Applications: Strategies for Safeguarding Analytical Performances in Biological Fluids.* Sensors, 2016. **16**(6): p. 780.
112. Tian, L. and L.L. Looger, *Genetically encoded fluorescent sensors for studying healthy and diseased nervous systems.* Drug discovery today. Disease models, 2008. **5**(1): p. 27-35.
113. Hall, M.D., A. Simeonov, and M.I. Davis, *Avoiding Fluorescence Assay Interference—The Case for Diaphorase.* Assay and Drug Development Technologies, 2016. **14**(3): p. 175-179.
114. Lee, G.J., et al., *Neurotransmitter detection by enzyme-immobilized CNT-FET.* Current Applied Physics, 2009. **9**(1, Supplement): p. S25-S28.
115. Braeken, D., et al., *Glutamate sensing with enzyme-modified floating-gate field effect transistors.* Biosensors and Bioelectronics, 2009. **24**(8): p. 2384-2389.

Achievements

I. Journal paper

1. **Nguyen Thanh Tung**, Phan Trong Tue, Truong Thi Ngoc Lien, Yasuhide Ohno, Kenzo Maehashi, Kazuhiko Matsumoto, Koichi Nishigaki, Manish Biyani, Yuzuru Takamura, **Peptide aptamer-modified single-walled carbon nanotube-based transistors for high-performance biosensors**, Scientific Reports (2017) 7: 17881, DOI:10.1038/s41598-017-18169-1.

II. Conference proceeding

1. **Nguyen Thanh Tung**, Trisha D. Farha, Hidekazu Tsutsui, Truong T.N. Lien, Yasuhide Ohno, Kenzo Maehashi, Kazuhiko Matsumoto, Manish Biyani, Phan T. Tue, Yuzuru Takamura, **Development of Glutamate biosensor based on the integration of network SWCNT-FET and Glutamate-binding protein**, *μ-TAS 2018*, p795-797, (Kaohsiung, Taiwan, November 11 – 15, 2018).

III. Presentation at academic conferences

1. **Nguyen Thanh Tung**, Trisha D. Farha, Hidekazu Tsutsui, Truong T.N. Lien, Yasuhide Ohno, Kenzo Maehashi, Kazuhiko Matsumoto, Manish Biyani, Phan T. Tue, Yuzuru Takamura, "Development of Glutamate biosensor based on the integration of network SWCNT-FET and Glutamate-binding protein", *μ-TAS 2018*, (Kaohsiung, Taiwan, November 11 – 15, 2018).

2. **Nguyen Thanh Tung**, T.D. Farha, H. Tsutsui, T.T.N. Lien, Y. Ohno, K. Maehashi, K. Matsumoto, P.T. Tue, Y. Takamura, "Glutamate-binding protein integrated into single-walled carbon nanotube field-effect transistor for ultrasensitive glutamate detection", *28th Anniversary World Congress on Biosensors (Biosensors 2018)*, No. P1.188, (Miami, USA, June 2018).

3. **Nguyen Thanh Tung** , Trisha Diba Farha, Hidekazu Tsutsui, Truong Thi Ngoc Lien, Yasuhide Ohno, Kenzo Maehashi, Kazuhiko Matsumoto, Phan Trong Tue, Yuzuru Takamura, "Study on Glutamate detection using Glutamate-binding protein modified network single-walled carbon nanotube field-effect transistor", *CHEMINAS37*, No. 3P17, (Ibaraki, Japan, May 2018).

4. **Nguyen Thanh Tung**, Phan Trong Tue, Truong Thi Ngoc Lien, Yasuhide Ohno, Kenzo Maehashi, Kazuhiko Matsumoto, Manish Biyani, Yuzuru Takamura, "Optimization of peptide aptamer immobilization onto single-walled carbon nanotube field-effect transistor for aptasensor", *The 9th International conference on Molecular Electronics and Bioelectronics (ME&B 2017)*, No. P-T2-007, (Kanazawa, Japan, June 2017).

5. **Nguyen Thanh Tung**, Phan Trong Tue, Truong Thi Ngoc Lien, Yasuhide Ohno, Kenzo Maehashi, Kazuhiko Matsumoto, Manish Biyani, Yuzuru Takamura, "Development of highly sensitive and specific aptasensor via combination of novel peptide aptamer bioreceptor and SWCNT FET", *CHEMINAS35*, No. 2P12, (Tokyo, Japan, May 2017).

6. **Nguyen Thanh Tung**, P.T. Tue, T.T.N. Lien, Y. Ohno, K. Maehashi, K. Matsumoto, M. Biyani, Y. Takamura, *"*Peptide aptamer-modified single-walled carbon nanotube field-effect-transistor-based biosensor for ultrasensitive cancer diagnostics", *The 5th International Conference on Bio-sensing Technology*, No. P193, (Riva Del Garda, Italy, May 2017).

7. **Nguyen Thanh Tung**, Phan Trong Tue, Truong Thi Ngoc Lien, Yasuhide Ohno, Kenzo Maehashi, Kazuhiko Matsumoto, Manish Biyani, Yuzuru Takamura, "Peptide aptamer-based single-walled carbon nanotube field-effect transistor biosensor for

cathepsin E biomarker detection", *The 64th JSAP Spring Meeting*, No. 16a-P7-10, (Pacifico Yokohama, Japan, March 2017).

8. **Nguyen Thanh Tung**, Phan Trong Tue, Truong Thi Ngoc Lien, Yasuhide Ohno, Kenzo Maehashi, Kazuhiko Matsumoto, Manish Biyani, Yuzuru Takamura, "Fabrication of Peptide-modified Single-Walled Carbon Nanotube Field Effect Transistor applying for Aptasensor", *Asia-Pacific Conference of Transducers and Micro-Nano Technology 2016 (APCOT2016)*, No. 4c.2, (Kanazawa, Japan, June 2016).

9. **Nguyen Thanh Tung**, Phan Trong Tue, Truong Thi Ngoc Lien, Yasuhide Ohno, Kenzo Maehashi, Kazuhiko Matsumoto, Manish Biyani, Yuzuru Takamura, "Study on peptide-functionalized single-walled carbon nanotube field-effect transistor for aptasensor", *The 63rd JSAP Spring Meeting*, No. 20p-P12-22, (Tokyo, Japan, March 2016).

10. **Nguyen Thanh Tung**, Phan Trong Tue, Truong Thi Ngoc Lien, Yasuhide Ohno, Kenzo Maehashi, Kazuhiko Matsumoto, Yuzuru Takamura, "Study on pre- and in-situ post-annealing effect on carbon nanotube growth for biosensing application", *The 76th JSAP Autumn Meeting*, No. 16a-PA2-4, (Nagoya, Japan, September 2015).

Appendix

1. Biacore X100

Biacore X100 is an automated and versatile system for comprehensive, label-free and flexible analysis and characterization of biomolecular interactions in real-time. This system is able to perform the accurate kinetic characterization, binding affinity and specificity determination, concentration measurements and detection of weak and transient binding events. The interaction of biomolecules can be measured in buffer solution or in physiological environment such as serum. These features of Biacore X100 make it highly suitable for many different assay formats and the study of a wide variety of molecular interaction research to boost the understanding of protein function and biological mechanisms.

In Biacore X100 system, molecular interactions are monitored quantitatively on the surface of a removable sensor chip by the surface plasmon resonance detector. Sample is introduced into the chip via microfluidic system which utilizes very small volume of sample (down to a few microliters). The operation of Biacore X100 system, data collection and valuation are handled by user-friendly software. The sensor chip contains glass slide coated with the thin film of gold to create the surface of sensor. A dextran matrix covalently covers the surface of gold film and plays a role as a substrate to which the ligand can be immobilized. There are many kinds of sensor chip using in Biacore system. In this work, we used the sensor chip CM5, which is the first choice for immobilization of protein via $–NH_2$, -SH, -CHO, -OH, -COOH and is suitable for low molecular weight molecules (typically < 1000 Da).

Biacore uses phenomenon of surface plasmon resonance (SPR) to detect the bimolecular interactions (Figure A1). In the setup, the light source pass through the prism,

reflects at the back side of the sensor chip surface and come to the detector. The light is absorbed by the electrons on the gold surface causing them to resonate. This resonating electron is also called SPR, which is sensitive to surrounding environment. SPR causes the sharp reduction in intensity of reflecting light at a specific angle from the glass slide of the sensor surface, which depends on the refractive index of the surface layer of a solution. The angle shifts when analytes bind to the surface and alter the refractive index of the surface layer. The change in SPR angle is proportional to the amount of binding analytes.

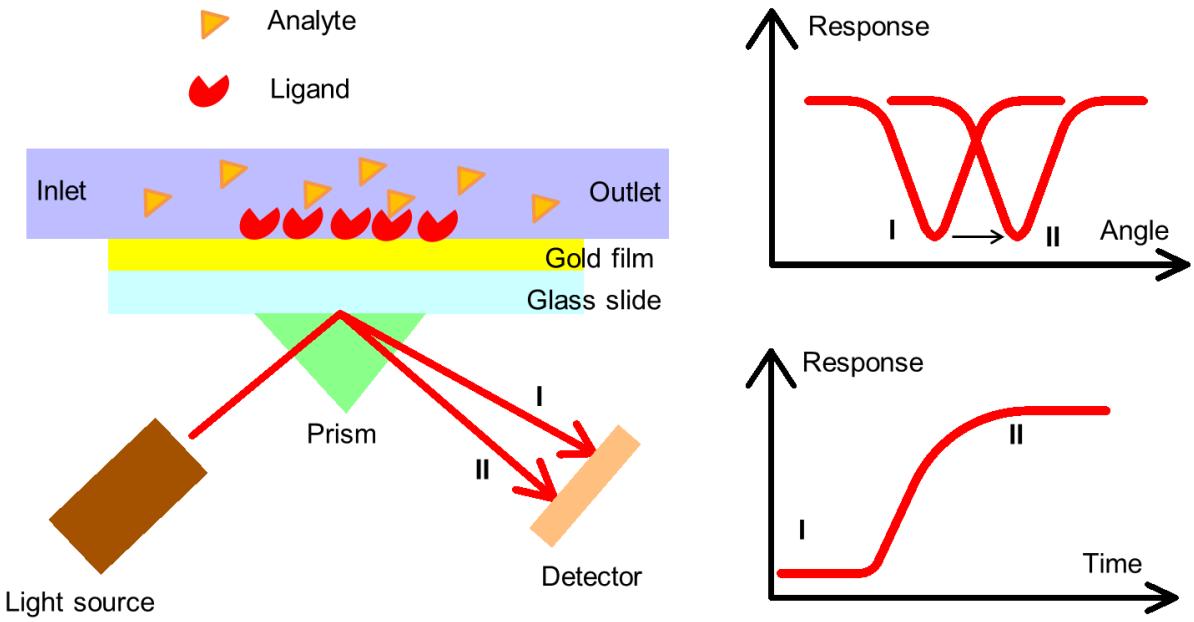

Figure A1: Schematic illustration of surface plasmon resonance.

2. Scanning electron microscope

Scanning electron microscope (SEM) is an improved model of an electron microscope. SEM is used to observe the two-dimensional image of the specimen. The SEM consists of component parts showing below (Figure A2):

- An electron gun to produce high energy electron beam.

- A magnetic condenser lens and objective lens to condense and produce the fine electron beam.

- A scanning coil to scan the electron beam along the surface of specimen.

- A specimen stage to place the specimen.

- A secondary electron detector to collect the secondary electrons.

- An image display to convert electrical signal into image.

- An operation system to perform various operations.

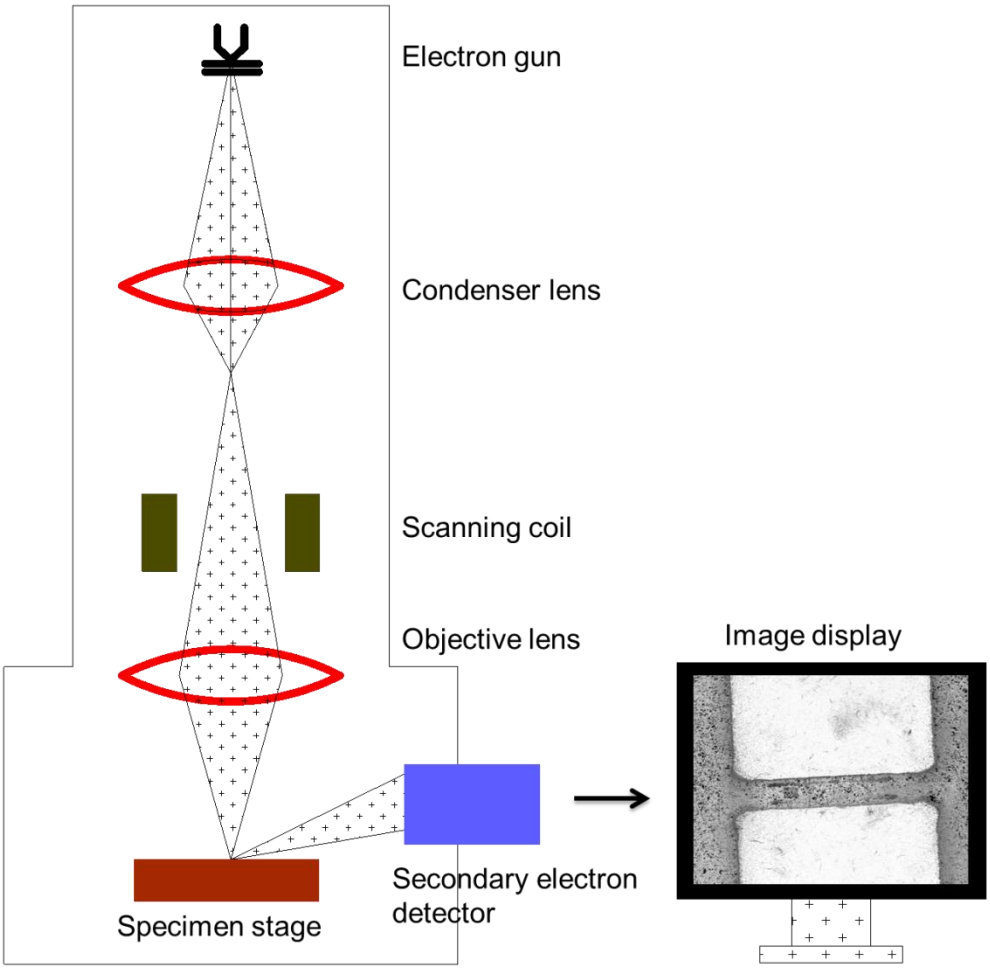

Figure A2: Schematic illustration of the SEM system.

The electron beam is generated by the electron gun and accelerated by the grid and anode. A fine electron beam is required for the SEM. Therefore, this accelerated primary electron beam is adjusted and focused the diameter to get a small electron beam by condenser and objective lenses. When the specimen is irradiated with a fine electron beam,

it produces secondary electrons emitted from the specimen surface. These secondary electrons are very difficult to be collected and hence a high voltage is applied to the secondary electron collector. These secondary electrons are converted into electrical signals and hence give the image of surface morphology of specimen.

There are three types of electron guns: thermionic emission gun (TE gun), field-emission electron gun (FE gun) and Schottkey-emission electron gun (SE gun).

- TE gun: Thermoelectrons are emitted from a thin tungsten wire filament (cathode) by heating the filament at high temperature of around 2800 K. By using TE gun, the electron source is generated with a diameter of 15 to 20 μm.

- FE gun: This electron gun is used for a high-resolution SEM. The FE gun utilizes the field-emission effect in which a high electric field is applied to force the electrons emitted from a thin tungsten wire cathode. By using FE gun, the electron source is generated with a diameter of 5 to 10 nm. The FE gun produces a much smaller electron source than the TE gun, thus suitable for high-resolution SEM.

- SE gun: The SE gun utilizes the Schottky-emission effect in which a high electric field is applied to a heated cathode. The cathode, which is generally made of a tungsten single crystal coated with ZrO, is heated at relatively low temperature of about 1800 K. Because SE gun consists of both thermal emission and field-emission effect, the SE gun is situated between TE and FE guns and its applications ranges from high-magnification observation to various analyses.

Atomic force microscope

The Atomic force microscope (AFM) is a kind of scanning probe microscope which based on the interactions between a tip and a sample surface to obtain a three-

dimensional topography of the sample surface. A typical AFM consists of a cantilever, a laser diode, a 4-quadrant photodiode and a scanner (Figure A3).

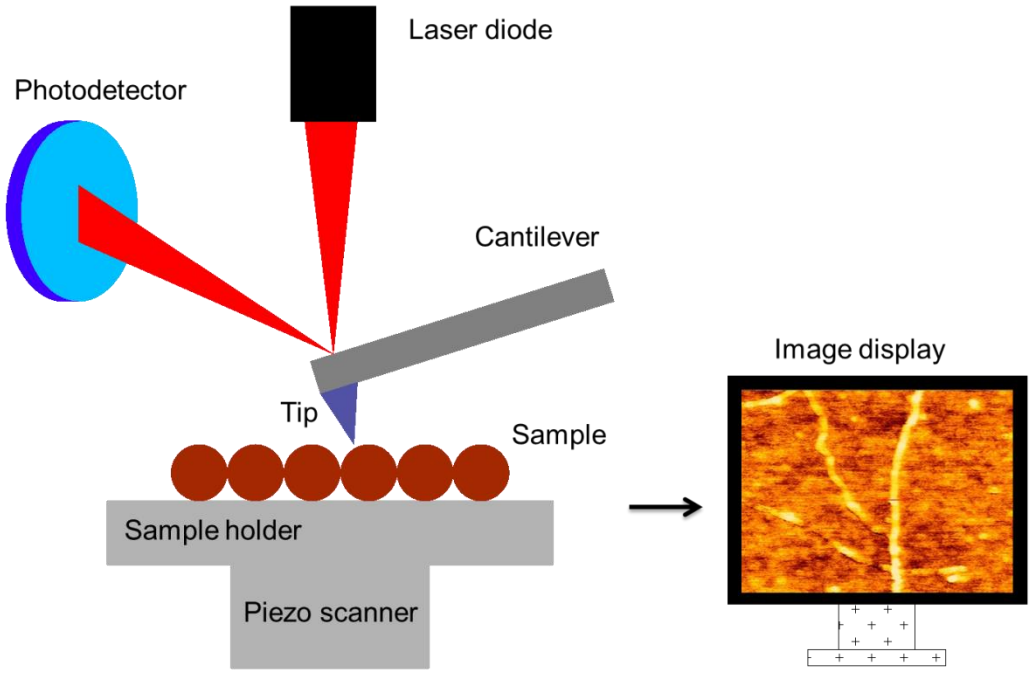

Figure A3: Schematic illustration of a typical AFM system.

Generally, the AFM cantilever does not move, instead the sample is moved in the x, y and z direction by a scanner. The movement of scanner is controlled by a piezoelectric material which can be enlarged or shrunk by applying voltage. A laser beam from laser diode is focused onto the back of the cantilever and be reflected back to the 4-quadrant photodiode detector. The interaction between tip of cantilever and sample surface makes the cantilever to deflect. Hence, the direction of laser is also deflected accordingly and be measured by photodiode detector to create the topographical image of sample. There are three operation modes: contact mode, dynamic (tapping) mode and non-contact mode.

- Contact mode: The tip of cantilever is softly contacted with the surface of sample and moves along the surface with a constant force. This movement may cause the damage to the sample due to the frictional and adhesive forces.

- Tapping mode: The tip of cantilever is intermittently contacted to the surface and oscillated with sufficient amplitude to prevent the frictional and adhesive forces. This operation mode offers less damage to sample rather than contact mode.

- Non-contact mode: In this operation mode, the tip of cantilever does not touch the sample. It oscillates above the surface of sample during scan. This operation mode offers a helpful measurement for soft samples.

Raman Spectroscopy

The Raman Spectroscopy is a highly versatile technique that provides a fast, precise and non-destructive analysis of both organic and inorganic chemicals. It provides qualitative and quantitative measurement of the rotational, vibrational and other low frequency modes of molecules, hence offers an important practical tool for quickly identifying molecules and minerals, and studying molecular structure. This technique requires no sample preparation. Since Raman spectroscopy is highly selective, it can easily differentiate molecules with very similar chemical structure. Metal nanoparticles-coated semiconductors can provide enhancement of Raman spectra by surface-enhanced Raman scattering effect. This system consists of main components as shown in the Figure A4.

- Single coloured light source (lasers): The laser wavelengths used for this Raman spectroscopy system are 488, 532, and 660 nm.

- Lenses: are used to focus the light onto the sample and to collect the scattered light.

- Filters: are used to prevent the undesired light and purify the reflected and scattered light so that only the Raman light is collected.

- Monochromator: Monochromator contains a pair of concave mirrors and a plain grating. The first mirror causes the light to become more aligned in a specific direction.

The plain grating splits the light into its constituent colours. The second mirror gathers the light from the grating and directs them to the detector.

- A highly sensitive charge coupled device (CDD) detector: to detect the photons from incident light.

- A computer: to control the whole system, display the spectrum and enable the information to be analysed.

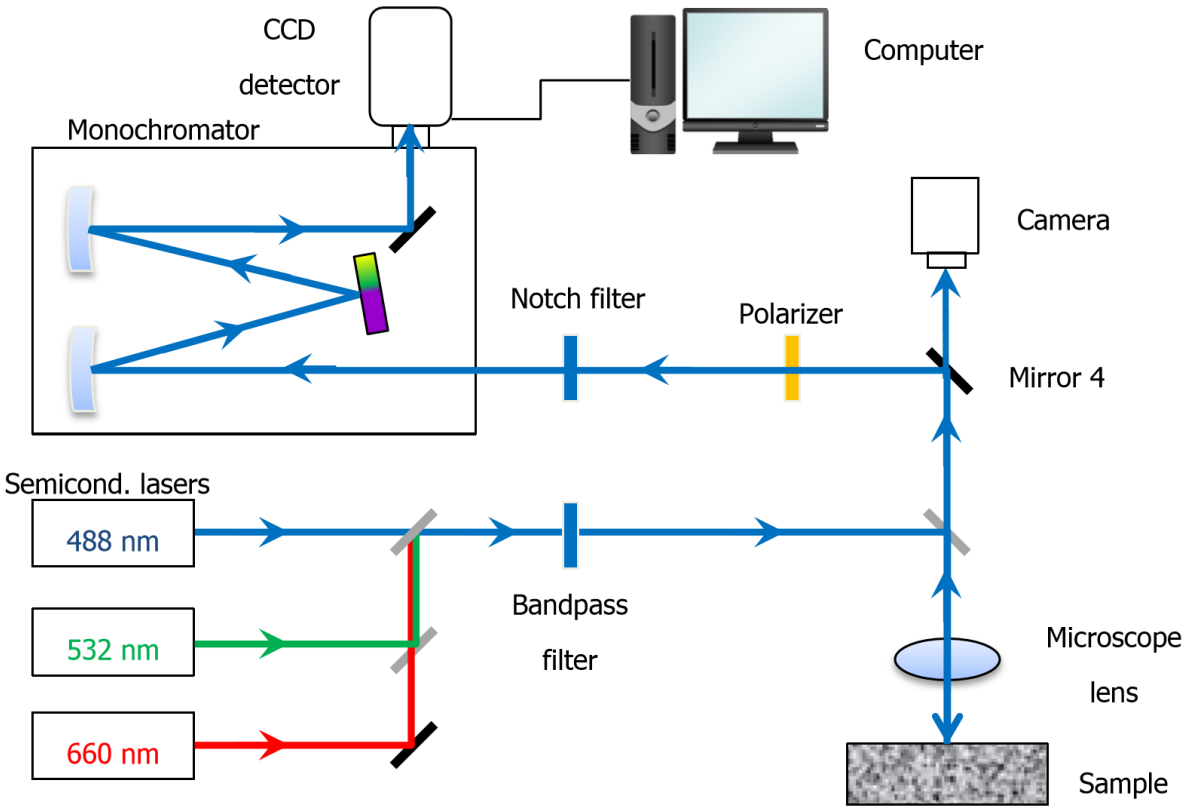

Figure A4: Schematic illustration of Raman spectroscopy system.

The operation of Raman spectroscopy is based on the inelastic scattering of a laser source. The laser beam is filtered by the Bandpass filter and be directed by a mirror. The beam is then focused on the measured semiconductor sample using Microscope lens. The incident light excites the surface particles of the sample and hence gives rise to emitted light. The emitted light is collimated into a parallel beam and be filtered before being

concentrated to the monochromator. Monochromator produces the monochromatic light which is collected by highly sensitive CCD camera, hence creating the optical spectrum.

Spectrofluorometer

Spectrofluorometer is a contactless, versatile, nondestructive and powerful optical method which takes advantage of fluorescent properties of some compounds in order to provide information regarding their concentration and chemical environment in a sample. A certain excitation wavelength is selected, a scan is performed to record the emission intensity versus wavelength, also called an emission spectra.

Photo excitation causes electrons within the material sample to jump from equilibrium states into the excited states. When these electrons return to their equilibrium states, they release the excess energy and give the emission of light (a radiative process) or a non radiative process (Figure A5). The excitation is provided by a laser light with energy much larger than the optical band gap of material.

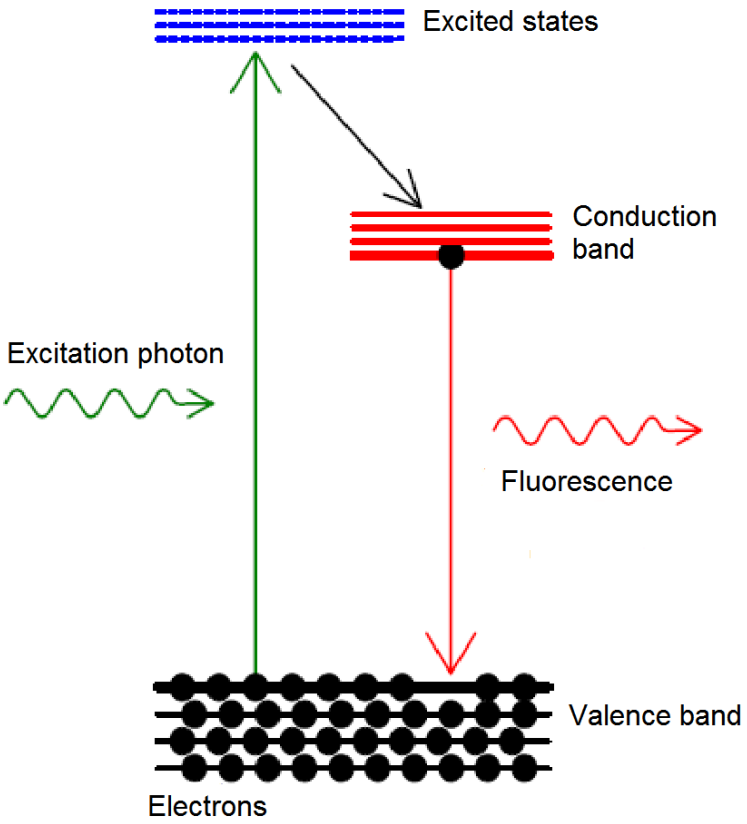

Figure A5: Principle of spectrofluorometer system.

The Spectrofluorometer is an analytical instrument used to measure and record the fluorescence of a sample by scanning excitation, emission or wavelength. Figure A6 shows the schematic diagram of Spectrofluorometer. The sample is placed in a cuvette. The excitation and emission wavelengths of light are selected using excitation and emission monochromator, respectively. The fluorescence intensity from the fluorophores is measured and recorded by a detector.

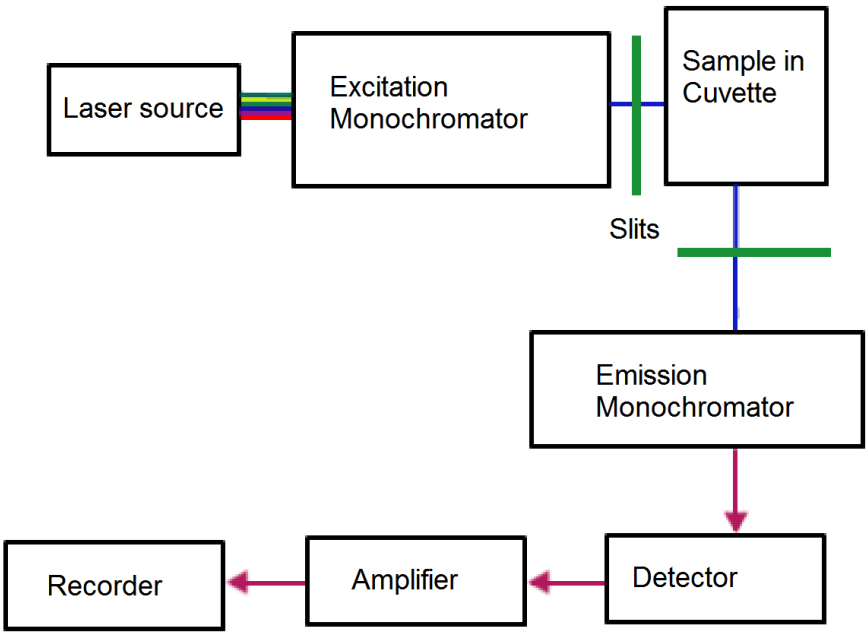

Figure A6: Schematic diagram of Spectrofluorometer system.

E-beam evaporation system

Electron beam evaporation is a physical vapour deposition (PVD) technique which allows for the thin film deposition of materials such as Au, Ti, etc. Figure A7 shows an image of schematic structure of an electron beam evaporation system.

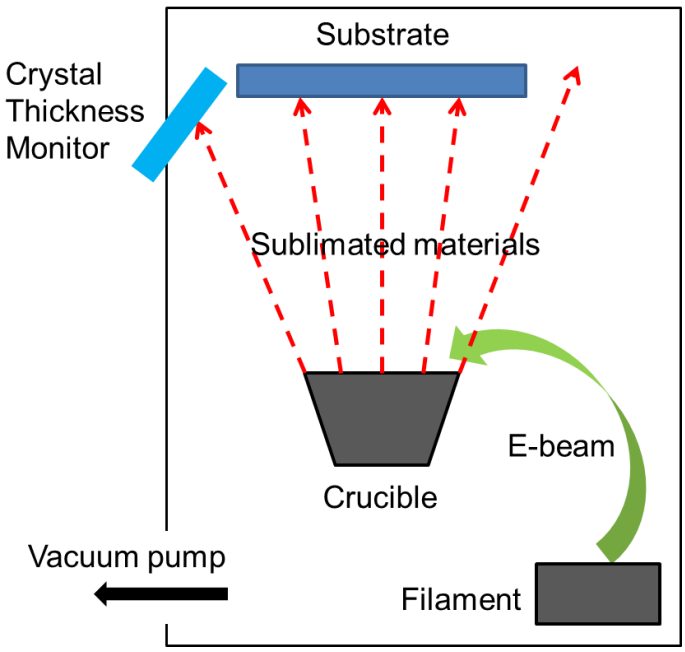

Figure A7: Schematic structure of an E-beam evaporator.

The chamber is kept at high vacuum during process. An electron beam is generated by applying an electrical current to a tungsten filament inside the vacuum chamber and using high electric field to extract the electrons from the filament. The electron beam is bent and focused into the crucible by magnetic force of electromagnetic coils. The material used for coating inside the crucible is heated and melted by the energy of incident electron beam; hence it is evaporated and condensed on the substrate which is located across from the crucible. The thickness is measured in-situ using a crystal thickness monitor which is based on the correlation between the oscillation frequency and the crystal's mass. The frequency data is converted into digital thickness data using an electronic instrument.

Peptide aptamer synthesis

The affinity-based selection used to synthesize peptide aptamer probe molecule is depicted in the Figure A8. First, the DNA molecules of the initial Y-ligation-based block shuffling (YLBS) library are converted into cDNA. The mRNA is generated from cDNA via transcription. The resultant mRNA can be linked to a puromycin linker by hybridization to make the RNA-puromycin conjugate. The ligation of mRNA and linker is subsequently translated *in vitro* to produce a population of RNA-peptide aptamer fusions. The CatE is immobilized onto the magnetic bead prior to be subjected to population of RNA-peptide aptamer fusions. The peptide aptamers bound to magnetic bead-immobilized CatE are isolated and collected by centrifugation, thence their cDNA is generated via reverse transcription and its sequences are amplified by polymerase chain reaction (PCR). The peptide aptamers of selected clones from the fusion of the peptide aptamer and its encoding cDNA is recovered by treatment with DNase I in buffer solution. The sequence of peptide aptamer is read via its cDNA sequence by DNA sequencing.

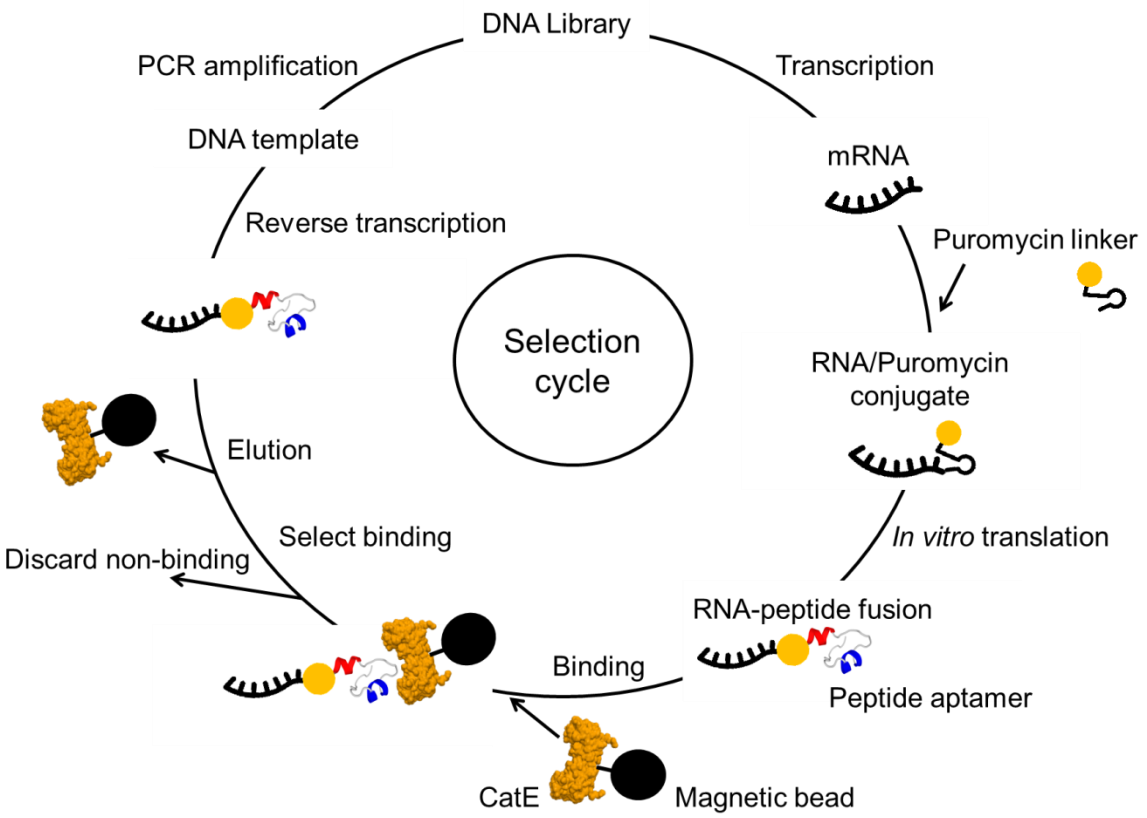

Figure A8: *In vitro* selection for obtaining peptide aptamer probe molecule.

Cloning of *E.coli* for Glutamate-binding protein

The glutamate/aspartate import solute-binding protein (GBP), pRSET B and *E. coli* cell were used as the cloned protein, cloning vector and competent cell. A 20 µL competent cell was dropped into Eppendorf tube, followed by adding 0.2 µL plasmid DNA (a pRSET B vector with GBP), then the solution was mixed briefly by vortex, and incubated on ice for 5 minutes in order to introduce plasmids into *E. coli* cells. The *E. coli* competent cells was given a shock by heating at 42 °C for 40 seconds to encourage them to take up plasmids, and then *E. coli* competent cells was placed on ice for 3 minutes to recover cells. The heat shock changes the fluidity of the *E. coli* membrane, hence causes the formation of pores, therefore making it easier for plasmid to enter the *E. coli* cell. After that, the *E. coli* cells were plastered onto an agar plate which has already contained an ampicillin. The plate was incubated at 37 °C overnight. A plasmid typically contains an

antibiotic resistance gene, which allows *E. coli* cells to survive in the agar plate with the presence of the ampicillin antibiotic. Therefore the *E. coli* that took up the plasmid can live and reproduce, while *E. coli* without a plasmid will die. Each surviving *E. coli* cell will make a colony, which contains the identical *E. coli* cells with the same plasmid. The medium of 13 mL LB and 13 µL ampicillin was prepared in a tube. Then a colony was picked up from the agar plate using toothpick and then was added to the LB/ampicillin tube. Then, this tube was shaken by Bioshaker with 180 rpm at 37 ^{0}C for about 3 hours. After that, the solution inside this tube was poured to a flask which contains a mixture of 90 mL LB and 90 µL ampicillin. This flask was then shaken by Bioshaker with 180 rpm at 22^{0} C for about 7 hours. This process is depicted in Figure A9. The solution in culture flask was transferred to Eppendorf tube. These tubes were performed 7000 rpm centrifugation at room temperature for 10 minutes, then discarding the upper solution and keeping pellet. The pellet was dissolved in 10 mL PBS, followed by 7000 rpm centrifugation at room temperature for 5 min. The pellet was collected and dissolved with 1 mL PBS in an Eppendorf tube, and then was mixed by vortex, then was placed in ice box. After that, 20 µL Lysozyme enzyme was added and incubated for 10 minutes, followed by sonication to make the *E. coli* cells be lysed to release GBP. This step was carried out in ice box to protect the living cells.

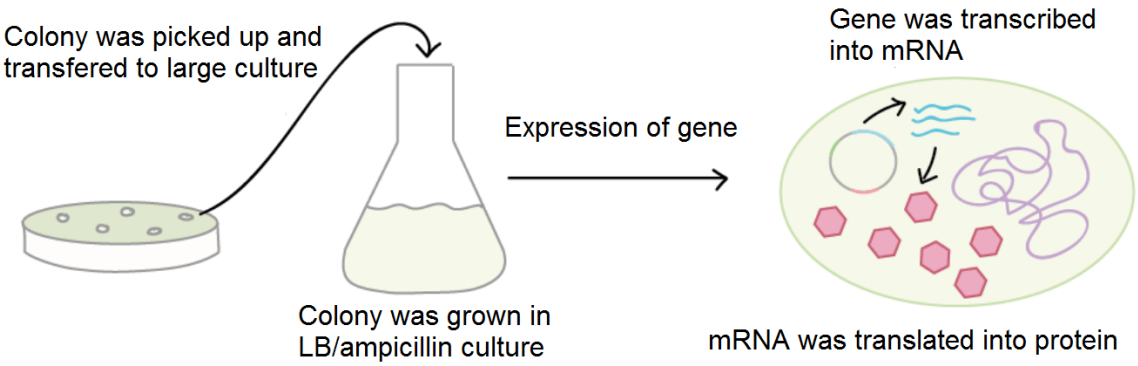

Figure A9: Colony culture and gene expression to produce Glutamate-binding protein

Since the *E. coli* bacteria contain many proteins and macromolecules, the culture product needs to be purified. To do it, affinity chromatography technique was used, in which a mixture of molecules extracted from the lysed *E. coli* bacteria is poured through a column. First, the ion exchange resin in ion exchange column was equilibrated by adding 500 µL PBS to column, followed by 5000 rpm centrifugation for 1 minute. Then, the sample solution was poured to column, followed by 3000 rpm centrifugation for 1 minute. In this step, GBP was retained by resin. After that, 200 µL of 0.5 M imidazole pH 7.4 was added to column for 1 minute, followed by 2000 rpm centrifugation at 4 ^{0}C for 1 minute to elute the GBP. The obtained solution contains GBP, PBS and imidazole. The imidazole was removed by 8000 rpm ultrafiltration at 4 ^{0}C for 10 min. This step was repeated three times. The retained GBP was collected and stored at -80 ^{0}C before use.

Subthreshold swing

Subthreshold swing (S) is defined as the gate voltage required changing the drain current by one order of magnitude.

$$S = \frac{\partial V_G}{\partial log I_D} \text{ (V/decade)}$$